이학박사 학위논문

Novel functions of lysyl-tRNA synthetase in invasive dissemination of colon cancer cells in 3D microenvironment

3차원적 콜라젠 환경에서 대장암세포의 침윤적 이탈을 위한 Lysyl-tRNA 합성효소의 기능

2017년 8월

서울대학교 대학원

자연과학대학 협동과정 유전공학전공

남 서 희

Novel functions of lysyl-tRNA synthetase in invasive dissemination of colon cancer cells in 3D microenvironment

A THESIS

Submitted to the Graduate School of

Seoul National University in Partial

Fulfillment of the Requirements

for the Degree of

Doctor of Philosophy

By

Seo Hee Nam

Interdisciplinary Graduate Program in Genetic Engineering

College of Natural Science

Seoul National University

August, 2017

TABLE OF CONTENTS

CHAPTER 1

LIST OF FIGURES

patient tissues.

Figure 2.1

Certain cytokines caused the dissemination phenotypes from colon cancer cell spheroids embedded in 3D collagen I gels.

Figure 2.2

Certain cytokines from KRS-positive tumor cells caused the polarization of macrophages from M1 to M2 populations.

Figure 2.3

KRS translocated into nucleus promotes GAS6 mRNA level and concomitantly KRS translocated on plasma membrane supports dissemination of colon cancer cells, respectively.

Figure 2.4

KRS-positive HCT116 tumor cells preferred to communicate with M2 macrophages rather than with M1 macrophages.

Figure 2.5

A positive relationship between KRS-positive colon cancer cells and M2 macrophages is important in favoring tumor microenvironment for KRS-positive metastatic phenotypes.

LIST OF ABBREBIATIONS

BSA	**Bovine Serum Albumin**
CM	**Conditioned medium**
COL	**Collagen**
FN	**Fibronectin**
IHC	**Immunohistochemistry**
KRS	**Lysyl-tRNA synthetase**
LN	**Laminin**
Mono	**Monocyte**
M1	**M1 macrophages**
M2	**M2 macrophages**
MSC	**Multi-tRNA synthetase complex**
PXN	**Paxillin**
qRT-PCR	**Quantitative Reverse Transcription PCR**
WCL	**Whole cell lysate**
WT	**Wild-Type**
3D	**3-Dimensional**
67LR	**67kDa laminin receptor**
37LRP	**37kDa laminin receptor precursor**

CHAPTER 1.

Noncanonical roles of membranous lysyl-tRNA synthetase in transducing cell-substrate signaling for invasive dissemination of colon cancer spheroids in 3D collagen I gels.

Abstract

The cell-adhesion properties of cancer cells can be targeted to block cancer metastasis. Although cytosolic lysyl-tRNA synthetase (KRS or KARS) functions in protein synthesis, KRS on the plasma membrane is involved in cancer metastasis. It may be hypothesized that KRS is involved in adhesion-related intracellular signaling for cancer cell migration and invasion. To test this hypothesis, colon cancer cells with modulated KRS protein levels were adhered on 2 dimension (2D) or embedded in 3D collagen I gel systems and analyzed for cell signaling and behaviors, in comparison to heterozygous $KRS^{-/+}$ mice and clinical colon cancer tissues. Although KRS suppression decreased expression of cell-cell adhesion molecules, cells still formed colonies without being scattered, supporting an incomplete EMT. Meanwhile, KRS-suppressed cells still exhibited focal adhesions on laminin, with Tyr397-phopshorylated FAK, but they lacked laminin-adhesion-mediated ERK and paxillin activation. Time-lapse imaging revealed KRS-dependent cell dissemination (e.g., outbound movement) from the spheroids, whereas KRS-suppressed spheroids remained static due to the absence of efficient cell-ECM adhesion-mediated outbound crawling movements. KRS, p67LR, and integrin α6β1 were found to interact, presumably to activate ERK for paxillin expression and activation even without involvement of FAK, so that specific inhibition of ERK or KRS in parental HCT116 spheroids blocked dissemination. Furthermore, KRS-suppressed spheroids recovered the capacity for dissemination upon the re-introduction of ERK or paxillin. The KRS/ERK/paxillin signaling axis was also observed in marginal areas of colon cancer or *KRS*$^{-/+}$ mouse tissues. Collectively, these observations indicate that KRS can cause cancer cell dissemination via the regulation of cell-cell and cell-ECM adhesion during KRS-mediated metastasis.

Introduction

Cancer metastasis is a complex process involving multiple steps, such as dissemination from the primary tumor mass via EMT, migration, and invasion, that occur even before intravasation processes [1]. Dissemination from the primary tumor mass can lead to a journey of metastatic cancer cells towards distal settlements, and the disseminated cancer cells migrate and invade through the stroma to reach vessels or lymph nodes along the way [2]. In addition to strategies aimed at the regression of the primary tumor mass through chemoprevention and/or radiation, anti-metastatic strategies that block dissemination process, which is an early step of metastasis, would be clinically important for achieving a higher cure rate for cancer. Numerous signaling or adaptor molecules have been shown to play critical roles in facilitating cancer cells to metastasize. Of these molecules, we are interested in revealing the mechanisms underlying the roles of aminoacyl-tRNA synthetases in tumorigenesis and metastasis [3]. Cytosolic aminoacyl-tRNA synthetases are traditionally and importantly involved in protein translation. However, lysyl-tRNA synthetase (KRS) was recently shown to function in immune responses [4, 5] as well as in tumor metastasis [6, 7], clearly suggesting additional biological functions beyond protein translation. KRS is phosphorylated at the Thr52 residue by p38MAPK, which causes it to dissociate from the cytosolic multi-tRNA synthetase (MTS) complex and translocate to the plasma membrane, where it associates with and stabilizes a 67 kDa laminin receptor (p67LR) that is involved in migration and metastasis [6]. p67LR is known to associate with integrin α6β1 [8] or α6β4 [9], which have roles in cell adhesion to the ECM and tumor cell invasion [10]. The association of KRS with p67LR is sufficiently targeted to allow the inhibition of KRS-dependent metastasis in a subcutaneously cell-injected animal model, suggesting that KRS is a promising target for anti-cancer metastatic strategies [7].

Therefore, as part of our efforts to develop anti-metastatic therapeutics by targeting KRS-mediated cellular behaviors, we found that KRS might cause cell dissemination from spheroids embedded in an ECM-surrounded 3-dimensional (3D) environment. This system would be beneficial if the dissemination process observed in 3D gels could be mechanistically related to KRS-dependent dissemination in *in vivo*-like circumstances and could also generally be useful as a template screening system for anti-metastasis reagents. This study revealed that KRS appears to play regulatory roles in cell adhesion by activating ERK and paxillin during cancer cell dissemination from primary tumor masses.

Experimental procedures

1. Cells

HCT116 and SW620 colon cancer (American Type Culture Collection, Manassas, VA, USA) and other colon cancer (Korean Cell Bank, Seoul National University) cells were stably transfected with shRNA against KRS (transcript 1, NM_001130089, lysyl-tRNA synthetase MISSION® shRNA Plasmid DNA, Sigma) using Truefect (United Biosystems, Herndon, VA) before antibiotic selections. The target sequences of shKRS and the names of the KRS-suppressed cell clones are shown in table 1. HCT116 cells overexpressing KRS were established via the stable transfection of a myc-tagged KRS plasmid [6]. ERK1 and ERK2 (ERK clones) and paxillin (PXN clones) were also stably transfected, either separately or together (PEE clones for paxillin, ERK1, and ERK2), into KRS-suppressed cell clones. Stable myc-tagged KRS and different stable shKRS-transfected clones were established by using 250 μg/ml G418 or 0.50 μg/ml puromycin (AG Scientific, Inc., San Diego, CA). The cells were maintained in RPMI-1640 (WelGene, Daegu, Korea) containing 10% FBS and antibiotics (Invitrogen, Grand Island, NY, USA).

2. Spheroid formation and embedding into 3D collagen I gels

HCT116 or SW620 cells with modulated KRS expression levels, or other colon cancer cells were processed for spheroid formation using Perfecta3D® 96-well hanging-drop plates (3D Biomatrix, Ann Arbor, MI). Spheroids were selected to be less than 70 m in size using a cell strainer sieve (SPL Life Science Co., Pocheon-si, Korea) prior to being embedded into 3D collagen I gels (BD Biosciences, San Jose, CA, USA). For embedding, polydimethylsiloxane (PDMS) chambers with an 8-mm diameter, or 10 well-slips for 22 x 60

mm coverslips (model No.: WL-2260-10, Live Cell Instrument, Seoul, Korea), were filled with 30 μl collagen I (2.0 mg/ml, BD Biosciences) to coat the bottom surfaces of the chamber. PDMS (Sylgard 184, Dow Corning, Midland, MI) prepolymer was prepared using a 10:1 (w/w) mixture of PDMS base and curing agent, cast against the master and thermally cured to obtain a negative replica-molded piece. Spheroids were then mixed with ice-cold collagen I solutions (2.0 mg/ml), which were prepared by diluting a concentrated collagen I (BD Biosciences) stock with 10 × reconstitution buffer (260 mM sodium bicarbonate and 200 mM HEPES), and 10 × RPMI-1640 with phenol red [11]. The pH was adjusted in the range of 7.2 to 7.4 using ice-cold 2 N NaOH. The mixture was transferred to a 37ºC CO_2 incubator to allow the collagen I to polymerize and form a fibrillar meshwork. The 3D culture was then refreshed each day with standard culture media containing 10 % FBS.

3. Extract preparation and Western blots

Colon cancer cells within collagen I gels were washed with ice-cold PBS and then homogenized with truncated pipette tips (3 times × 20 min on ice) in modified RIPA buffer (50 mM Tris-HCl, 150 mM NaCl, 1% NP-40, and 0.25% sodium deoxycholate) with a protease inhibitor cocktail (GenDepot, Barker, TX). The extracts were centrifuged for 30 min at 15,000 *g* and 4°C, and then the lysates were collected from the supernatant. The protein amounts were normalized with the band intensities for -tubulin or -actin via standard Western blots, before further immunoblotting with different antibodies. The primary antibodies used in the study were as follows: α-tubulin, α-SMA, talin, pY^{822}vinculin, and vimentin (Sigma, St Louis, MO); pY^{416}c-Src, ERKs, phospho-ERKs, FLAG, pS^{473}Akt, pS^{425}talin, caspase 3, Tensin 2, and Akt (Cell Signaling Technol. Danvers, MA); paxillin, N-cadherin, and FAK (BD Biosciences); pY^{397}FAK, p67LR, laminin, vinculin, and Twist1 (Abcam, Cambridge, UK); c-Src, pY^{118}paxillin, pY^{577}FAK, pY^{861}FAK, pY^{925}FAK, Snail1, E-cadherin, β-catenin, and Slug

(Santa Cruz Biotech., Santa Cruz, CA); ZO1 (Zymed Laboratories, Camarillo); pY^{483}Tensin 2 (Biorbyt, San Francisco, CA); vinculin, integrin α6, β1, and β4 (Millipore, Billerica, MA); fibronectin (DAKO, Carpinteria, CA); and KRS (Atlas Antibodies, Stockholm, Sweden).

4. Normal 2D culture or replating on 2D ECM layer

Cells were kept in suspension or replated on ECM (10 μg/ml, laminin or fibronectin, BD Biosciences)-precoated dishes or coverglasses in the absence (in the case of fibronectin) or presence of low serum (2%, in the case of laminin) for 1 h before being analyzed for cell-ECM adhesion signaling by standard Western blotting or for the formation of focal adhesions by indirect immunofluorescence, as described previously [12]. Function blocking antibodies against human integrin α6 (Millipore, 20 μg/ml) were preincubated with cells by rocking at 37ºC for 1 h prior to replating. Pharmacological inhibitors were added to the culture media for 24 h or to replating media at the reseeding time. Cells were reseeded on coverglasses precoated with standard media containing 10% FBS, before imaging to monitor cell growth patterns or immunofluorescence to detect the formation of cell-cell contacts. Confluent cells were wounded with a pipette tip and washed twice with PBS. After treatment with DMSO, U0126 (10 μM, LC Labs., Woburn, MA), or YH16899 (10 μM) and incubation in a CO_2 incubator for 24 h, the marginal edges of the wounds were imaged (CKX41, Olympus, Japan).

5. Time-lapse FRET analysis for ERK activity

HCT116 cells were cultured on a laminin-coated (5 μg/ml) 35-mm glass-base dish and were transfected with FRET-based indicators [13] using the lipofectamine 2000 transfection reagent (Life Technologies, Grand Island, NY), according to the manufacturer's instructions. FRET images were obtained on a Nikon Ti-E inverted microscope (Nikon, Tokyo, Japan) equipped with PFS, a CoolSNAP HQ camera (Roper Scientific, Trenton, NJ), and excitation

and emission filter wheels. Images were acquired by using the 4×4 binning mode and 200-ms exposure time. All systems were controlled by MetaMorph software (Molecular Devices, Sunnyvale, CA). For dual-emission ratio imaging of the intramolecular FRET probe, we obtained images for CFP and FRET. After background subtraction, pseudo-colored images of FRET/CFP were created using eight colors from red to blue to represent the FRET/CFP ratio via the intensity modulated display (IMD) mode using MetaMorph software. Filters used for the dual-emission ratio imaging were purchased from Semrock (Rochester, NY): an FF01-438/24-25 excitation filter, an FF458-Di02-25×36 dichroic mirror, and two emission filters, FF01-483/32-25 for CFP and FF01-542/27-25 for FRET.

6. Time-lapse imaging of cells in 3D ECM gels

Parental or stable cells were transfected with mCherry-MT1-MMP for 24 h before spheroid formation. Three hours after spheroids were embedded in 3D collagen I gels, time-lapse images were collected for the indicated periods using IX81-ZDC microscope (Olympus, Tokyo, Japan). The microscope was equipped with a 10-well Chamlide Incubator system (Live Cell Instrument, Seoul, Korea), and an environmental chamber mounted on the microscope maintained constant conditions of 37°C, 5% CO_2, and 95% humidity. Pharmacological inhibitors such as U0126 (50 μM) or YH16899 [50 μM, [7]] were mixed during the process of embedding the cells into 3D collagen I gels.

7. Coimmunoprecipitations

Whole-cell extracts prepared from cells in standard media containing 10% FBS or from cells kept in suspension or reseeded onto laminin (10 μg/ml) in media containing 2% FBS for 2 h were immunoprecipitated overnight using anti-myc tag antibody-coated agarose beads (Sigma). The immunoprecipitated proteins were boiled in 2 × SDS-PAGE sample buffer before

standard Western blot analysis.

8. Indirect immunofluorescence

Cells reseeded on 2D normal culture media- or ECM-precoated glass coverslips or embedded in 3D collagen I gels within PDMS were immunostained using antibodies against E-cadherin, snail1, pERK, K14, or paxillin in addition to DAPI staining for the nucleus. Immunofluorescence images were acquired on a fluorescence microscope (BX51TR, Olympus, Tokyo, Japan) or a confocal laser scanning microscope with a Nikon Plan-Apochromat 60×/1.4 N.A. oil objective (Nikon eclipse Ti microscope, Nikon, Tokyo, Japan), and then analyzed using the IMARIS imaging software (Bitplane AG, Zurich, Switzerland).

9. Chromatin immunoprecipitation (ChIP)

ChIP assays were performed using the ChIP-IT Express kit (Active Motif, Carlsbad, CA), following the manufacturer's protocols. Briefly, cells embedded in collagen I gels for 24 h were fixed for 30 min with 2% formaldehyde, and the chromatin was then prepared by sonication shearing to aid nuclear release and enzymatic shearing. The sheared chromatin was immunoprecipitated using c-Jun (Cell Signaling) or Elk-1 (Santa Cruz Biotech.,) antibodies and captured with protein G magnetic beads. The chromatin was eluted from the purified immunoprecipitates, reversed cross-linked, and digested with proteinase K. The reaction was then stopped using proteinase K stop solution. The isolated chromatin was analyzed by 36 cycles of PCR. Ten microliters of each PCR product was separated via 2% agarose electrophoresis and visualized by ethidium bromide staining.

10. Generation of KRS heterozygote mouse

For the generation of KRS heterozygote animals, KRS genetrap ES cells (AJ0130) were purchased from the MMRRC and used to generate a chimeric mouse at the UCSD

transgenic mouse core facility. The disruption of the gene via the insertion of the genetrap cassette into intron 13 was confirmed by genomic PCR using primers flanking the breakpoint (forward: 5'- TGG GTT TCA TCC TGA GGT CT - 3'; reverse: 5'- GCT TTC TTT CCC AGG TCC TC - 3'; genetrap reverse: 5'-TGT CCT CCA GTC TCC TCC AC - 3'). No viable homozygous pups were born, nor were any viable embryos observed (up to embryonic day 9.5). We confirmed the reduction of KRS expression levels in the heterozygote in multiple organs (Fig. S9). No gross phenotypic differences, including size, weight and movement behavior, were observed between wild-type and KRS heterozygote mice (data not shown). MMTV-PyVT transgenic mice were purchased from The Jackson Laboratory.

11. Measurement of metastasis in the MMTV-PyVT transgenic mice

MMTV-PyVT mice were crossed to KRS heterozygotes to generate the MMTV-PyVT; $KRS^{+/+}$ and MMTV-PyVT; $KARS^{+/GT}$ mice. Female mice were sacrificed at 16 and 18 weeks. After the lungs were dissected out and fixed, each lobule was carefully examined under the microscope to count the total number of metastatic nodules. A white round bump of over 100 μm on the lung surface was counted as a nodule.

12. Analyses of murine or human tissues

All procedures for animal and human tissues were performed in accordance with the procedures of the Seoul National University Laboratory Animal Maintenance Manual and Institutional Review Board (IRB) agreement approved by the Institute of Laboratory Animal Resources Seoul National University (ILARSNU) and SNUIRB, respectively. Human colon tissues were obtained with informed content from patients who received surgery at Samsung Medical Center (Sungkyunkwan University School of Medicine, Seoul, Korea) or National Biobank of Korea-Pusan National University Hospital (PNUH) in accordance with IRB agreements. Whole-tissue extracts were prepared with modified RIPA buffer [12] using a

Bullet Blender BBX24 surrounded by dry ice and containing 1.0 mm zirconium silicate beads (Next Advance, Inc. Averill Park, NY), prior to standard Western blots for the indicated molecules.

13. Immunohistochemistry

Dissected breast tumors were fixed and stored in 10% NBF. The tissues were processed, paraffin embedded, and sectioned at 6-μm thickness. After deparaffinization, antigen retrieval was performed by boiling the sections for 5 min in sodium citrate solution (0.01 M, pH 6). The sections were incubated he at 4ºC with the indicated antibodies in PBST (0.3% Triton X-100 in PBS) containing 5% goat serum or 3% BSA. After washing, the sections were incubated with biotin-conjugated anti-rabbit, mouse or goat IgG (1:100, Sigma) antibody and ExtrAvidin-peroxidase (1:50, Sigma) at RT for 1 h each for 3,3′-diaminobenzidine detection. The sections were counterstained with hematoxylin and imaged under the microscope. Immunohistochemistry of serial sections of paired normal or tumor colon tissues was performed using normal rabbit IgG, normal mouse IgG, phospho-ERKs (Cell Signaling), KRS (Atlas Antibodies), and paxillin (BD Biosciences).

14. RT-PCR

Total RNA was extracted from cells in 2D normal 10% FBS-containing condition or ECM-precoated culture dishes with low (2%) serum-containing conditions, or in 3D collagen I gels, using TRIzol (Invitrogen) according to the manufacturer's protocol. One microgram of total RNA was reverse transcribed using the amfiRivert Platinum cDNA Synthesis master mix (GenDepot). Primers were designed using Primer3 software as follows: human *E-cadherin* (*CDH1*) mRNA, forward 5'-TGCCCAGAAAATGAAAAAGG-3' and reverse 5'-GTGTATGTGGCAATGCGTTC-3'; human *N-cadherin* (*CDH2*) mRNA, forward 5'-ACAGTGGCCACCTACAAAGG-3' and reverse 5'-CCGAGATGGGGTTGATAATG-3';

human *Vimentin* (*VIM*) mRNA, forward 5'-GAGAACTTTGCCGTTGAAGC-3' and reverse 5'-GCTTCCTGTAGGTGGCAATC-3'; human *Twist* (*TWIST*) mRNA, forward 5'-GGAGTCCGCAGTCTTACGAG-3' and reverse 5'-TCTGGAGGACCTGGTAGAGG-3'; human *paxillin (PXN)* mRNA, forward 5'-GAAATCAGCTGAGCCTTCAC-3' and reverse 5'-TTAGGCTTCTCTTTCGTCAGG-3', *Snail1*, forward 5'-GGTTCTTCTGCGCTACTGCT-3' and reverse 5'-TAGGGCTGCTGGAAGGTAAA-3'; *slug*, forward 5'-GGGGAGAAGCCTTTTTCTTG-3' and reverse 5'-TCCTCATGTTTGTGCAGGAG-3; human *KRS* (*KARS*) mRNA, forward 5'- CAATGCCCATGCCCCAGCCA-3' and reverse 5'-ACCCCACCCTTCCGGCGAAT-3', and human *β-actin* (*ACTB*) mRNA, forward 5'-TGACGGGGTCACCCACACTGTGCCCATCTA-3' and reverse 5'-CTAGAAGCATTTGCGGTGGACGACGGAGGG-3'.

15. Statistical methods

Student's *t*-test was performed for statistical comparisons of mean values to determine significance. A p value less than 0.05 was considered statistically significant.

Results

Incomplete EMT phenotype upon KRS suppression

To explore the roles of KRS in metastatic dissemination, HCT116 colon cancer cells with endogenous, suppressed, or overexpressed KRS levels were analyzed for EMT phenotypes. Using an RT-PCR approach, we found that KRS suppression decreased *E-cadherin* mRNA (an epithelial marker) but increased the mRNAs of mesenchymal markers (Fig. 1.1A). Furthermore, these KRS suppression-dependent changes in EMT markers also carried over to protein levels; epithelial markers including E-cadherin were expressed at higher levels in KRS-expressing parental and KRS-overexpressing HCT116 cells, whereas KRS-suppressed cell clones decreased epithelial marker expression and concomitantly enhanced the expression of mesenchymal markers (Fig. 1.1B). The increased levels of mesenchymal marker proteins after the suppression of KRS to certain levels, without caspase 3 activation, supported additional roles for KRS other than protein translation. Meanwhile, KRS-suppressed cell clones did not show altered expression of laminin and p67-laminin receptor (p67LR), which are important for KRS-mediated tumorigenic roles [3], or integrin chains α6, β1, or β4 compared with KRS-expressing cells (Fig. 1.1B). E-cadherin and β-catenin were not clearly observed in cell-cell junctions when KRS was suppressed, as compared with KRS-expressing cells (Fig. 1.1C). Therefore, the inverse relationship between KRS and epithelial marker expression may suggest the induction of EMT phenotypes. However, cell-cell contacts were not disrupted after KRS suppression (Figs. 1.1C and D), suggesting that KRS suppression caused an incomplete EMT.

KRS-dependent cell-laminin adhesion

We then examined the relationship between KRS expression and cell-ECM adhesion

properties. First, cells with various KRS expression levels were adhered under normal 10% FBS-containing culture conditions and examined for adhesion-related signaling activities. Under normal 10% serum-containing 2D culture conditions, KRS suppression abolished the signaling activities of FAK, ERK, c-Src, and paxillin (Fig. 1.2A) compared with KRS-expressing (or overexpressing) cells. Cell adhesion-related signaling activities were then analyzed after the cells were kept in suspension or reseeded onto ECM-precoated culture dishes. Because KRS has been shown to translocate to the plasma membrane in a laminin-dependent manner [6] and because KRS suppression did not change laminin expression (Fig. 1B), we explored the biological significance of KRS expression after reseeding onto laminin under reduced (2%) serum-containing conditions. The adhesion-dependent phosphorylation of FAK was not abolished by KRS suppression, nor was it affected by treatment with a KRS inhibitor [YH16899, which blocks the interaction between KRS and p67LR [7]], when compared with KRS-expressing cells (Fig. 2B, lanes 2, 5, 7, and 9). However, the phosphorylation of ERK, paxillin, and c-Src in KRS-expressing cells increased upon adhesion to laminin and was abolished by additional YH16899 treatment, whereas no effect was observed in KRS-suppressed cells (Fig. 1.2B). KRS-dependent FAK activity in 2D 10% serum-containing normal condition appeared not to be the case when HCT116 cells were manipulated to be newly adhered on laminin under a lower serum condition. When the cells were treated with the addition of soluble laminin to the culture media, paxillin expression and ERK phosphorylation were lower in KRS-suppressed cells than in KRS-expressing cells. We next examined the subcellular localization of phospho-ERK or phospho-Tyr118 paxillin in cells with various KRS expression levels. When the cells were reseeded onto laminin-precoated coverglasses in 2% serum-containing media, KRS-positive (but not KRS-suppressed) cells showed obvious phospho-ERK staining in the nucleus (Fig. 1.2C). Phospho-Tyr118 paxillin was also clearly localized to focal adhesions in a KRS-dependent manner (Fig. 1.2D).

Interestingly, replating cells on laminin for a shorter (2 h) or a longer (24 h) period showed phospho-Tyr397 FAK independent of KRS expression, although ERKs phosphorylation and paxillin expression and phosphorylation depended on KRS expression (Figs. 1.2E), suggesting that FAK activity upon laminin stimulation in 2D condition might not be relevant for KRS expression. Given that KRS suppression induced fibronectin (Fig. 1.1B), we also examined how the cells would respond to fibronectin simulation. Reseeding KRS-suppressed cells onto fibronectin-precoated dishes did not result in any significant difference in Tyr397-phosphorylated FAK, compared with KRS-expressing cells, although ERK phosphorylation depended on KRS expression. Meanwhile, wounds were made in confluent cells in normal 10% FBS-containing 2D conditions, and KRS-expressing parental cells exhibited clear outbound movement at the wound boundary, whereas KRS-suppressed cells did not (Fig. 1.2F). These KRS-dependent differential movements toward free spaces might be intrinsically correlated with non-effective cell-ECM adhesion for crawling out.

KRS-dependent dissemination of HCT116 spheroids in 3D collagen I gels

Because KRS-expressing (but not KRS-suppressed) cells efficiently moved toward free spaces during wound healing, we wondered whether KRS could be important for cell dissemination from the tumor masses. In particular, we explored the significance of KRS expression in cell dissemination by time-lapse monitoring of HCT116 spheroids (with various KRS expression levels) embedded into 3D collagen I gels. Hanging drops of HCT116 cell clones with various KRS expression levels efficiently formed spheroids. When spheroids with diameters between 70 and 100 μm were sieved and embedded into collagen I (2.0 mg/ml) gels, the KRS-expressing cells exhibited outbound movement or dissemination of single or as well as small groups of cells (Fig. 1.3A, top and bottom panels). However, KRS-suppressed cell clones did not show any such dissemination even when monitored for 28 h (Fig. 1.3A, middle

panels). Because imaging commenced 3 h after embedding, signaling activities were also examined at 3 or 24 h after separate embedding into collagen I gels. Consistent with the laminin-adherent 2D condition, c-Src, ERK, and paxillin (but not FAK) activity were similarly dependent on KRS expression, decreasing with time after embedding, although only phospho-Tyr118 paxillin increased as time passed after the embedding (Fig. 1.3B). Decreases in ERK and paxillin signaling activities upon KRS suppression were also observed in another colon cancer cell line, SW620, in 3D collagen gels (Fig. 1.3C). SW620 cells also showed dissemination from spheroids in a KRS expression-dependent manner. Furthermore, KRS-suppressed cells showed increased mesenchymal markers and decreased epithelial markers 24 h after embedding (Fig. 1.3D), although they did not disseminate (Fig. 1.3A). The lack of dissemination from spheroids by KRS-suppressed cells in 3D collagen I gels might be related to an incomplete EMT. Consistent with the absence of outbound movements and lack of scattering in 2D conditions (Fig. 1.1), no dissemination from or cell scattering of spheroids in 3D collagen I gels was observed, although the cells showed reduced E-cadherin at cell-cell contacts (Fig. 1.3E). When one epithelial marker (cytokeratin 14, K14) was immunostained in the spheroids in 3D collagen I gels, KRS-expressing parental or KRS-overexpressing cells were positive for K14 staining in cells at the dissemination margins, whereas KRS-suppressed or U0126- or YH16899-treated parental cells were negative for K14 (Fig. 1.3F), suggesting a role for K14 in dissemination. Furthermore, ERK phosphorylation and paxillin expression in KRS-expressing parental HCT116 spheroids in 3D collagen I gels were also decreased by KRS-suppression (Figs. 1.3G and H). Meanwhile, KRS suppression did not alter other focal adhesion molecules such as vinculin, talin, and tensin 2 expression and talin phosphorylation levels but decreased vinculin and tensin 2 phosphorylations (Fig. 1.3I), suggesting specific effects on paxillin expression and FA molecule phosphorylations via KRS suppression. These observations indicate that KRS-mediated dissemination appears to involve cell-cell adhesion

properties, as well as cell-ECM adhesion signaling for ERK activity and paxillin expression/activity-mediated phosphorylations of FA molecules.

KRS/p67LR/integrin a6β1 linkage correlates for ERKs activation

Because KRS-suppression decreased ERK phosphorylation, we attempted to measure the *in situ* ERK activity using an ERK biosensor. On laminin-precoated coverglasses in 2% serum-containing media, KRS-expressing parental or KRS WT-overexpressing cells showed greater FRET signals, indicating highly active ERK with activity oscillations, compared to KRS-suppressed cells, which showed gradual declines (Figs. 1.4A). This KRS-dependent ERK activation was consistent with the observation that ERK phosphorylation was increased by KRS overexpression (Fig. 1.2A). Comparising of the mean FRET signal intensities showed that ERK activity clearly depended on KRS expression (Fig. 1.4B). Interestingly, transient transfection of ERK1 or 2 into KRS-suppressed cells resulted in somewhat increased paxillin expression and Tyr118 phosphorylation, but not FAK Tyr397 phosphorylation, in addition to dramatically increased phospho-ERK levels (Fig. 1.4C). This observation suggests the presence of a link between pERK and paxillin expression/phosphorylation in KRS-expressing cells. Given that KRS expression led to ERK phosphorylation, we examined how ERK could be activated through KRS. KRS can translocate to the plasma membrane after Thr52-phosphorylation-dependent disassociation from cytosolic MSC and associate and collaborate with p67LR in the presence of laminin [6]. Different HCT116 cell clones with various KRS expression levels did not show altered laminin, p67LR, or integrin α6, β1, and β4 expression levels (Fig. 1.1B). Integrin α6β1 and α6β4 are responsive to laminin and are known to bind p67LR [8, 9]. Furthermore, integrins are well-known to activate ERK for different cell functions in many cell and tissue systems [14]. Therefore, to determine whether the interaction between KRS, p67LR, and integrin α6β1 could be correlated to ERK activation, we examined

possible physical interactions between these proteins via coimmunoprecipitation. Myc-KRS prepared from normal 10% FBS-containing culture conditions co-precipitated with integrin α6 and p67LR, and this interaction was reduced by anti-KRS inhibitor (YH16899) treatment (Fig. 1.4D). To further analyze the significance of laminin stimulation for this association, myc-KRS immunoprecipitates were prepared from cells kept in suspension or reseeded onto laminin-precoated dishes in culture media containing 2% FBS. Whereas p67LR was shown to bind to KRS in lysates from suspended cells, KRS binding to integrin α6 and β1 was observed to be adhesion-dependent, and was disrupted by additional treatment with YH16899 (Fig. 1.4E). Those molecules including KRS, laminin, p67LR, and integrin α6 were positively correlated around the invasive marginal area of breast tumor tissues from the PyVT mouse model (Fig.1. 4F). We then examined how ERK activity could be related to paxillin levels. First, we found that c-Jun expression and Ser63 phosphorylation, but not Elk-1, p38, or JNKs expression and phosphorylation, were correlated with KRS expression (Fig. 14G). In addition, the suppression of Elk-1, an ERK-mediated transcription factor, did not down-regulate paxillin expression and Tyr118 phosphorylation (Fig. 1.4H). Thus, we speculated that c-Jun might be involved in ERKs activity-mediated paxillin expression in a KRS-dependent manner. We therefore examined whether ERK activity could be linked to paxillin transcription via c-Jun by chromatin immunoprecipitation approaches. Promoter regions that bind c-Jun (Region 1 with two putative binding sites at -380 or -460 base pairs upstream of the starting point +1, and nonbinding control Region 2) or Elk-1 (putative binding sites at CG-enriched -10 base pair and -498 base pair for Region 3 and nonbinding control Region 4) following ERK activation were identified (Fig. 1.4I). Chromatin immunoprecipitated with anti-c-Jun, but not normal IgG, showed a PCR product for the *PXN* promoter region, which was abolished in KRS-suppressed or YH16899-treated HCT116 cells (Fig. 1.4J). Meanwhile, Chromatin immunoprecipitated with anti-Elk-1 did not show any amplified PCR product (Fig. 1.4K), indicating that ERK activated in KRS-

expressing cells may transcriptionally induce paxillin via c-Jun rather than Elk-1. In addition to HCT116 cells, other colon cancer cells showed decreases in ERK and paxillin activities and paxillin expression upon YH16899 treatment (Fig. 1.4L), suggesting that this signaling axis depends on the compound to regulate the interaction between KRS, p67LR, and integrin α6β1. Furthermore, in the PyVT breast tumor mouse model, staining of the invasive marginal area showed a positive relationship for these signaling molecules (Fig. 4M). Therefore, the interaction between KRS and integrin α6β1 via p67LR may be correlated with KRS expression-mediated ERK activity and paxillin expression/activity during dissemination from cell masses.

KRS-dependent cell dissemination require ERKs and paxillin phosphorylations

We then explored whether KRS-dependent ERK activation was important for dissemination. KRS-expressing parental HCT116 spheroids exhibited the dissemination of single cells or cell groups, and this was not observed when the spheroids were embedded in the presence of a MEK inhibitor (U0126, leading to ERK inhibition) or YH16899 [to block the interaction between KRS and p67LR, as shown in Figs. 4D and 4E and in a previous study [7], Supplementary movie 14], although outbound processes or spikes still formed (Figs. 1.5A). Treating SW620 cells with U1026 or YH16899 also blocked dissemination. Furthermore, the L142A KRS mutant, which does not interact with p67LR [6], caused decreased ERK activity and paxillin expression and Tyr118 phosphorylation and did not cause dissemination, much like KRS suppression. In addition, whereas EGF treatment of KRS-expressing parental or KRS-overexpressing cells showed more dramatic dissemination, KRS-suppression-inhibited dissemination was not recovered by exogenous EGF treatment, indicating that growth factor-mediated ERKs activation might not be sufficient for dissemination under KRS-suppressed conditions. Being consistent, EGF treatment-mediated ERK and Elk-1 (but not c-Jun) activities

could not be linked to paxillin induction in KRS-suppressed cells. Therefore, these observations suggested that the complex formed by KRS, p67LR, and integrin α6β1 upon cell-laminin adhesion might also be important for ERKs activation for dissemination. Treating KRS-expressing cells with either U0126 or YH16899 decreased both *paxillin* and *E-cadherin* mRNA levels (Fig. 1.5B). Each inhibitor decreased ERK phosphorylation, and paxillin expression and phosphorylation without activating caspase 3 and resulted in the loss of epithelial markers (Figs. 1.5C and D). These inhibitor-mediated effects were very similar to the effects of KRS suppression (Figs. 1.1B, 1.3C, and 1.3D). Meanwhile, YH16899 treatment of KRS-expressing cells did not result in changes in focal adhesions containing Tyr397-phosphorylated FAK or in cellular morphology (Fig. 1.5E) but decreased phospho-ERK (Fig. 1.5F) and phospho-Tyr118 paxillin under 2D laminin-precoated conditions (Fig. 1.5G) or phospho-ERK in 3D collagen I gels (Fig. 1.5H). YH16899 or U0126 treatment decreased paxillin protein levels in KRS-suppressed cells in 3D collagen I gels (Fig. 1.5I). Interestingly, U1026 or YH16899 treatment also decreased the K14 epithelial protein that was localized along the outbound dissemination (Fig. 1.5J). Furthermore, it was tested whether the lack of dissemination in KRS-suppressed cells might be attributed to no protease activity in these cells. MT1-MMP-transfection in KRS-suppressed cells did not cause dissemination, although MT1-MMP transfected cells were disseminated from parental HCT116 spheroids (Fig. 1.5K, upper panels). However, the treatment of U0126 and YH16899 blocked the dissemination of parental cells even after MT1-MMP transfection (Fig. 1.5K, lower panels). Thus, the lack of dissemination in KRS-suppressed cells might be irrelevant to MMP-based proteolytic activity. These observations therefore suggest that the KRS-dependent dissemination of HCT116 spheroids in 3D collagen I gels may be regulated by ERK and paxillin expression and activity.

KRS-suppression-inhibited dissemination is recovered by ERK1 and/or paxillin expression

We explored whether ERK activity in KRS-expressing cells depended on FAK. Because KRS-dependent ERK activity appeared to occur via the formation of a signaling complex between KRS, p67LR, and integrin α6β1, we examined whether and how functionally blocking of integrin α6 affected the phosphorylation of FAK and ERK. When HCT116 parental cells were preincubated with neutralizing anti-human integrin α6 antibodies, ERK activity that was dependent on cell adhesion to laminin for 24 h decreased, as did paxillin expression and Tyr118 phosphorylation, but not FAK phosphorylation (Fig. 1.6A). To examine whether FAK was important for dissemination, we examined the correlation between FAK activity, ERK activity, and paxillin expression and activity downstream of KRS. First, the expression of kinase-dead (R454) FAK in KRS-expressing cells decreased FAK phosphorylation, but not ERK activity, paxillin expression or Tyr118 phosphorylation (Fig. 1.6B, lanes 1 and 2). In addition, the expression of active FAK [N-terminal deleted FAK [15]] or wild-type FAK in KRS-suppressed cells increased FAK phosphorylation, but did not alter ERK activity or paxillin expression and Tyr118 phosphorylation (Fig. 1.6B, lanes 3 to 8). The lack of a link between FAK and ERK/paxillin activity and expression downstream of KRS was also observed for the dissemination of cells from spheroids in 3D collagen I gels; although R454 FAK expression in KRS-expressing cells did not significantly block dissemination, expressing active FAK in KRS-suppressed cells also did not cause dissemination (Fig. 1.6C). In addition, L37A mutant FAK, which is shown to be active [15], was stably transfected into KRS-suppressed cells. The expression of L37A FAK did not cause ERK activation, paxillin expression or Tyr118 phosphorylation or dissemination (Fig. 1.6C). These experiments suggested that KRS-dependent dissemination might involve FAK-independent ERK activation. Because KRS-dependent cell dissemination was inhibited by ERK inhibition and because pERK might induce

paxillin expression, we examined whether the inefficient dissemination of KRS-suppressed cells in 3D collagen I gels could be recovered by the overexpression of ERK1 alone, paxillin alone, or both together. Stable transfection of ERK1 resulted in ERK activation, and a slight induction of paxillin expression and Tyr118 phosphorylation (Fig. 1.6D), as shown also in Fig. 4C. In addition, stable transfection of paxillin alone or together with ERK1 resulted in moderately increased Tyr118 phosphorylation in paxillin (Fig. 1.6D). The stable transfection of ERK1 alone, paxillin alone, or both together caused the KRS-suppressed cell clones to undergo dissemination from the spheroids (Fig. 1.6E). Therefore, the blockade of dissemination in KRS-suppressed cells may be due to decreased ERK and paxillin activity in these cells.

KRS appear to play pro-metastatic roles at the invasive margins of KRS-/+ mouse breast tumor and human colon tumor tissues

Next we explored the roles of KRS in lung metastasis of breast tumors using KRS-heterozygous MMTV-PyVT mice. To generate the *KRS* genetrap mouse, a genetrap cassette was inserted into intron 13 to disrupt KRS gene expression. A comparison of KRS immunoblots in various organs from wild-type and heterozygous mice demonstrated the overall reduction of KRS. When breast tumor sections in PyVT mice were stained with hematoxylin-eosin or immunostained for KRS, the compact core region of the tumor section showed very weak KRS-staining, whereas marginal regions with highly complex lumen structures showed strong KRS-staining (n = 4, Fig. 1.7A). KRS-heterozygous PyVT mice showed a lower incidence of metastasis than KRS wild-type mice, as determined by counting metastatic lung nodules in the PyVT mice (TG) with the indicated *krs* genotype at 16 or 18 weeks of age (Fig. 1.7B). Therefore, this $KRS^{-/+}$ mouse model suggested that KRS might play important roles at the invasive margins of tumor masses. We then examined the correlation between KRS, pERK,

and paxillin in clinical colon cancer tissues. Compared with normal colon tissues from colon cancer patients, tumor tissues showed higher KRS and paxillin expression (7/7, Fig. 1.7C), suggesting a positive correlation between KRS and paxillin, which support the KRS-mediated metastatic dissemination phenotypes as well as the positive staining of invasive margins in $KRS^{-/+}$ mouse tumor models. Interestingly, pERK was not easily detected to access the correlation with KRS or paxillin expression in either normal or tumor colon tissue extracts (Fig. 1.7C), presumably because the extracts were from mixed populations of different cell types around the tumor lesions. Furthermore, an online database (i.e., Oncomine, www.oncomine.org) showed a positive correlation between the significant overexpression of KRS and paxillin in colon carcinoma samples (Fig. 1.7D). Therefore, we examined the molecular correlation in serial sections of normal and tumor colon tissues. Tumor tissues identified as grade II or III clearly showed marginal and local staining for pERK, whereas KRS and paxillin were observed not only in local areas but also in massive core areas (Fig. 1.7E). These observations indicated that KRS might mediate ERK and paxillin activation around invasive margins during an early metastatic step.

Fig. 1

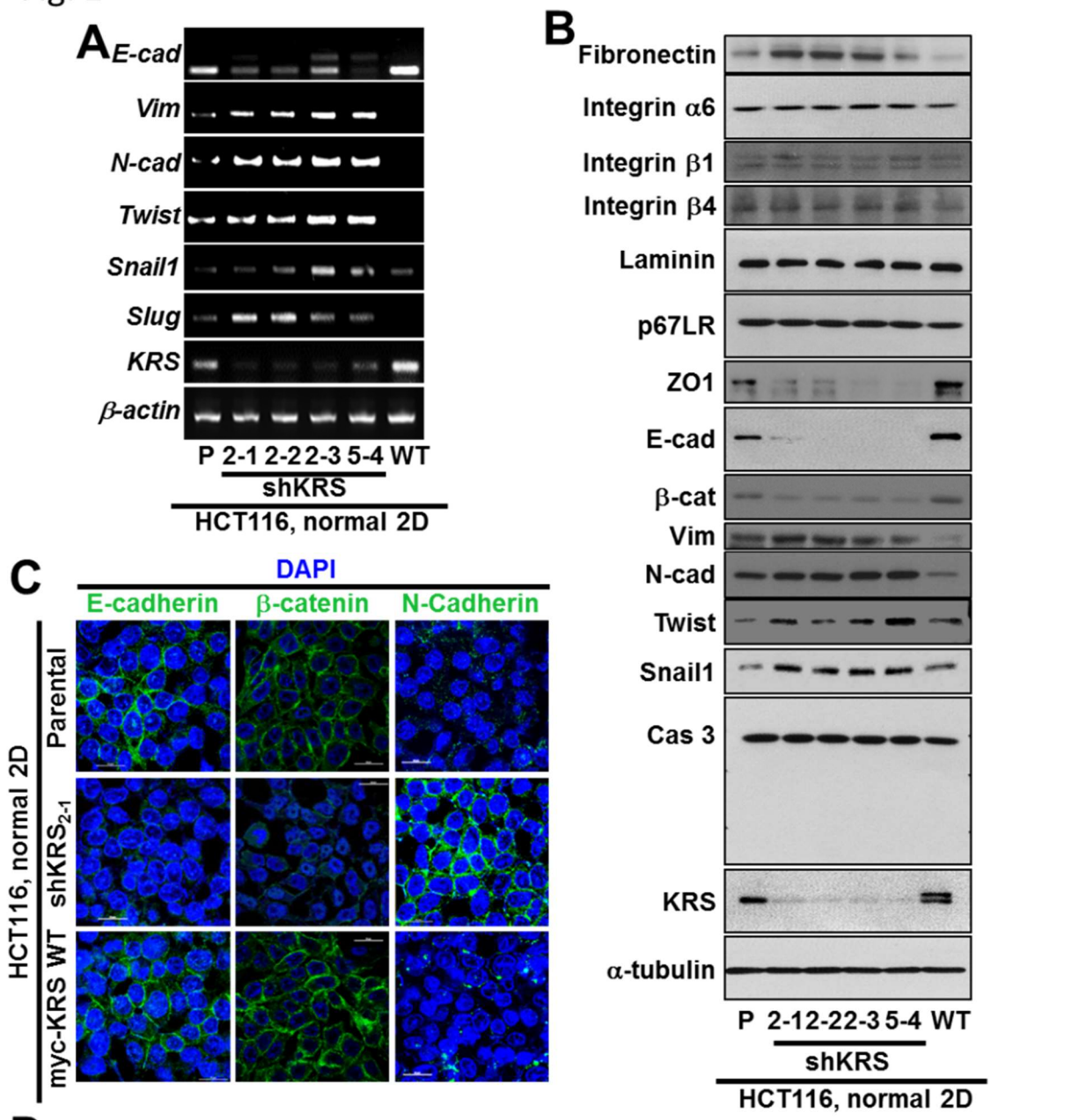
A
E-cad
Vim
N-cad
Twist
Snail1
Slug
KRS
β-actin
P 2-1 2-2 2-3 5-4 WT
shKRS
HCT116, normal 2D
B
Fibronectin
Integrin α6
Integrin β1
Integrin β4
Laminin
p67LR
ZO1
E-cad
β-cat
Vim
N-cad
Twist
Snail1
Cas 3
KRS
α-tubulin
P 2-1 2-2 2-3 5-4 WT
shKRS
HCT116, normal 2D
C
DAPI
E-cadherin
β-catenin
N-Cadherin
HCT116, normal 2D
Parental
shKRS2-1
myc-KRS WT
D
Parental
Myc-KRS WT
HCT116, normal 2D
KRS-pos
shKRS2-1
shKRS5-4
KRS-neg
E
HCT116, normal 2D
Parental
shKRS2-1
Myc-KRS WT
F-actin/DAPI

Fig. 1.1. KRS-dependent incomplete EMT phenotypes in normal 2D conditions.

(A and B) RT-PCR **(A)** or standard Western blots **(B)** for the indicated epithelial or mesenchymal markers from KRS-expressing parental HCT116 (P), stably myc-KRS wildtype-overexpressing HCT116 (KRS WT), and stably KRS-suppressed HCT116 cell clones (2-1, 2-2, 2-3, and 5-4 for shKRS) normally cultured 1n 2D 10% FBS-containing condition. **(C)** Cells were cultured on coverglasses precoated with 10% FBS-containing culture media until confluence and then immunostained for E-cadherin or β-catenin along with DAPI costaining. **(D)** Subconfluent cells from the normal 2D condition were imaged using a phase contrast microscope. Data shown represent at least three independent experiments.

Fig. 2

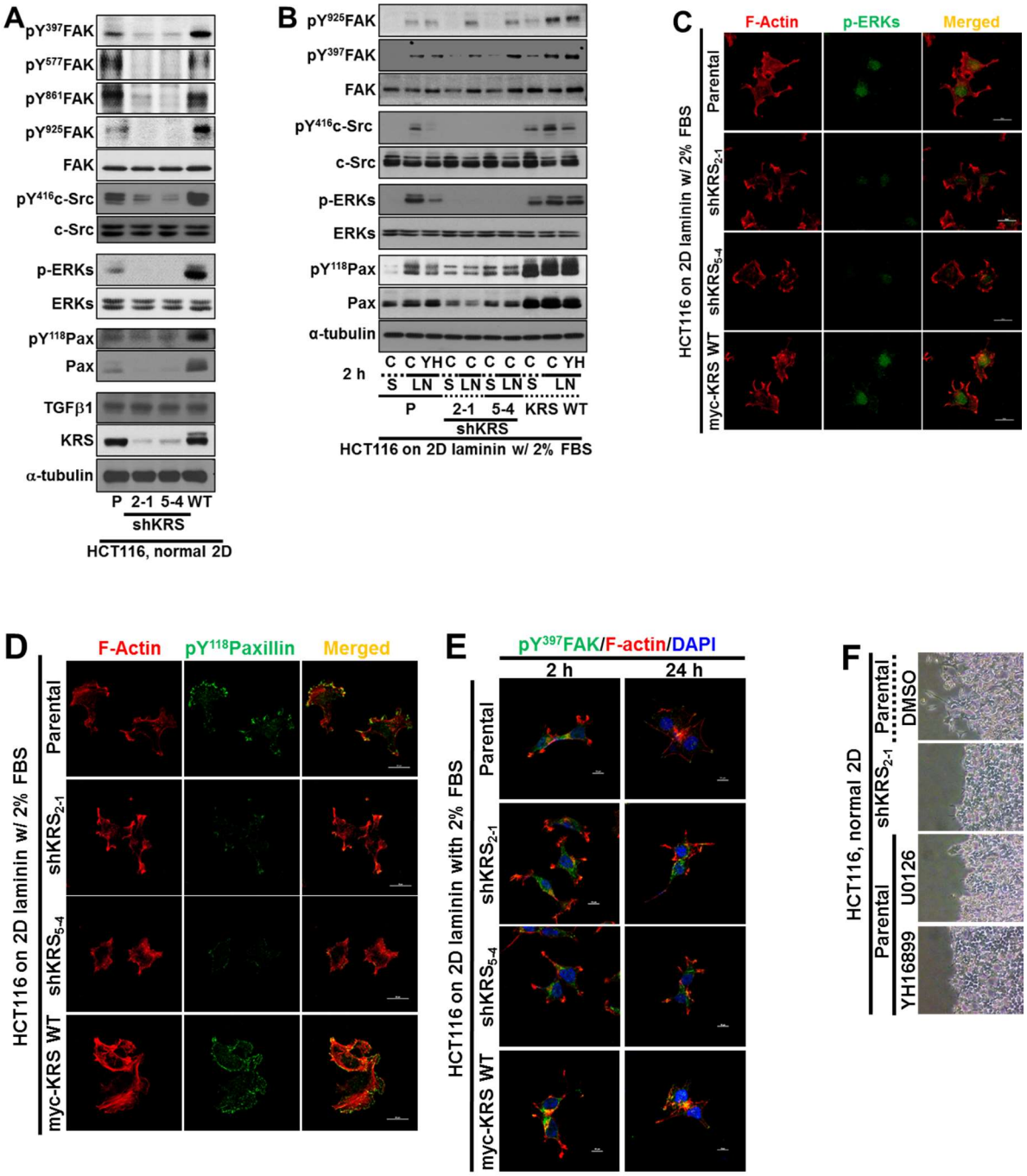
A
pY397FAK
pY577FAK
pY861FAK
pY925FAK
FAK
pY416c-Src
c-Src
p-ERKs
ERKs
pY118Pax
Pax
TGFβ1
KRS
α-tubulin
P 2-1 5-4 WT
shKRS
HCT116, normal 2D
B
pY925FAK
pY397FAK
FAK
pY416c-Src
c-Src
p-ERKs
ERKs
pY118Pax
Pax
α-tubulin
2 h
C C YH C C C C C YH
S LN S LN S LN S LN
P 2-1 5-4 KRS WT
shKRS
HCT116 on 2D laminin w/ 2% FBS
C
F-Actin
p-ERKs
Merged
HCT116 on 2D laminin w/ 2% FBS
Parental
shKRS2-1
shKRS5-4
myc-KRS WT
D
F-Actin
pY118Paxillin
Merged
HCT116 on 2D laminin w/ 2% FBS
Parental
shKRS2-1
shKRS5-4
myc-KRS WT
E
pY397FAK/F-actin/DAPI
2 h
24 h
HCT116 on 2D laminin with 2% FBS
Parental
shKRS2-1
shKRS5-4
myc-KRS WT
F
HCT116, normal 2D
Parental
shKRS2-1
DMSO
Parental
U0126
YH16899

Fig. 1.2. KRS suppression impair cell-ECM adhesion and signaling activities.

(A) HCT116 cells with various KRS expression levels [parental P, KRS-suppressed 2-1 and 5-4 clones, and myc-KRS WT overexpressed (WT) cells] were analyzed for the indicated molecules via standard Western blots. KRS-suppressed cells in normal 2D conditions showed decreased FAK, ERKs (A), c-Src, and paxillin phosphorylation, compared with KRS-expressing cells. **(B to D)** Cells were kept in suspension (S) or reseeded onto laminin (Ln) -precoated dishes or coverglasses with DMSO (C) or YH16899 (YH) treatment for 2 h, prior to harvesting for standard Western blots for the indicated molecules (B) or immunostaining for pERK (C) or Tyr118-phsophorylated paxillin (D) together with phalloidin staining for F-actin. **(E)** Cells were replated onto laminin-precoated culture dishes containing reduced (2%) FBS (to make cells healthy while minimizing effects from serum components) for 2 or 24 h, prior to immunostaining using anti-Tyr397-phosphorylated FAK (green), phalloidin (red), and DAPI (blue) staining. **(F)** Confluent cells grown under normal 2D conditions were wounded, washed, and treated with either DMSO or the indicated inhibitor. Fifteen hours later, cells near the wound edges were imaged. Data shown represent three independent experiments.

Fig. 3

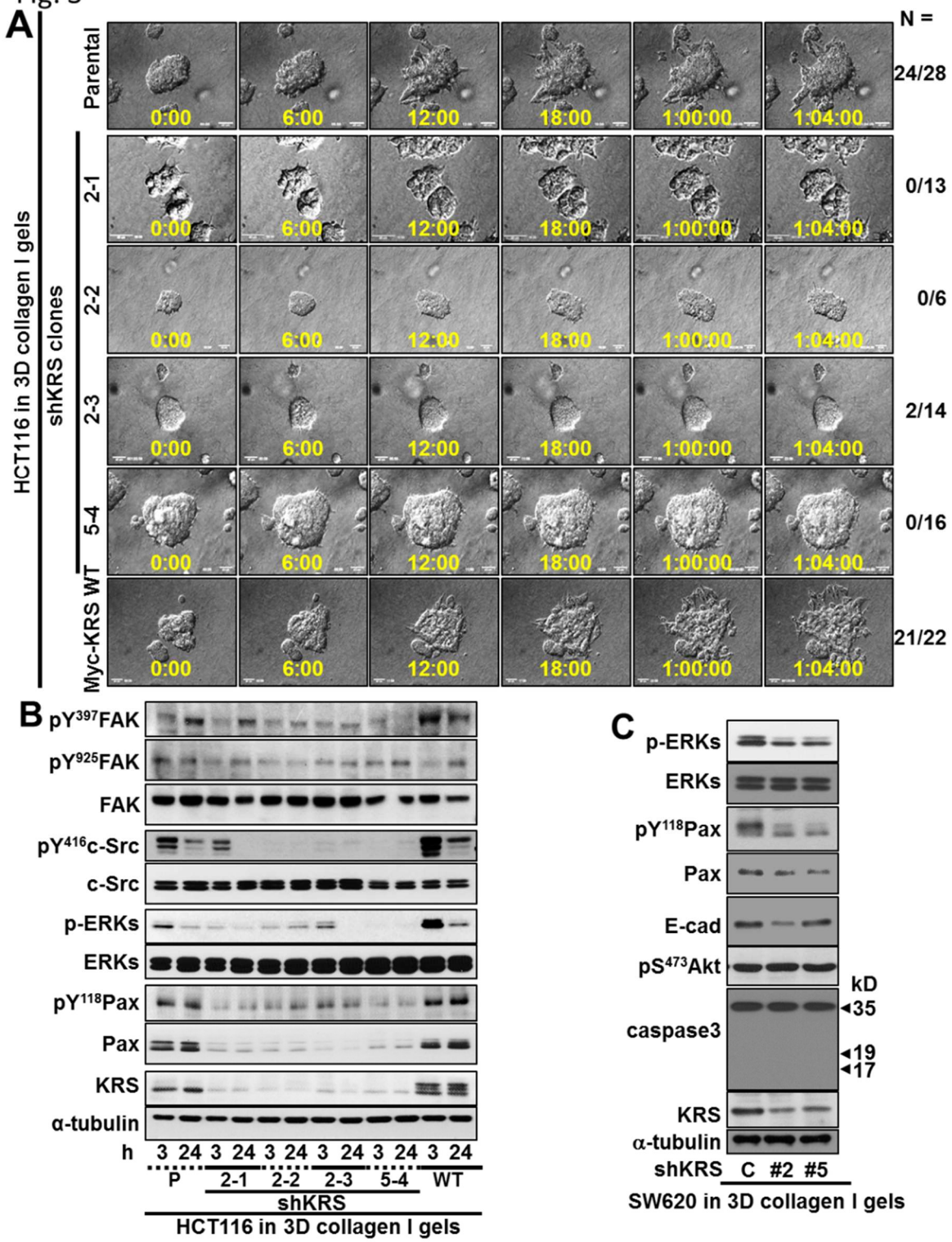
A
HCT116 in 3D collagen I gels
shKRS clones
Parental
2-1
2-2
2-3
5-4
Myc-KRS WT
N =
24/28
0/13
0/6
2/14
0/16
21/22
0:00
6:00
12:00
18:00
1:00:00
1:04:00
B
pY397FAK
pY925FAK
FAK
pY416c-Src
c-Src
p-ERKs
ERKs
pY118Pax
Pax
KRS
α-tubulin
h
3 24 3 24 3 24 3 24 3 24 3 24
P
2-1
2-2
2-3
5-4
WT
shKRS
HCT116 in 3D collagen I gels
C
p-ERKs
ERKs
pY118Pax
Pax
E-cad
pS473Akt
caspase3
KRS
α-tubulin
kD
35
19
17
shKRS
C
#2
#5
SW620 in 3D collagen I gels

Fig. 3-continued

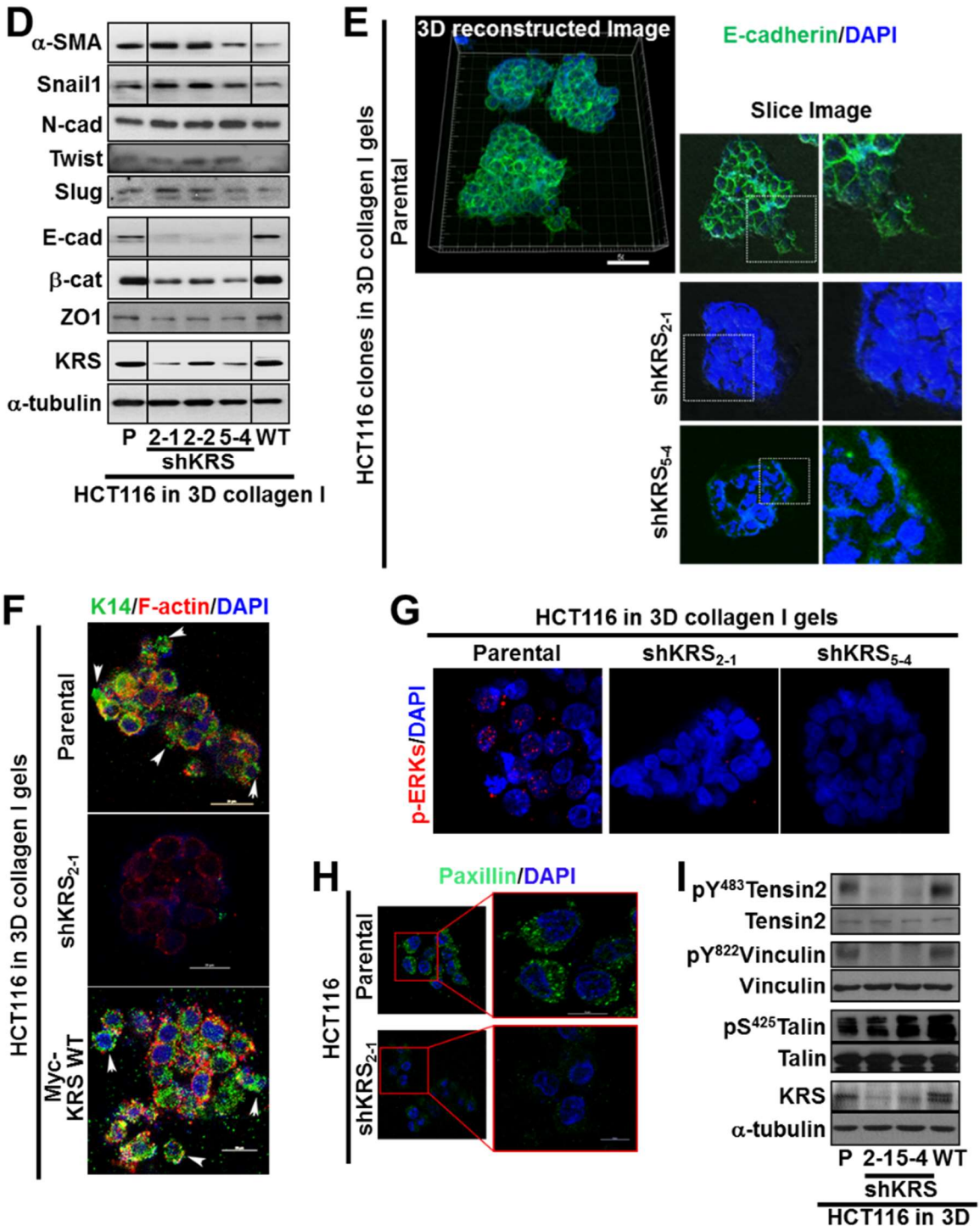

Fig. 1.3. Impaired adhesion-related signaling in KRS-suppressed cells correlates to a lack of dissemination from spheroids in 3D collagen I gels.

(A) Spheroids of HCT116 colon cancer cells (parental, stable shKRS-transfectant clones of 2-1, 2-2, 2-3, and 5-4, and stably myc-KRS WT overexpressing cells) embedded in 3D collagen I gels were imaged by time-lapse microscopy for 28 h. Note that KRS-expressing parental and myc-KRS WT cells showed dissemination of single cell or small groups of cells from the spheroids. **(B to D)** HCT116 (B and D) or SW620 (C) cells embedded in 3D collagen I gels for 3 (B) or 24 h (B, C, and D) were harvested for whole-cell extracts prior to performing standard Western blots for the indicated molecules. **(E)** Spheroids of HCT116 parental cells (*left*) or HCT116 shKRS cells (2-1 clone, *middle*), and HCT116-KRSWT (*right*) cells embedded in 3D collagen I gels for 24 h were double-stained with DAPI (blue) and anti-E-cadherin (green) antibody. Note that spheroids in the 3D environment retained their shapes without dispersion. **(F)** Cells were embedded in 3D collagen I gels for 24 h before fixation, permeabilization, and immunostaining for K14 (green) in parallel with phalloidin (red) and DAPI (blue) staining. Arrow heads depict cells presumably disseminating with K14 expression. **(G and H)** Cell spheroids embedded in 3D collagen I gels for 24 h were immunostained for pERK (G, red) or paxillin (H, green), with DAPI (blue) costaining. **(I)** Cells were embedded in 3D collagen I gels for 24 h were harvested and processed for standard Western blots for the molecules. Data represent three independent experiments.

Fig. 4

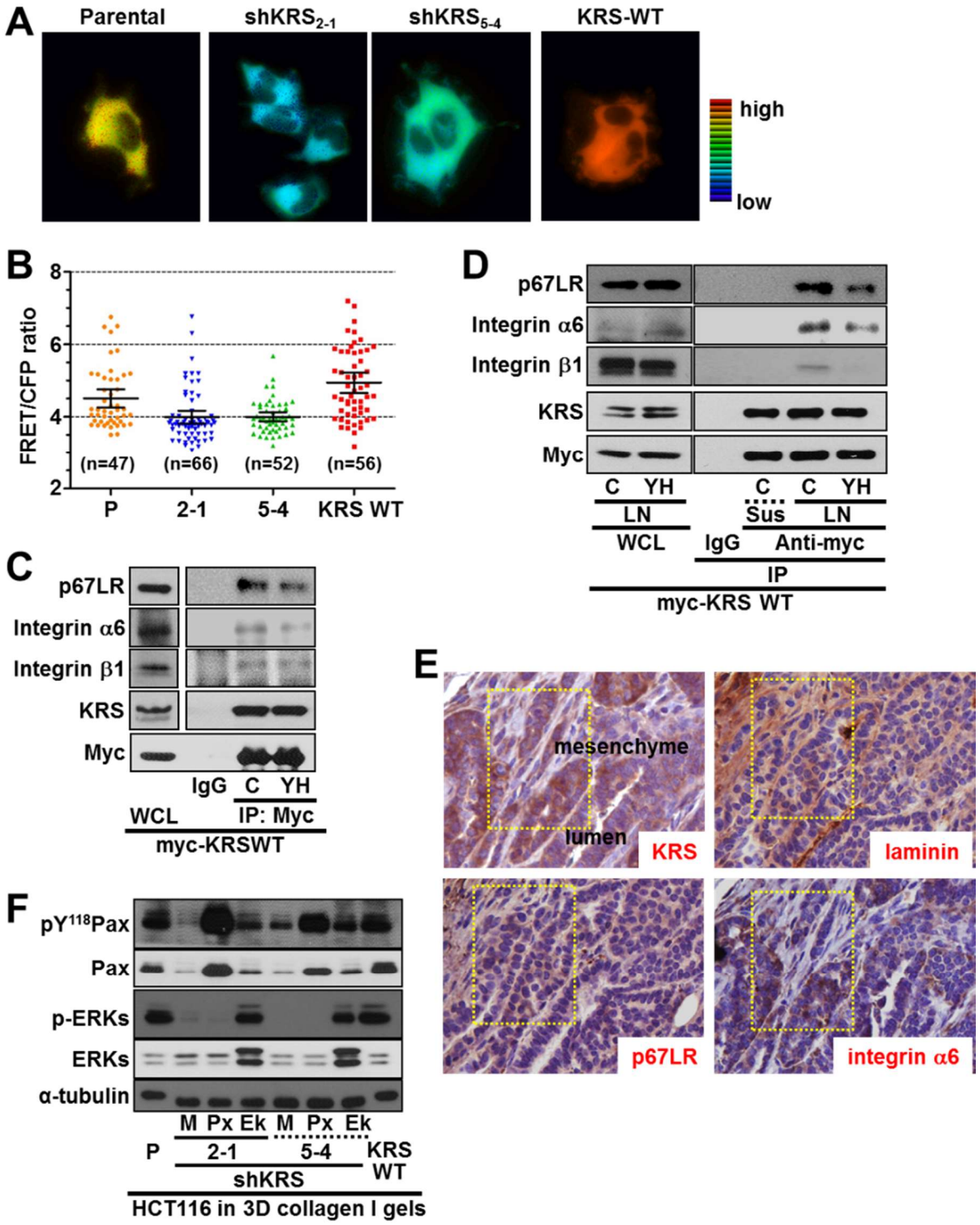
A
Parental
shKRS2-1
shKRS5-4
KRS-WT
high
low
B
FRET/CFP ratio
8
6
4
2
(n=47)
(n=66)
(n=52)
(n=56)
P
2-1
5-4
KRS WT
C
p67LR
Integrin α6
Integrin β1
KRS
Myc
IgG
C
YH
WCL
IP: Myc
myc-KRSWT
D
p67LR
Integrin α6
Integrin β1
KRS
Myc
C
YH
C
C
YH
LN
Sus
LN
WCL
IgG
Anti-myc
IP
myc-KRS WT
E
mesenchyme
lumen
KRS
laminin
p67LR
integrin α6
F
pY118Pax
Pax
p-ERKs
ERKs
α-tubulin
M Px Ek M Px Ek
P
2-1
5-4
KRS WT
shKRS
HCT116 in 3D collagen I gels

Fig. 4-Continued

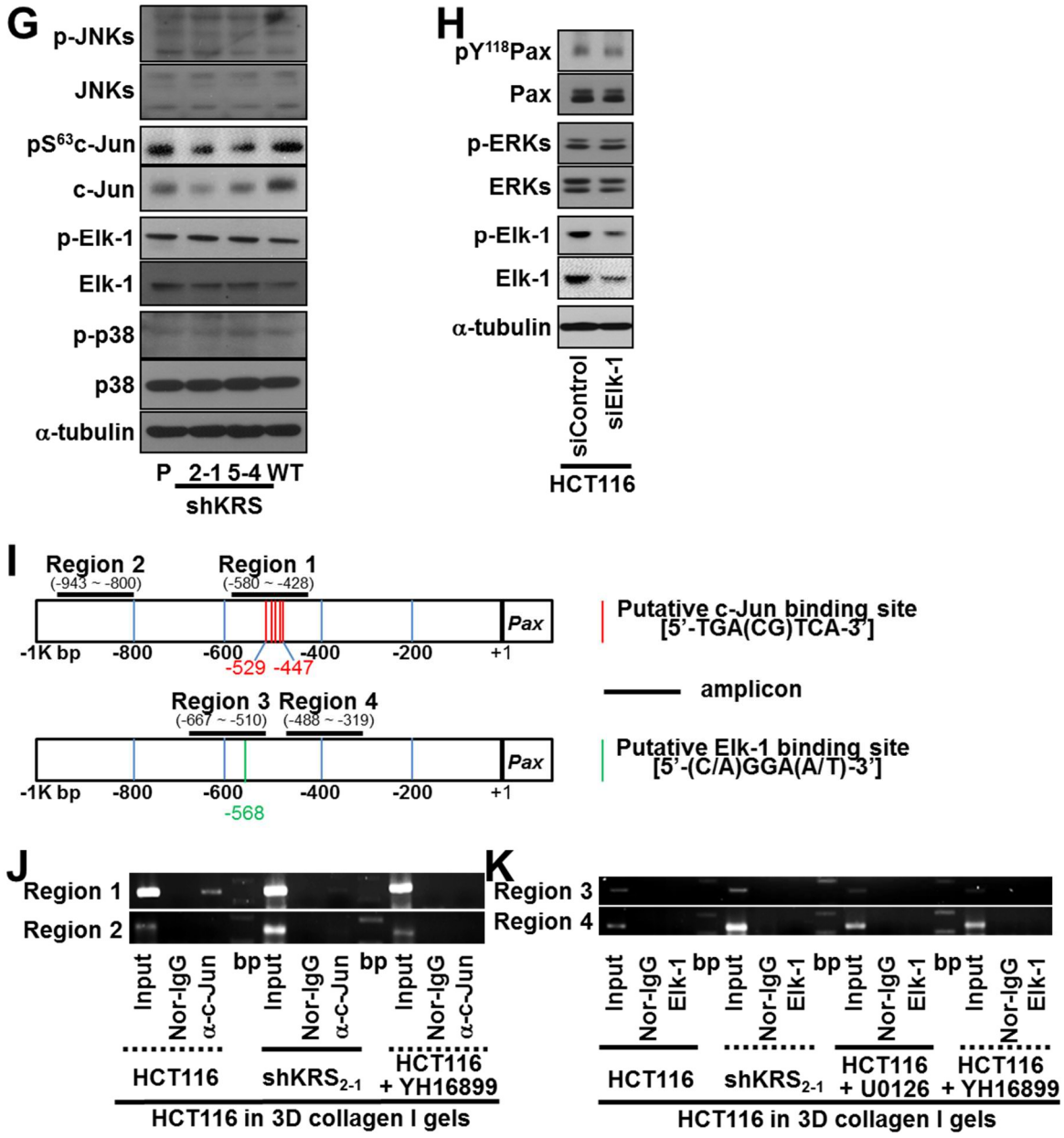

Fig. 4-Continued

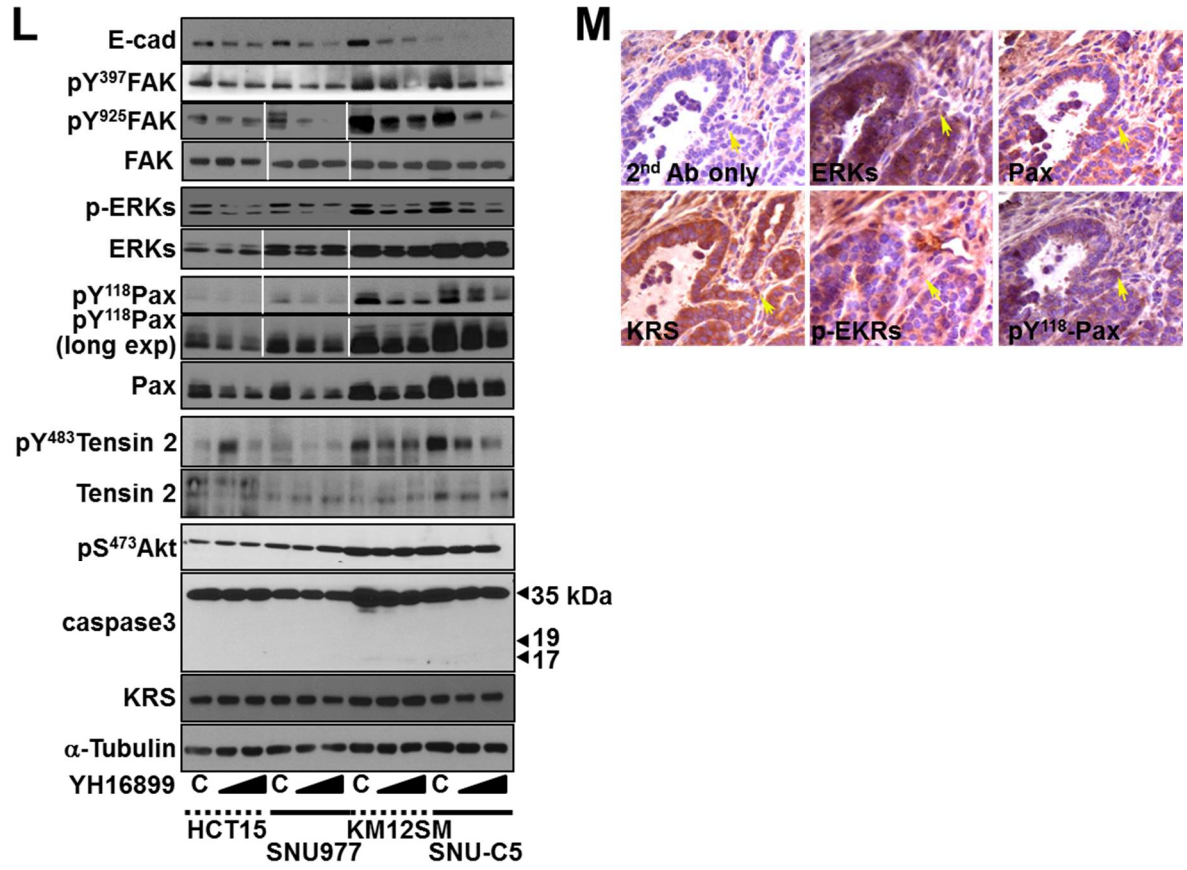

Fig. 1.4. KRS-mediated ERK activation correlates with the formation of a p67LR/integrin α6β1 complex.

(A) Cells reseeded onto laminin-precoated cover glasses for 24 h were processed for ERK activity analysis using an ERK1 FRET biosensor. **(B)** The mean fluorescence intensities of each cell from separate cell images (n= separately imaged cell numbers) were measured using the MetaMorph software and presented as a graph of the mean ± standard deviation (SD) of the FRET value/CFP ratio. **(C)** In addition to KRS-expressing parental (P) and KRS WT-overexpressing cells, KRS-suppressed cells were transiently transfected with mock (M),

paxillin (Px), or ERK1/2 (Ek) expression vectors for 24 h, and then their spheroids were embedded into 3D collagen I gels for another 24 h, before harvesting and standard Western blotting for the indicated molecules. **(D and E)** Myc-KRS WT cells grown in normal 2D conditions (D), kept in suspension (S), or reseeded onto laminin (Ln)-precoated dishes in the presence of DMSO (C) or YH16899 (YH) treatment were harvested for whole cell lysates (WCL) prior to immunoprecipitation using normal IgG (IgG) or anti-myc antibody and standard Western blotting for the indicated molecules. **(F)** Serially-sectioned breast tumor tissues from PyVT mice were stained for the indicated molecules and visualized at ×200 magnification. Black-dotted boxes depict the marginal area invasive to mesenchyme. **(G and H)** Subconfluent cells (G) or cells transiently transfected with siRNA against a control sequence (siControl) or Elk-1 (siElk-1) (H) were harvested for whole-cell lysates and normalized and processed for standard Western blots for the indicated molecules. **(I)** Schematic representation of the promoter regions of the human *paxillin* gene with putative c-Jun or Elk-1 binding sites and the PCR amplification region of the chromatin immunoprecipitates. **(J and K)** Chromatin immunoprecipitated from cells using normal IgG or anti-c-Jun (H) or anti-Elk-1 (I) antibodies without or with U0126 or YH16899 treatment were processed for PCR using primers for the *PXN* promoter regions (5 putative c-Jun binding sites within Region 1, a putative binding site in Region 3 for Elk-1) or control regions without binding sites (Region 2 for c-Jun, Region 4 for Elk-1). Bp depicts the DNA ladders. **(L)** Subconfluent colon cancer cells were treated with DMSO (C) or YH16899 (increasing doses at 50 and 100 μM) for 24 h, prior to harvesting of whole-cell lysates and immunoblotting for the indicated molecules. **(M)** Immunohistochemistry of PyVT breast tumor tissues with invasive marginal area (boxed) for the indicated molecules. Data represent three independent experiments.

Fig. 5

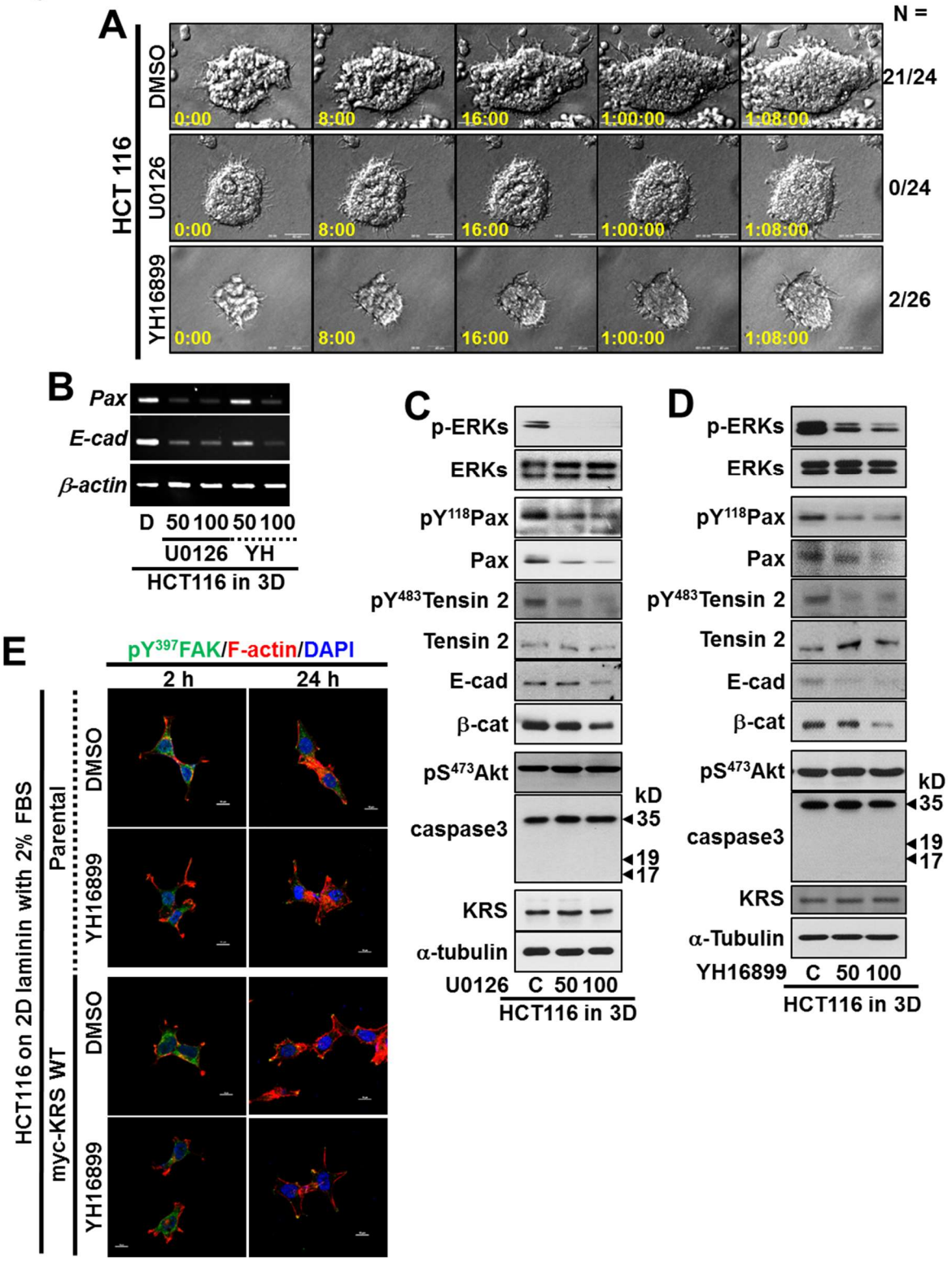
A
HCT 116
DMSO
U0126
YH16899
N =
21/24
0/24
2/26
0:00
8:00
16:00
1:00:00
1:08:00
B
Pax
E-cad
β-actin
D 50 100 50 100
U0126 YH
HCT116 in 3D
C
p-ERKs
ERKs
pY118Pax
Pax
pY483Tensin 2
Tensin 2
E-cad
β-cat
pS473Akt
caspase3
KRS
α-tubulin
kD
35
19
17
U0126 C 50 100
HCT116 in 3D
D
p-ERKs
ERKs
pY118Pax
Pax
pY483Tensin 2
Tensin 2
E-cad
β-cat
pS473Akt
caspase3
KRS
α-Tubulin
kD
35
19
17
YH16899 C 50 100
HCT116 in 3D
E
pY397FAK/F-actin/DAPI
2 h
24 h
HCT116 on 2D laminin with 2% FBS
Parental
myc-KRS WT
DMSO
YH16899
DMSO
YH16899

Fig. 5-continued

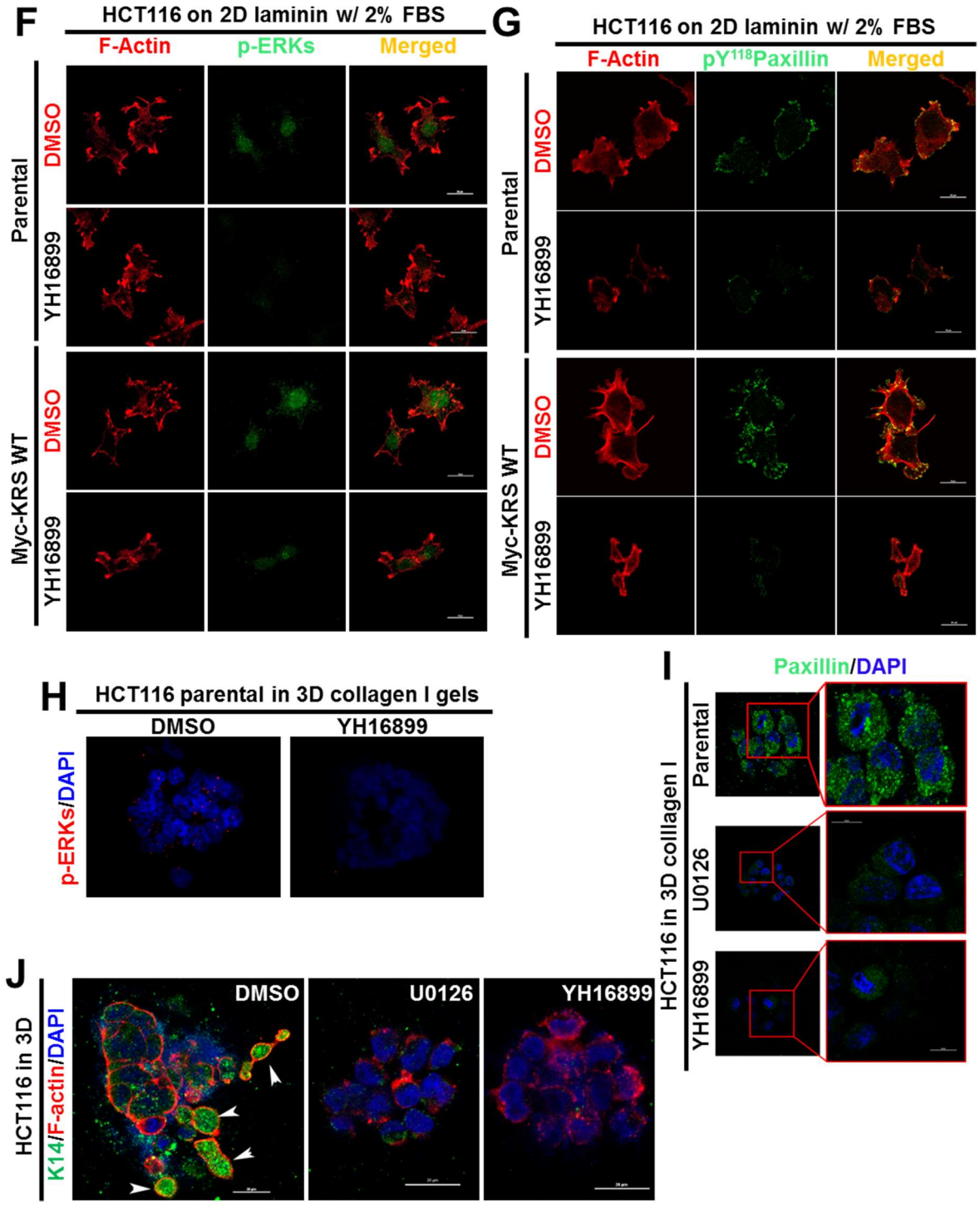

Fig. 5-continued

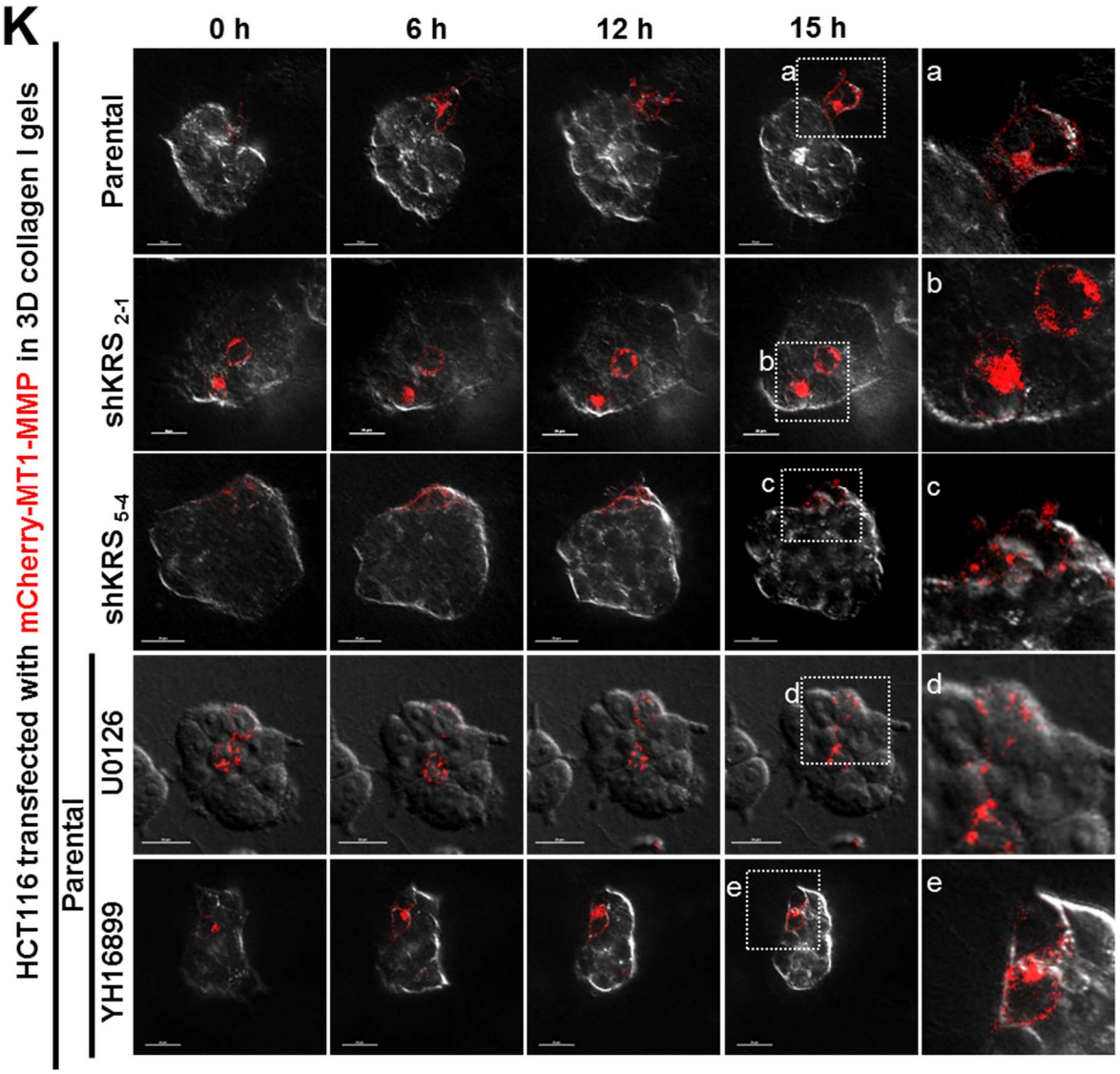

Fig. 1.5. KRS-dependent cell dissemination from spheroids in 3-D collagen I gels is blocked by anti-MEK/ERK U0126 or anti-KRS YH16899 treatment.

(A) Spheroids of HCT116 parental cells embedded in 3D collagen I gels in the presence of the ERK inhibitor U0126 (50 μM) or the KRS inhibitor YH16899 (50 μM) were imaged by time-lapse microscopy after embedding for 32 h. **(B to D)** HCT116 parental spheroids in 3D collagen I gels were treated with U0126 (50 or 100 μM) or YH16899 (50 or 100 μM) for 24 h, and the cells were then processed for RT-PCR for the indicated molecules (B) or harvested for standard Western blots, using antibodies against the indicated molecules (C and D). **(E and G)** Cells were reseeded onto laminin-precoated coverglasses for 2 h in the presence of YH16899 (50 μM) treatment before immunostaining for Tyr397 FAK-phosphorylated FAK (E, green), pERK (F, green), or Tyr118-phosphorylated paxillin (G, green) with phalloidin for F-actin (red) and DAPI for DNA (blue) costaining. **(H)** HCT116 parental spheroids in 3D collagen I gels were immunostained for pERK (red) with DAPI (blue) costaining. **(I and J)** Spheroids embedded in 3D collagen I gels for 24 h in the presence of DMSO (vehicle control), U0126, or YH16899 were immunostained for paxillin together with DAPI staining (I) or the epithelial marker K14 (green, J) together with F-actin (red) and DAPI staining (I). Right panels are enlarged from the red boxes in the corresponding left panels (I). Arrow heads depict cells presumably disseminating with K14 expression (J). **(K)** Cells transiently transfected with mCherry-conjugated MT1-MMP (red) plasmid were embedded into 3D collagen I for 3 h and then live-imaged for dissemination in the absence or presence of U0126 or YH16899 treatment. Data represent three independent experiments.

Fig. 6

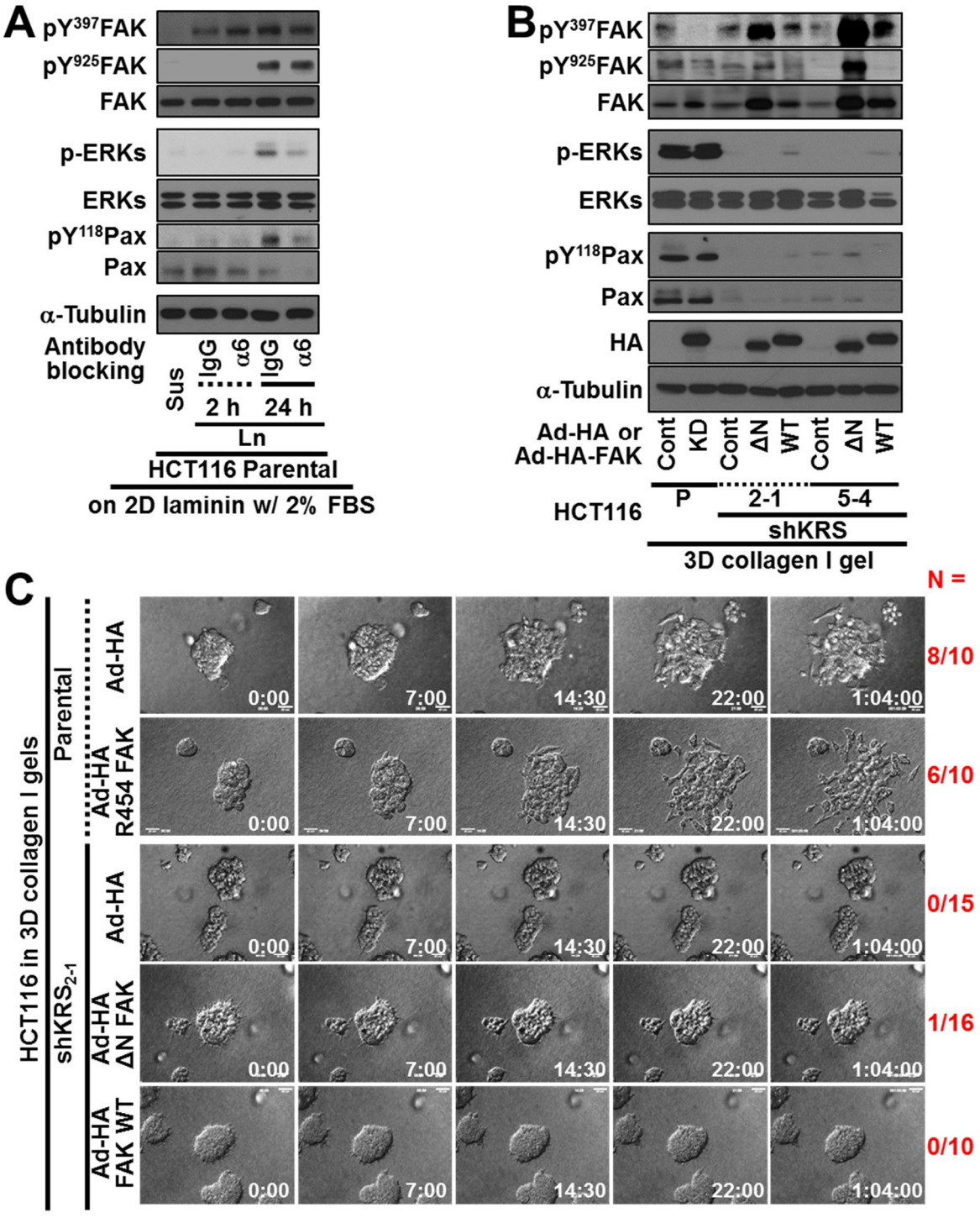
A
pY397FAK
pY925FAK
FAK
p-ERKs
ERKs
pY118Pax
Pax
α-Tubulin
Antibody blocking
Sus
IgG
α6
IgG
α6
2 h
24 h
Ln
HCT116 Parental
on 2D laminin w/ 2% FBS
B
pY397FAK
pY925FAK
FAK
p-ERKs
ERKs
pY118Pax
Pax
HA
α-Tubulin
Ad-HA or Ad-HA-FAK
Cont
KD
Cont
ΔN
WT
Cont
ΔN
WT
HCT116
P
2-1
5-4
shKRS
3D collagen I gel
C
HCT116 in 3D collagen I gels
Parental
shKRS2-1
Ad-HA
Ad-HA R454 FAK
Ad-HA
Ad-HA ΔN FAK
Ad-HA FAK WT
0:00
7:00
14:30
22:00
1:04:00
N =
8/10
6/10
0/15
1/16
0/10

Fig. 6-continued

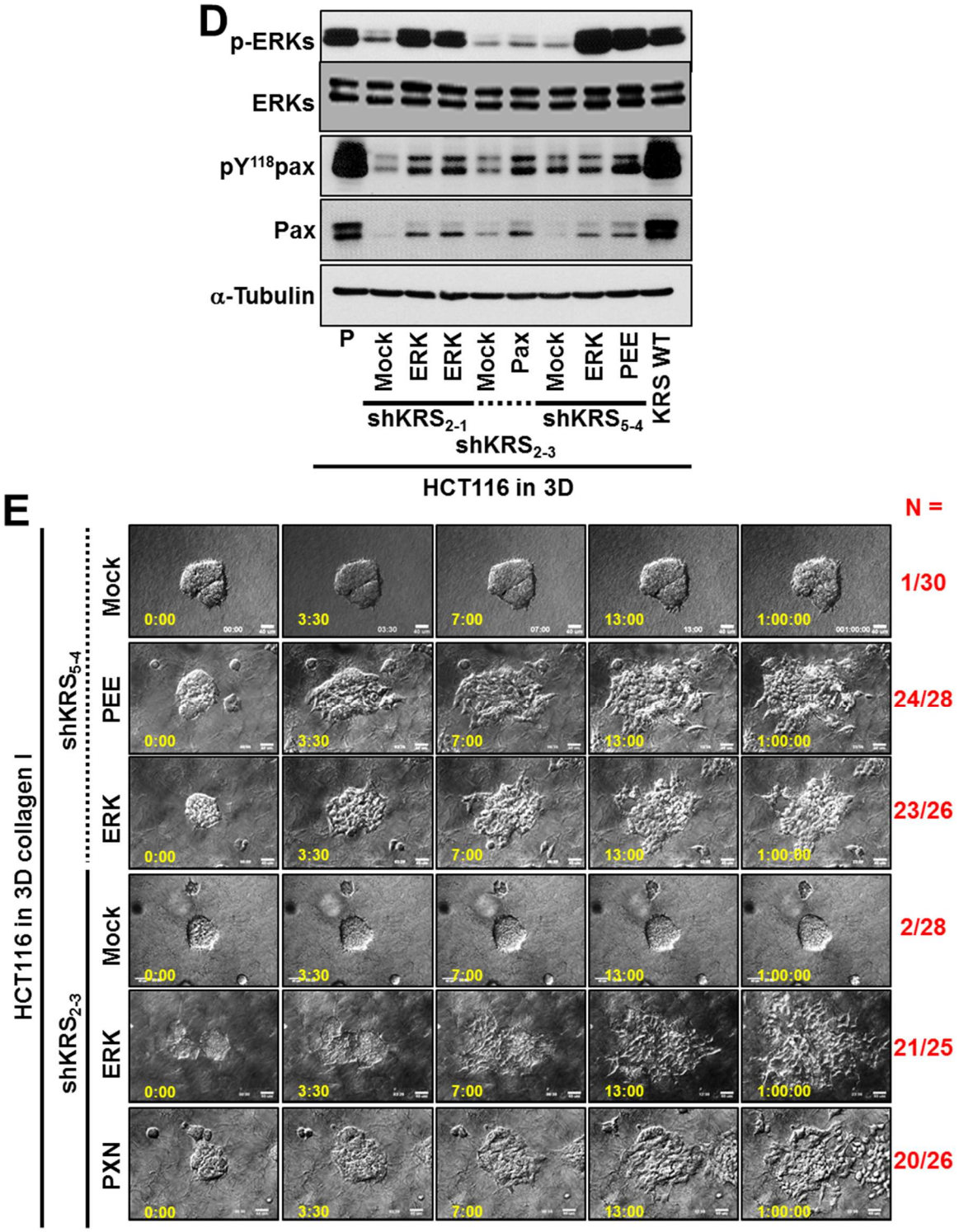

Fig. 1.6. Blockade of dissemination by KRS-suppression is relieved by ERK and/or paxillin expression.

(A) HCT116 parental cells were suspended in serum-free BSA containing media, preincubated with normal IgG or functional anti-human integrin α6 blocking antibody (20 μg/ml) for 30 min, and then kept in suspension or reseeded onto laminin-precoated culture dishes with 2% serum-containing media for 2 or 24 h. Whole-cell lysates were immunoblotted for the indicated molecules. **(B and C)** Cells were transduced with adenovirus (Ad-HA) for R454 (kinase dead) FAK, ΔN(1-100) FAK, or FAK WT for 12 h, or stably transfected with the L37A FAK mutant. The cells were embedded in 3D collagen I gels, and 3 h later, cell lysates were prepared for immunoblotting (B) or time-lapse imaging was performed for a further 28 h (1:04:00, C). **(D and E)** KRS-expressing cells and KRS-suppressed HCT116 cell spheroids (2-1, 2-3 and 5-4 clones) with stable transfection of ERK1 (ERK), paxillin (PXN), or ERK1/paxillin (PEE) were embedded in 3D collagen I gels for 24 h, prior to harvesting whole-cell lysates for immunoblotting for the indicated molecules (A). Alternatively, the spheroids were embedded for 3 h and then time-lapse imaged for another 24 h (B). Note that KRS-suppressed cells did not disseminate, whereas spheroids with ERK1, paxillin, or ERK1/paxillin overexpression showed dissemination. Data represent three independent experiments.

Fig. 7

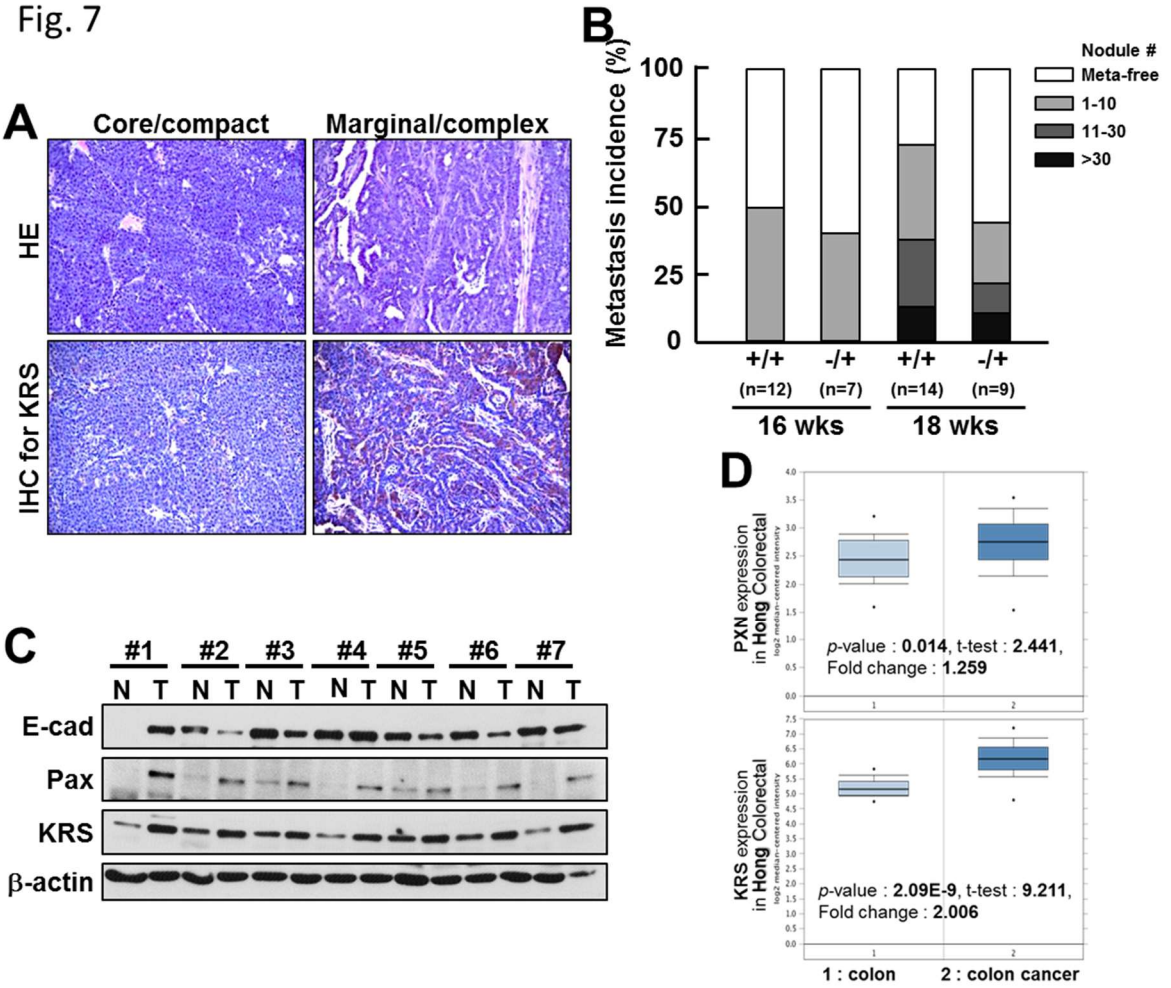
A
Core/compact
Marginal/complex
HE
IHC for KRS
B
Metastasis incidence (%)
100
75
50
25
0
Nodule #
Meta-free
1-10
11-30
>30
+/+ (n=12)
-/+ (n=7)
+/+ (n=14)
-/+ (n=9)
16 wks
18 wks
C
#1 #2 #3 #4 #5 #6 #7
N T N T N T N T N T N T N T
E-cad
Pax
KRS
β-actin
D
PXN expression in Hong Colorectal
p-value : 0.014, t-test : 2.441,
Fold change : 1.259
KRS expression in Hong Colorectal
p-value : 2.09E-9, t-test : 9.211,
Fold change : 2.006
1 : colon
2 : colon cancer
E
p-Erk1/2
KRS
Pax
Rb IgG
MS IgG
Grade II
Normal
Tumor
Grade III
Normal
Tumor

Fig. 7-continued

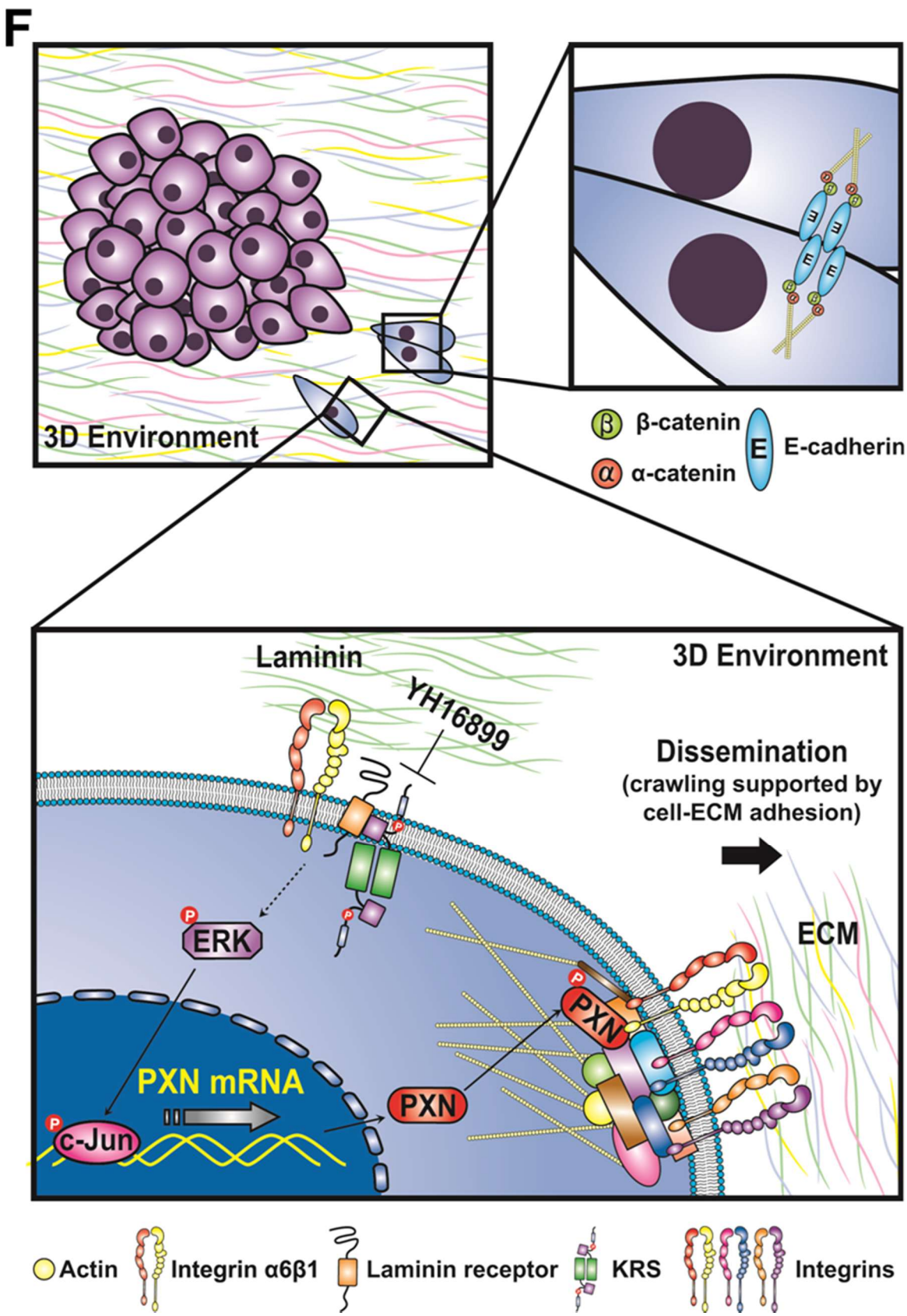

Fig. 1.7. Positive relevance in tumor metastasis of KRS in KRS$^{-/+}$ PyVT mouse and colon cancer patient tissues.

(A) Breast tumor sections of the compact core or marginal region in PyVT mice were stained with hematoxylin-eosin (HE, upper panels) or immunostained for KRS (KRS IHC, lower panels). **(B)** Metastatic lung nodules were counted in the PyVT mice (TG) with the indicated *Kar*s genotypes (WT or KRS$^{-/+}$ heterozygosity, Het) at 16 or 18 weeks of age. **(C)** Serial sections (6 μm) from normal (N) or tumor (T) tissues from grade II or grade III colon cancer patients were processed for immunohistochemistry using anti-pERK, KRS, or paxillin antibodies in addition to controls using normal rabbit (Rb) or mouse (MS) IgG. **(D)** Data from Oncomine online cancer genomics data analysis tools showed the significant overexpression of KRS and paxillin in a positively-correlated manner in colon carcinoma, compared with normal colon tissues. **(E)** Normal (N) or tumor (T) colon tissues from different clinical colon cancer patients were harvested for whole-tissue extracts at 4ºC, prior to standard Western blotting for the indicated molecules. Data shown represent three independent experiments. **(F)** Scheme to represent KRS-mediated cell dissemination from spheroids in 3D collagen I gels via regulations of cell-cell and cell-ECM adhesion. Laminin expressed in an autocrine manner binds to p67LR, which forms a complex with KRS and integrin α6β1, leading to ERK activation that in turn causes paxillin expression, via c-Jun-dependent transcriptional activation, and Tyr118 phosphorylation. Activated paxillin can mediate cell-ECM adhesion-related signaling and/or force generation to facilitate dissemination or crawling out.

Discussion

The observations in this study, made using diverse systems, such as *in vitro* cells adherent on 2D layers or embedded in 3D collagen I gels, $KRS^{-/+}$ heterozygous mice, and clinical colon tissues, support the notion that KRS functions together with p67LR/integrin α6β1 receptors to mediate cell dissemination from (tumor) cell masses via the laminin adhesion-dependent regulation of ERK and paxillin expression and activity. During the regulation of dissemination, KRS was also involved in regulating cell-cell contacts and cell-ECM adhesion. The outbound movement or dissemination from the boundaries of KRS-expressing cell spheroids appeared to be supported by KRS-dependent signaling to facilitate outbound crawling upon the adhesion of cells to laminin. ERK activity and paxillin expression/activity leading to efficient FA formation and signaling, following the formation of a complex between KRS, p67LR and integrin α6β1, were important for cell dissemination from colon cancer spheroids embedded in 3D collagen I gels (Fig. 7F). Inactivating ERK or disrupting complex formation blocked dissemination and the reintroduction of ERK or paxillin in KRS-suppressed cells restored dissemination. Although FAK-mediated ERK activity in cell adhesion is well known [16] and KRS-expressing A549 cells activate FAK upon being reseeded on laminin [6], here FAK appears not to paly importantly in the 3D dissemination of HCT116 cells. KRS-suppressed HCT116 cells showed still detectable FAK activity, whereas KRS-overexpressed HCT116 cells showed more FAK activity than parental HCT116 cells, indicating a correlation between KRS and FAK might be valid only when KRS is highly expressed. Furthermore, FAK activity was not relevant for KRS-dependent ERK activation and dissemination. This KRS/ERK/paxillin signaling axis was implicated in marginal invasiveness and metastasis in mouse animal and in clinical colon tissue models. This study provides further

evidence of a platform for KRS-dependent cell dissemination from tumor masses in 3D collagen I gels, which may be useful to screen anti-metastatic reagents against KRS-dependent colon cancers.

This study revealed that KRS was involved in the regulation of cell-cell contacts as part of its pro-metastatic functions. However, such a role for KRS has never been explored. Here, we observed that whereas KRS suppression (to certain levels) did not cause any apoptotic caspase 3 activation, KRS suppression modulated the epithelial-mesenchymal properties of cells; KRS suppression decreased the expression of epithelial markers (i.e., E-cadherin, β-catenin, ZO1, etc.) and concomitantly increased mesenchymal markers (i.e., Vimentin, N-cadherin, Twist, Snail1, etc.), although it is not currently known how KRS causes these alterations. However, KRS suppression did not cause cell scattering, supporting an incomplete EMT phenotype in KRS-suppressed cells, and indicating that KRS-suppressed cells retained certain characteristics of epithelial cells that prevent them from scattering. Furthermore, the lack of proteolytic activity of MMPs such as MT1-MMP appeared not to be the cause of no dissemination in KRS-suppressed cells. KRS-suppressed cells could not move outbound or disseminate from the boundaries of cell masses, presumably because losses of epithelial markers would not be all enough for the outward movement or dissemination, with further cell-ECM adhesion capacity also being required for these processes. Consistent with this hypothesis, cells disseminating from spheroids in a KRS-dependent manner were positive for the epithelial marker K14, although its role in dissemination as an epithelial marker protein remains to be explained.

We observed that KRS-dependent dissemination might not depend solely on either epithelial or mesenchymal characteristics; KRS-suppressed cells could not efficiently disseminate from cell masses in either 2D or 3D conditions, although they obviously lost E-

cadherin and other epithelial markers. It is well established that circulating tumor cells (CTCs) originating from primary breast tumors consist of cells with epithelial, mesenchymal, or both characteristics [1, 17]. The EMT is a key process that results in morphological changes and altered adhesion characteristics and is crucial to the metastasis of CTCs [18]. Several previous studies have examined biomarkers from colorectal cancers (CRCs)-derived CTCs, which include hepatocyte growth factor receptor c-Met, melanoma antigen gene-A3 family (MAGEA3), β1-4-*N*-acetylgalactoaminyltransferase (GalNAc-T), and cytokeratin-20 (CK20) [19], or human telomerase reverse transcriptase (hTERT), cytokeratin-19 (CK19)/cytokeratin-20 (CK20), and carcinoembryonic antigen (CEA) [20]. In these reports, CTCs derived from colorectal cancer cells could commonly be marked by CK20, which is a typical epithelial marker, suggesting that epithelial characteristics may also be at least somewhat important for metastasis, presumably by playing roles during colonization and proliferation at secondary metastatic sites. Therefore, it may be likely that KRS-expressing cells with certain epithelial characteristics resulted in dissemination for eventual metastasis.

In addition to regulating cell-cell adhesion, KRS was involved in the regulation of cell-ECM adhesion as part of its pro-metastatic functions. KRS translocates from the cytosolic MSC to the plasma membrane after p38 MAPK-dependent Thr52 phosphorylation upon extracellular laminin stimulation, where it protects p67LR from ubiquitination-mediated degradation [6]. Furthermore, the interaction between KRS and p67LR is critically involved in the lung metastasis of subcutaneously-injected mouse breast carcinoma 4T1 cells with KRS overexpression [7]. We observed here that the KRS/p67LR complex also included integrin α6, allowing KRS-expressing cells to transduce intracellular signals under extracellular laminin-stimulated conditions. Although the 3D culture in this study was performed using collagen I gels supplied with 10% FBS-containing culture media, cells efficiently expressed laminin

independent of KRS expression, suggesting that laminin was available during the experiments in the 3D collagen I gels. Interestingly, KRS-suppressed cells expressed more fibronectin, and their adhesion onto fibronectin still caused similar or slightly reduced adhesion-related FAK phosphorylation but decreased ERK phosphorylation compared with KRS-expressing cells on fibronectin. Moreover, extracellular laminin but not collagen I causes KRS translocation to the plasma membrane for binding to p67LR [6]. Thus, it is likely that KRS may mediate ERK activation for pro-metastatic roles following specific signals from the extracellular microenvironment, including laminin. Consistent with this role, KRS expression around the invasive margins in animal or human cancer tissues was correlated with laminin and p67LR expression.

Within laminin-containing 3D collagen I gels, KRS mediated ERK and paxillin activations. FAK, SFKs, paxillin, and ERK1/2 are key regulators of focal adhesion dynamics, especially during cell adhesion and migration [21, 22]. Cell-ECM adhesion activates ERK, via a FAK Tyr925 phosphorylation-mediated signaling pathway from FAK to the Ras cascade upon integrin/ECM engagement [16]. FAK-independent ERK activation is also possible upon cell adhesion; the association of integrins with caveolin-1 and Fyn (a c-Src family kinase member) recruits Shc for ERK activation [23-25]. Furthermore, the cell adhesion-dependent activation of CaMKII in vascular smooth muscle (VSM) cells leads to ERK activation independent of FAK activity [26].

Meanwhile, FAK phosphorylation in 3D collagen I appeared not to support KRS-dependent dissemination in this study, and KRS was not correlated with FAK/c-Src phosphorylation upon cell adhesion to laminin or embedding in 3D collagen I gels. We observed that YH16899 inhibitor treatment to block the binding of KRS to p67LR resulted in decreased formation of the KRS/p67LR/integrin $\alpha 6\beta 1$ complex, the phosphorylation of ERK,

and the dissemination of HCT116 parental cells. Functionally blocking integrin α6 to prevent ERK activation during laminin adhesion by KRS-expressing cells still maintained efficient FAK activity. Transduction of WT or active FAK adenovirus or stably transfecting active L37A FAK [15] into KRS-suppressed cells did not rescue ERK activity, paxillin expression/activity, or the dissemination of KRS-suppressed cells. KRS was also previously shown to be phosphorylated at Ser209 or Thr52 by either ERK for nuclear translocation [5] or p38MAPK for plasma membrane localization [6], respectively. However, KRS-mediated intracellular signal transduction has not been explored any further. KRS expression was shown to cause ERK phosphorylation/activity by several approaches in this study: (a) the overexpression of KRS caused ERK phosphorylation even in suspended cells: (b) cell adhesion-dependent ERK phosphorylation depended on KRS expression: (c) *in situ* ERK activation upon reseeding onto laminin was observed using a FRET ERK biosensor approach: (d) KRS-dependent biological behaviors, including dissemination from the cell masses, were blocked by ERK inhibition: and (e) overexpressing ERK1 rescued the dissemination of KRS-suppressed cells.In this study, KRS-dependent ERK activity was positively correlated with expression and phosphorylation of paxillin, vinculin and tensin 2, but not of other focal adhesion molecules, indicating that KRS suppression-mediated effects on paxillin (expression and activity) led to secondary effects on other FA molecule phosphorylations. Although paxillin is known to be phosphorylated by active FAK [27], this study further revealed that paxillin expression was regulated by ERK activity, because (a) ERK overexpression in KRS-suppressed cells enhanced paxillin expression and Tyr118 phosphorylation: (b) pharmacological ERK inhibition decreased paxillin expression and phosphorylation: and (c) chromatin immunoprecipitation showed that downstream of active ERK, c-Jun bound to the promoter region, presumably to regulate paxillin transcription, in a KRS inhibitor-dependent manner. It was also previously shown that activated ERK correlated with total paxillin expression and Ser178 phosphorylation but not

with Tyr118 phosphorylation during EGF/TGFβ1-mediated hepatocyte migration [28]. Paxillin localizes to focal adhesions, which are the structure in which adhesion receptor integrins bind extracellular matrix proteins such as laminin [29]. This linkage from the KRS/p67LR/integrin α6β1 complex to paxillin expression/phosphorylation via ERK/c-Jun activity could thus be the underlying mechanism by which KRS regulates cell-ECM adhesion and dissemination presumably as a pro-metastatic molecule. Therefore, KRS may represent a promising therapeutic target to address (colon) cancer metastasis.

CHAPTER 2

Lysyl-tRNA synthetase (KRS) promotes dissemination from colon cancer spheroids via recruitment and reprogramming of macrophages in 3D collagen I gels.

Abstract

It is well established that tumor microenvironment plays an important role in cancer development and metastasis. Cell-cell and cell-substrate adhesion properties of cancer cells can be targeted to block cancer metastasis. Although cytosolic lysyl-tRNA synthetase (KRS or KARS) canonically functions in protein synthesis, it is reported that KRS on the plasma membrane is involved in cell migration/invasion and cancer metastasis. We found that KRS-positive cells in 3D collagen I gels showed clear disseminative phenotypes from cancer spheroids, whereas KRS-suppression was enough to block the phenotype. It is reasonable that the close vicinity of cancer cells and tumor-associated macrophages (TAMs) at the invasive front of tumors suggests that these two cell types may mutually interact leading to a promotion of KRS-mediated cell migration/invasion and cancer metastasis. Analysis of cytokines secreted by KRS-positive spheroids showed a greater secretion of cytokine GAS6 than KRS-negative spheroids, which caused polarization of macrophages from M1 to M2 population. Nucleus KRS upregulated expression of GAS6 mRNA through MiTF to bind the promotor region of GAS6. This KRS-mediated cancer cell dissemination appeared to be depending on the role of nucleus KRS to cause the expression of cytokine (including GAS6) for M2 polarization and also membraneous KRS to cause intracellular signaling linkage for cell-ECM engagement-mediated tractive force generation, as explained in the chapter 1. In return, the treatment of conditioned media (CM) from M2 macrophage to cancer spheroids caused a greater dissemination from KRS-positive spheroids, and a recovery of the disseminative phenotype even from KRS-negative spheroids, which was to a degree less than those from KRS-positive spheroids. FGF2/GRO-α/M-CSF in the conditioned media of M2 macrophage mediated activation of intracellular signaling pathways that involved paxillin, ERKs, STAT3, and NF-κB in cancer cells to cause disseminative phenotypes. Therefore, KRS-positive cancer cells

appeared to cause macrophage infiltration and M2 polarization, which then supported for disseminative invasion of (KRS-negative and/or positive) cancer cells. Normal fibroblasts appeared to be differentiated to CAFs (cancer-associated fibroblasts) by treatment of M2 macrophage CM, and CAFs induced laminin and thereby dissemination/migration of KRS-positive cancer cells presumably under the laminin-containing microenvironment, as shown in the chapter 1. Altogether, the KRS-positivity in colon cancer cells allow metastatic cells to efficiently gain functions at the cancer-stromal interface, suggesting that KRS can be a promising target to block the colon cancer metastasis.

Introduction

Tumor microenvironment plays a pivotal role in tumor progression and metastasis, and there are a variety of cells that help cancer cells, including cancer cells [30, 31]. Among them, tumor-associated macrophages (TAM) are the most notable, and many studies have been reported recently. Correlation of poor prognosis and TAM in various types of cancer, including colorectal cancer have been showed many studies and clinical evidence [32]. Macrophages differently respond to a variety of microenvironmental signals, and therefore have different functions depending on the microenvironment [33]. Recent studies have shown that macrophages can undergo significant phenotypic changes due to their diverse interactions with tumor cells, by entering the tumor microenvironment and then retain its character. It is usually described in two phenotypes depending largely on the characters of the macrophage; M1 (classically activated) macrophages that produce pro-inflammatory cytokines are strong inhibition factor of pathogens and tumor cells, and M2 (alternatively activated) macrophages, which produce a large amount of anti-inflammatory cytokines, show anti-inflammatory effects [34, 35]. In malignant tumors, TAM is mostly similar to the M2 phenotype, but the exact phenotype and characters are still unclear [36]. It has been shown that TAM promotes the progression and metastasis of colorectal cancer by secretion of a variety of cytokines. TAM-derived cytokines can promote migration and invasion of cancer cells by increasing cell-extracellular matrix (ECM) interaction in the tumor microenvironment [37, 38].

Where TAM is usually found, it has been reported that it is often observed in the invasive portion of advanced tumors [39]. It has already been studied that the expression of KRS is high in invasive cancer tissues, and therefore the relationship between TAM and cancer cells with high expression of KRS can be expected [40]. Previous studies have shown that

cancer cells with high expression of KRS are advantageous for metastasis, suggesting that such KRS-expressing cancer cells can regulate tumor microenvironment and thus have a selective advantage in migration [7]. In this study, we present a fundamental mechanism for studying the interaction between TAMs and cancer cells and their positive-loop phenomenon that promotes metastasis.

Experimental Procedures

1. Cells.

Human colon cancer cell lines HCT116, SW620 and mouse colon carcinoma CT-26 cells (American Type Culture Collection, Manassas, VA, USA) were stably transfected with shRNA against KRS (transcript 1, NM_001130089, lysyl-tRNA synthetase MISSION® shRNA Plasmid DNA, Sigma). DNA construct (in PLKO.1 lentiviral vector backbone) was isolated from bacterial culture. Lentiviral production was performed by transfection of HEK293T cells using Fugene 6 (Promega). Supernatants were collected 24–48 h after transfection and then filtered through 0.22-mm syringe filter. Cells were infected with lentivirus with 8 mg ml^{-1} polybrene for 24 h and then the medium was replaced with fresh growth media containing puromycin (1–2 mg ml^{-1}) for selection. HCT116 cells overexpressing KRS were established via the stable transfection of a myc-tagged KRS plasmid [6]. The cDNAs encoding Myc-KRS mutants at S207A were cloned using a QuikChange II kit (Agilent Technologies, Santa Clara, CA, USA) following the manufacturer's instruction. Other HCT116 KRS mutant stable cell lines(ΔC5, T52A) were kindly provided by Dr. Sunghoon Kim (Seoul National University, Seoul, Korea). Stable myc-tagged KRS and different stable shKRS-transfected clones were established by using 250 μg/ml G418 or 0.50 μg/ml puromycin (AG Scientific, Inc., San Diego, CA). The cells were maintained in RPMI-1640 (WelGene, Daegu, Korea) containing 10% FBS and antibiotics (Invitrogen, Grand Island, NY, USA). Human monocyte THP-1 cells were kindly provided by Dr. Mi-Ok Lee (Seoul National University, Seoul, Korea). THP-1 cells were differentiated by treatment with 100 nM phorbol-12-myristate-13-acetate (PMA) for 1 day. The adhered cells were further differentiated with 100 ng/ml lipopolysaccharide for 72 h and 20 ng/ml IFN-γ during the last 72 h (M1) or 20 ng/ml IL-4 and 20 ng/ml IL-13 for 72 h (M2). Fibroblasts from normal colon CCD-18CO were obtained from

American Type Culture Collection (ATCC) and grown according to standard protocols. Human monocytes from the peripheral blood of healthy donors were kindly provided by Dr. Eun-Kyung Jo (Chungnam National University, Daejeon, Korea).

2. Animals

Balb/c mice and C57BL6 mice, 10 weeks of age, were purchased from Orient Bio,KOREA. All care administered to the animals was in accordance with protocols approved by the Seoul National University Institutional Animal Care and Use Committee. Colorectal cancer was induced using the protocol described by [41] with slight modifications. . In brief, BALB/c mice or C57BL6 mice were intraperitoneally administered azoxymethane (AOM) to initiate colon carcinogenesis. And then, mice were given two cycles of dextran sodium sulfate (DSS) in drinking water, in which each cycle consisted of one week of DSS water followed by two weeks of tap water. Experiments were performed with 8-week-old female Balb/c mice. CT-26 cells were harvested, washed three times in phosphate-buffered saline and resuspended in sterile phosphate-buffered saline at a cell concentration of 1×10^5/200 μl. Cells were injected into mouse tail veins using a 25-gauge needle. (n = 5 per group, 2 groups). At days 21, mice were sacrificed, and peritoneal tumors were histologically examined.

3. Spheroid formation and embedding into 3D collagen I gels

HCT116, SW620 and CT-26 cells with modulated KRS expression levels, or other colon cancer cells were processed for spheroid formation using Petri dishes on rotary orbital shakers or Perfecta3D® 96-well hanging-drop plates (3D Biomatrix, Ann Arbor, MI). Spheroids were selected to be less than 70 μm in size using a cell strainer sieve (SPL Life Science Co., Pocheon-si, Korea) prior to being embedded into 3D collagen I gels (BD Biosciences, San Jose, CA, USA). For embedding, polydimethylsiloxane (PDMS) chambers

with an 8-mm diameter, or 10 well-slips for 22 x 60 mm coverslips (model No.: WL-2260-10, Live Cell Instrument, Seoul, Korea), were filled with 70 μl collagen I (2.0 mg/ml, BD Biosciences) to coat the bottom surfaces of the chamber. PDMS (Sylgard 184, Dow Corning, Midland, MI) prepolymer was prepared using a 10:1 (w/w) mixture of PDMS base and curing agent, cast against the master and thermally cured to obtain a negative replica-molded piece. Spheroids were then mixed with ice-cold collagen I solutions (2.0 mg/ml), which were prepared by diluting a concentrated collagen I (BD Biosciences) stock with 10 × reconstitution buffer (260 mM sodium bicarbonate and 200 mM HEPES), and 10 × RPMI-1640 with phenol red [11]. The pH was adjusted in the range of 7.2 to 7.4 using ice-cold 2 N NaOH. The mixture was transferred to a 37ºC CO_2 incubator to allow the collagen I to polymerize and form a fibrillar meshwork. The 3D culture was then refreshed each day with standard culture media containing 10 % FBS.

4. Extract preparation and Western blots.

Colon cancer cells within collagen I gels were washed with ice-cold PBS and then homogenized with truncated pipette tips (3 times × 20 min on ice) in modified RIPA buffer (50 mM Tris-HCl, 150 mM NaCl, 1% NP-40, and 0.25% sodium deoxycholate) with a protease inhibitor cocktail (GenDepot, Barker, TX). The extracts were centrifuged for 30 min at 15,000 *g* and 4°C, and then the lysates were collected from the supernatant. The protein amounts were normalized with the band intensities for α-tubulin or β-actin via standard Western blots, before further immunoblotting with different antibodies. The primary antibodies used in the study were as follows: α-SMA (Sigma, St Louis, MO); Hsp90, pY^{701}STAT1, pY^{705}STAT3, STAT6, pY^{641}STAT6, ERKs, phospho-ERKs, pY^{845}EGFR and phospho-FGFR(pY653/654) (Cell Signaling Technol. Danvers, MA); paxillin (BD Biosciences); p67LR, laminin, p-MerTK(pY749/753/754) and MiTF (Abcam, Cambridge, UK); pY^{118}paxillin, E-cadherin,

IκBα, STAT1, STAT3, CXCR2, M-CSF, FGFR1, FGFR2, Axl, Histone H1, angiogenin, c-Myc, β-actin and α-tubulin (Santa Cruz Biotech., Santa Cruz, CA); integrin αvβ1, (Millipore, Billerica, MA); Gas6, phospho-Axl, MerTK (R&D systems) EGFR (Thermo) and KRS (Neomics, KOREA).

5. Time-lapse imaging of cells in 3D ECM gels.

Various stable cell lines were processed for spheroid formation using Petri dishes on rotary orbital shakers or Perfecta3D® 96-well hanging-drop plates (3D Biomatrix, Ann Arbor, MI). One hour after spheroids were embedded in 3D collagen I gels, time-lapse images were collected for the indicated periods using IX81-ZDC microscope (Olympus, Tokyo, Japan). The microscope was equipped with a 10-well Chamlide Incubator system (Live Cell Instrument, Seoul, Korea), and an environmental chamber mounted on the microscope maintained constant conditions of 37°C, 5% CO_2, and 95% humidity.

6. Coimmunoprecipitations.

Whole-cell extracts prepared from cells in standard media containing 10% FBS were immunoprecipitated overnight using anti-myc tag antibody-coated agarose beads (Sigma). The immunoprecipitated proteins were boiled in 2 × SDS-PAGE sample buffer before standard Western blot analysis.

7. Indirect immunofluorescence.

Human normal colon fibroblast CCD-18CO embedded in 3D collagen I gels within PDMS were immunostained using antibodies against α-SMA, laminin in addition to DAPI staining for the nucleus. Immunofluorescence images were acquired on a confocal laser scanning microscope with a Nikon Plan-Apochromat 60×/1.4 N.A. oil objective (Nikon eclipse

Ti microscope, Nikon, Tokyo, Japan).

8. Chromatin immunoprecipitation (ChIP).

ChIP assays were performed using the ChIP-IT Express kit (Active Motif, Carlsbad, CA), following the manufacturer's protocols. Briefly, cells seeded in a plate for 48 h were fixed for 10 min with fixation solution, and the chromatin was then prepared by sonication shearing to aid nuclear release and enzymatic shearing. The sheared chromatin was immunoprecipitated using MiTF (Abcam) or c-Jun (Cell Signaling) antibodies and captured with protein G magnetic beads. The chromatin was eluted from the purified immunoprecipitates, reversed cross-linked, and digested with proteinase K. The reaction was then stopped using proteinase K stop solution. The isolated chromatin was analyzed by 36 cycles of PCR. Ten microliters of each PCR product was separated via 2% agarose electrophoresis.

9. Co-culture in 3D collagen I gels.

Operetta ® / Harmony ® High Content Screening (HCS) Platform was used to analyze the migration and invasion of cancer cells toward macrophages, and vice versa, in 3D collagen 1 gels. Monocytes or macrophages were embedded at the bottom of the gels, and KRS level-modulated HCT116 cancer cells were embedded at the upper side of the gels. KRS level-modulated HCT116 cancer cells were embedded at the bottom of the gels, and monocytes or macrophages were embedded at the upper side of the gels. HCT116 cancer cells were stained with Cell Tracker Green (CMFDA), and macrophages were stained with Cell Tracker Red (CMTPX). The location of cells in the gels was taken at Day 5 and Day 10 after embedding. The confocal image acquisition performed by the Operetta High Content Screening System allows robust and reliable cell counting within different planes of the matrix, leading to graphic presentations of the cell numbers in each plane (Y-axis) to depict relative migrations (X-axis)

10. Cytokine antibody array.

Human cytokine antibody array was used to measure the synthesis or secretion levels of 42 cytokines by HCT116 cells (parental, KRS-suppressed cells, or KRS-overexpression cells) in 3D collagen I gels. Shown in rectangle enclosed boxes are the factors that are highly down-regulated upon KRS suppression in conditioned medium of HCT116 cells. The Human Cytokine Array was used to simultaneously detect differences in cytokine secretion profiles in the supernatants of THP-1, human macrophage (monocyte, M1-, M2-polarized) cells. The relative expression levels of 102 human soluble proteins were determined.

11. Analysis of Subcellular Proteome Extraction.

Cells were then subjected to membrane and cytosol fractionation using Subcellular Proteome Extraction Kit (Calbiochem, Billerica, MA), as indicated by the manufacturer. HCT116 shControl, HCT116 cells stably transfected with shKRS (clones of #2 or #5), myc-KRS-overexpressing cells (KRS WT) and other KRS mutants (ΔC5, T52A, S207A) were harvested for membrane, nucleus and cytosol fractions. The cell fractions were normalized for standard western blot analysis, and probed using antibodies against the indicated molecules. The data shown represent three independent experiments.

12. Immunohistochemistry.

Dissected colon and lung were fixed and stored in 4% Formaldehyde. The tissues were processed, paraffin embedded, and sectioned at 6-μm thickness. After deparaffinization, antigen retrieval was performed by boiling the sections for 5 min in sodium citrate solution (0.01 M, pH 6). Immunohistochemistry of serial sections of paired normal or tumor colon tissues was performed using normal rabbit IgG, normal mouse IgG, KRS (Neomics), CD206 (Abcam) and CD11c (Invitrogen).

13. Real-Time PCR.

Total RNA was extracted from cells in 10% FBS-containing condition or in 3D collagen I gels, using QIAzol (QIAGEN) according to the manufacturer's protocol. One microgram of total RNA was reverse transcribed using the amfiRivert Platinum cDNA Synthesis master mix (GenDepot) and ReverTra Ace qPCR RT Master Mix with gDNA Remover (TOYOBO). Primers were designed using Integrated DNA Technologies (IDT) software as follows : human CD11b mRNA, forward 5'-CAGTGTGACATCCCGTTCTT-3' and reverse 5'-CACGATCAGGAGGTGGTTATG-3'; human CD11c mRNA, forward 5'-GTTAGCAGCCACGAACAATTC-3' and reverse 5'-TCCCTCTGTCCCAGGTTATT-3'; human TNFα mRNA, forward 5'-GATCCCTGACATCTGGAATCTG-3' and reverse 5'-GAAACATCTGGAGAGAGGAAGG-3'; human IL-1β mRNA, forward 5'-CTCTCACCTCTCCTACTCACTT-3' and reverse 5'-TCAGAATGTGGGAGCGAATG-3'; human IL-6 mRNA, forward 5'-ATAGGACTGGAGATGTCTGAGG-3' and reverse 5'-GCTTGTGGAGAAGGAGTTCATAG-3', CD206, forward 5'-GGACGTGGCTGTGGATAAAT-3' and reverse 5'-ACCCAGAAGACGCATGTAAAG-3'; IL-10, forward 5'-GCTGGAGGACTTTAAGGGTTAC-3' and reverse 5'-GATGTCTGGGTCTTGGTTCTC-3; GAS6, forward 5'- TCTGTGGCACTGGTAGACTAT-3' and reverse 5'- CGCAGACCTTGATCTCCATTAG-3; Fibronectin, forward 5'-CCACAGTGGAGTATGTGGTTAG-3' and reverse 5'- CAGTCCTTTAGGGCGATCAAT-3; human KRS (KARS) mRNA, forward 5'- GAGAAGGAGGCCAAACAGAA-3' and reverse 5'- CTCAGGACCCACACCATTATC-3', and human GAPDH mRNA, forward 5'-GGTGTGAACCATGAGAAGTATGA-3' and reverse 5'-GAGTCCTTCCACGATACCAAAG-3'.

Results

FGF2/GROa/M-CSF cause the dissemination from colon cancer spheroids embedded in 3D collagen I gels.

Previous results have shown that the physical distance between cancer cells with high expression of KRS and surrounding macrophages in cancer tissues is close, suggesting that there may be an interaction between cancer cell and macrophages. Therefore, we conducted an experiment to check the effect of surrounding macrophages on cancer cells. The effect of macrophages around the cancer cells mimics by treating the conditioned medium (CM) of macrophages with cancer cells. Previous studies have shown that cancer cells with higher expression of KRS are more capable of dissemination and migration in a 3D collagen environment. Thus, the dissemination ability of stable cell lines with different KRS expression by macrophage effect was observed through time-lapse microscope. CM of macrophages was obtained by differentiating human monocytes and human monocyte cell lines THP-1 into M1 and M2, respectively. HCT116 cells (shControl, shKRS#2, shKRS#5(data not shown)) or SW620 cells (shControl, shKRS#2, shKRS#5 (data not shown)) spheroids were embedded in collagen 1 gel and treated with CM of macrophages isolated from healthy donor blood. Inhibition of KRS expression in HCT116 and SW620 cell lines showed that the suppressed dissemination ability was restored by treating CM of M2 macrophages (M2 CM). However, when treated with CM of M1 macrophages (M1 CM), KRS-suppression inhibited dissemination ability was not recovered. The CM of M1 or M2 macrophages differentiated in THP-1 cell line were both disseminated in the KRS-suppression cell lines. (Fig. 2.1A) The difference in the CM of macrophages differentiated from healthy donor blood and CM of differentiated macrophages from THP-1 cell line is thought to be due to the fact that THP-1 is

a cell line isolated from leukemia patient rather than monocytes isolated from the heathy state body. The CM of monocytes or THP-1 monocytes isolated from human blood could not affect KRS-suppression cell lines. (data not shown) It was observed that phospho-Tyr705 and phospho-ERKs were reduced by KRS suppression in HCT116 and SW620 cell lines. We found that phospho-Tyr705 and phospho-ERKs were restored when treated with CM of macrophages isolated from healthy donors. Especially, it was confirmed that this phenomenon is prominent when M2 CM is treated than M1 CM. (Fig. 2.1B) Similarly, phospho-Tyr705 and phospho-ERKs were also increased when CM of THP-1 macrophages was treated in the same cell lines. In addition, we confirmed the expression of Paxillin and phosphor-Tyr118 Paxillin, which is a signal required for dissemination. The expression of IκBα is inhibited by treatment with CM of THP-1 macrophages, which suggests that NF-κB is activated. And, when the CM of macrophages is treated with cancer cells, it can be seen that the effect of M2 CM is larger than monocyte, M0, and M1 CM. (Fig. 2.1C and D) We confirmed that KRS-suppression stable cell lines, which inhibited the dissemination phenomenon, showed activation of various molecules and showed dissemination phenotype when cancer cells were treated with CM of macrophages. Therefore, we analyzed CM of macrophages using a cytokine antibody array in order to investigate whether any substance present in the CM of macrophages affects the dissemination of cancer cells. Because M2 CM affects the dissemination of cancer cells than M1 CM, we analyzed cytokines secreted more in M2 CM than monocyte CM or M1 CM. In the CM of THP-1 cell line, nine cytokines were more prominent than monocyte or M1 CM. We also found that the CM of macrophages isolated from the blood of healthy donor secreted more 18 substances in M2 CM than monocyte CM or M1 CM. When the results of THP-1 CM and the CM of macrophages isolated from blood were combined, it was common that there were six cytokines secreted by M2 CM in common. Among them, it was able to be compressed into three cytokines (FGF basic, GROalpha, M-CSF) from the results obtained through repeated

experiments. (Fig. 2.1E) To confirm whether these three cytokines could affect the dissemination of cancer cells, we examined the dissemination of SW620 cell lines in a 3D collagen environment. These three cytokines not only increased the dissemination capacity of the KRS positive cell line, but also restored the suppressed dissemination ability of the KRS suppression cell line. (Fig 2.1F) In the dissemination ability of cancer cells, immunoblotting was performed to confirm whether FGF basic had a specific effect on cancer cells and whether other growth factors were not affected. As a result, activation of signal related to dissemination could be confirmed only when FGF basic was treated in HCT116 cell lines without being influenced by other growth factors, PDGF and VEGF. (Fig. 2.1G) Furthermore, when the CM of THP-1 macrophages was treated with HCT116 cell lines, it was confirmed that the phosphorylation of FGFR was increased. (Fig. 2.1H) Similarly, when GROα and M-CSF were treated with cancer cells, phosphorylation of STAT3 and ERKs were increased. Interestingly, we found that GROα and M-CSF treatment in cancer cells in the 3D environment resulted in signal activation early in the treatment, unlike FGF basic treatment. (Fig. 2.1I) In the HCT116 cell lines, mRNAs of these three molecules were examined and it was confirmed that mRNA expression was not different between cancer cells that regulated KRS expression. This may be due to the dissemination of cancer cells by the effect of paracrine by macrophages. (Fig. 2.1J) In order to determine whether these three molecules directly affect the dissemination of cancer cells, experiments were conducted to neutralize them by treating the antibodies that can target them. The KRS suppression cell lines of HCT116 and SW620 were treated with M2 CM to induce dissemination and to mix the antibodies together, respectively. As a result, in the HCT116 cell lines, the dissemination phenomenon observed by treating M2 CM with KRS suppressed spheroids was not observed in single cells disseminated by treating the antibodies, but some protrusive phenotypes were showed. In the SW620 cell lines, when the antibodies were treated, there was almost no dissemination of the cancer cells. (Fig. 2.1K) Activation of

FGFR by FGFbasic is known to be associated with integrin αvβ3. We investigated whether the phenomenon of dissemination by M2CM is due to the interaction between FGFR and integrin αvβ3. When the integrin signal was blocked by treatment with M2CM and integrin αvβ3 antibody, the dissemination ability of cancer cells was decreased. However, it did not completely prevent the dissemination of cancer cells. The dissemination of cancer cells by M2CM suggests that the FGFR-integrin αvβ3 dependent pathway and the FGFR-integrin avb3 independent pathway are present. (Fig. 2.1L) Likewise, when the antibody that can target the KRS on the membrane was treated, it was confirmed that the cancer cell was partially prevented from dissemination. KRS on the membrane is known to provide the crawling force of cancer cells through the KRS-Laminin receptor (LR)-integrin α6β1 interaction in the dissemination process of cancer cells. This KRS-LR-integrin α6β1 pathway also partially contributed to the dissemination of cancer cells by M2CM. It is suggested that KRS-independent pathway is also present in dissemination by M2CM. (Fig. 2.1M) Taken together, cytokines such as FGF basic, GROα, and M-CSF secreted by TAM induce dissemination of surrounding cancer cells. The dissemination of cancer cells is an important first step leading to the metastasis of tumor, suggesting that modification of the tumor microenvironment by TAM may play an important role in cancer cell metastasis.

GAS6 from KRS-positive tumor cells causes the polarization of macrophages from M1 to M2 populations.

To investigate the effect of cancer cells on peripheral macrophages in the tumor microenvironment, CM of HCT116 stable cell lines, which regulated KRS expression, was treated with THP1 macrophages (differentiated into M1 and M2, respectively). The mRNA expression of IL6, which is known to be secreted mainly from M1 macrophages and The mRNA expression of IL10, which is known to be secreted mainly from M2 macrophages, was

examined. We also confirmed the mRNA expression of mannose receptor (CD206), a marker of M2 macrophages. Interestingly, when CMs of KRS expression-regulated colon cancer cell lines were treated, there was no difference in the expression of IL10 and CD206 in M1 macrophages was found to be increased by treatment of CM of KRS positive cancer cell lines. (Fig. 2.2A) Many researches have been conducted on the transition of macrophages with the M1 phenotype to macrophages with the M2 phenotype. The mRNA level of several molecules known to affect these transitions was examined in the cancer cell lines that regulated KRS expression. Among the various molecules, only GAS6 and IL8 showed a marked decrease in mRNA expression in KRS suppressed cell lines, and it was confirmed that the expression of GAS6 and IL8 was increased as KRS expression was increased. (Fig. 2.2B) In addition, we examined 48 cytokines secretion in the CM of KRS expression- regulated cancer cells through cytokine antibody array. These results indicate that the higher the expression of KRS in colorectal cancer cells, the more cytokines such as angiogenin (ANG) and IL8 are secreted. (Fig. 2.2C) To investigate whether GAs6, IL8, and ANG, which have different levels of expression and secretion in KRS expression-regulated cancer cells, affect the transition from M1 macrophages to M2 macrophages, experiments were conducted to directly treat these molecules with macrophages. When Gas6, IL8, and ANG were treated with THP-1 monocyte or M1, M2 macrophages, in particular, the mRNA expressions of IL10 and CD206 were increased by treating GAS6 in M1 macrophages. (Fig. 2.2D and E) When IL8 and ANG were individually treated with macrophages, they did not significantly affect the transition from M1 to M2. (data not shown) When examined by FACS under the same conditions, it was confirmed that the expression of M2 macrophage marker, CD206, was increased by the treatment of Gas6, IL8, ANG with M1 macrophages, although there was no significant difference in expression of M1 marker, CD11b. (Fig. 2.2F) When CM of stable cell lines regulated KRS expression was treated on M1 macrophages, CM of KRS positive cancer cells was found to increase phospho-

STAT6 in M1 macrophages. (Fig. 2.2G) It is generally known that phospho-STAT1 is increased in M1 macrophages and phospho-STAT6 is increased in M2 macrophages. Similarly, it was confirmed that phospho-STAT6 was increased by treating Gas6 (and IL8/ANG) with M1 macrophages.(Fig. 2.2H) It is known that MerTK acts on the transition from M1 to M2 through GAS6 in macrophages. Thus, we confirmed whether GAS6 secreted by KRS positive cancer cells induces a transition from M1 to M2 macrophages through activation of MerTK. As a result, when M1 macrophages were treated with GAS6 (IL8 and ANG), MerTK was activated through MerTK phosphorylation.(Fig. 2.2I) Because of this, KRS positive cancer cells secrete GAS6, IL8 and ANG, and these cytokines induce the transition from surrounding M1 macrophages to M2 macrophages. Cancer cells secrete a number of cytokines, which change the surrounding macrophages into TAM, thereby creating a favorable environment for cancer cells.

KRS translocated into nucleus promotes GAS6 mRNA level through transcription factor MiTF.

It was confirmed that GAS6 secreted by KRS positive cancer cells affects peripheral macrophages, causing the transition of M1 macrophages to M2 macrophages. To examine the mechanism of KRS in cancer cells to regulate the mRNA of Gas6, various KRS mutants were used. It has been reported in various researches that KRS is located in various places within the cell, and that KRS functions differently depending on its location. There are three ways in which KRS can regulate the mRNA of Gas6, depending on where KRS is located in the cell. First, KRS in cytosol regulates the expression and activation of transcription factor, which can regulate GAS6 mRNA. The second is that KRS directly enters the nucleus and regulates the transcription factor to regulate GAS6 mRNA. Finally, the third method is to regulate the expression of gas6 by stimulating cancer cells with autocrine effect by KRS secreted from

cancer cells. KRS mutants that inhibit intracellular transport of KRS were constructed in HCT116 cell lines and gas6 mRNA expression was examined in these mutants such as the KRS T52A mutant, which fails to migrate to the membrane, KRS ΔC5 mutant that is not secreted out of the cells and the KRS S207A mutant, which does not enter the nucleus. (Fig. 2.3A) However, except for the KRS T52A mutant, there was no problem with the dissemination of KRS mutants. (Fig. 2.3B) Interestingly, only the KRS S207A mutant was found to show a decrease in GAS6 mRNA expression. Other KRS mutants were found to have no effect on Gas6 mRNA expression. (Fig. 2.3C) When the CM of KRS mutants were treated to M1 macrophage, the treatment of KRS S207A mutant CM showed that the M1 macrophages did not transition to the M2 macrophages more than the treatment of the other mutants CM. (Fig. 2.3D) KRS has been reported to enter the nucleus and activate the transcription factor MiTF to regulate gene expression in dendritic cells. In the colon cancer cells, the ChIP assay was performed to examine the effect of KRS on the transcription factor to regulate GAS6 mRNA expression. Based on previous studies, we examined the transcription factors MiTF and c-JUN, which are expected to be regulated by KRS. Thus, an experiment to confirm that two transcription factors bound to the promoter of GAS6 was designed and shown in a schematic diagram. (Fig. 2.3E) As a result, it was confirmed that the transcription factor regulating GAS6 mRNA by KRS in colon cancer cells was MiTF, not c-JUN. When M2 CM was treated with the KRS suppressed cell line, MiTF was attached to the gas6 promoter. (Fig. 2.3F) YH 16899 inhibits KRS - LR interaction on membrane, which is known to inhibit dissemination by KRS. We also examined whether YH 16899 could affect the expression of GAS6, which is regulated by KRS present in the nucleus. When several KRS mutants were treated with YH 16899, GAS6 mRNA expression was not affected at all. (Fig. 2.3G) Since FGF basic, M-CSF, and GROα secreted by macrophages induce dissemination of KRS suppressed cells, we examined whether these molecules could affect GAS6 expression. (Fig. 2.3H) These three molecules, which

induced dissemination of cancer cells, had no effect on GAS6 mRNA expression. Because of this, it is anticipated that other substances present in M2CM will affect KRS or MiTF and affect GAS6 mRNA expression.

KRS-positive HCT116 tumor cells prefer to communicate with M2 macrophages rather than with M1 macrophages.

Many results have confirmed that the relationship between these cancer cells and macrophages in the tumor microenvironment is affecting each other. Through the co-culture in 3D collagen 1 gel of cancer cells and macrophages, we attempted to mimic what this relationship would be in the tumor microenvironment. 3D co-culture was performed in a cornining 48-well plates for 5-10 days, and images were obtained and analyzed through Operetta. The cells to be traced were embedded in the bottom part of the collagen gel, and the migration distance of the cells was measured every 5 days. When macrophages are tracked, it was confirmed that the M2 macrophages migrated more toward the cancer cells than the monocytes or M1 macrophages. In addition, the co-culture with KRS positive cancer cells showed that the migration of macrophages was further increased. (Fig. 2.4A) Conversely, when tracking cancer cells, we confirmed that KRS positive cancer cells migrated more toward macrophages than KRS suppressed cancer cells. When co-cultured with M2 macrophages, the migration of cancer cells was prominent on 5 days after co-culture. Interestingly, however, when we observed 10 days after co-culture, the migration of cancer cells co-cultured with M1 or M2 macrophages was not significantly different. In other words, when co-cultured for 5 days, only M2 macrophages and KRS positive cancer cells were largely attracted. However, when co-cultured for 10 days, M1 macrophages and KRS positive cancer cells were also increased attraction each other. (Fig. 2.4B) Indeed, in the tumor, cancer cells with different levels of KRS expression will be present in the form of solid tumors. In order to mimic such a situation, the

KRS positive cell line and the KRS negative cell line were made into one spheroid, and 3D co-culture was performed. Each cell line was stained with a different fluorescent dye to track KRS positive cells (cell tracker green; CMFDA) and KRS negative cells (cell tracker red; CMPTX). We confirmed that KRS positive cells only disseminated in spheroids composed of two cell lines. However, when M2 CM was treated, both KRS positive cell and KRS negative cell were found to be disseminated. This suggests that KRS positive cells are inadequate to induce dissemination of KRS negative cells in an environment composed only of cancer cells with different levels of KRS expression. (Fig. 2.4C) It has been reported that there are many macrophages in the peripheral region other than the core region of the tumor, and cancer cells with high expression of KRS are reported to be present in the marginal portion of these tumors. To investigate the relationship between macrophages and highly expressed KRS - expressing cancer cells in tumors, we examined the inducible colon carcinoma model in Balb / c female mice. KRS expression was higher than normal tissues in tumors generated by chronic inflammation, and CD206, which is a marker of M2 macrophages, was present around the tumor. (Fig. 2.4D) In addition, inducible colon carcinoma was induced by treatment with AOM-DSS in C57BL6 male and female mice KRS $^{+/+}$, KRS $^{+/-}$ mice. According to the differences in expression of KRS, the degree of tumor formation and severity was more prominent in KRS $^{+/+}$ mice than in KRS $^{+/-}$ mice. (Fig. 2.4E) Interestingly, KRS $^{+/-}$ mice showed higher KRS expression than other normal tissues in the area of colon carcinoma. In addition, we observed more macrophages with M2 phenotype than macrophages with M1 phenotype around tumor. (Fig. 2.4F) In this regard, in colorectal cancer, KRS expression is increased in the tumor region, and M2 macrophages are present around cancer cells having increased expression of KRS. Interaction may be expected between the two cells with close physical distance, suggesting that such interactions may have a large impact on the tumor microenvironment. A stable cell line regulating KRS expression was constructed by CT26, a

mouse colon cancer cell line, and confirmed by in vivo system through IV injection. The characteristic signaling pathway observed when KRS expression was regulated in cancer cells could be obtained in the CT26 cell line as in the case of human colon cancer cell lines. (Fig. 2.4G) Three weeks after the injection of CT26 cell line, which regulated KRS expression, the mice were sacrificed and the tumor formation of the lungs was confirmed. When shControl cell lines were injected, the formation of the tumor was markedly greater than that of shKRS # 2 cell lines. These results suggest that the greater the expression of KRS in cancer cells, the more excellent the ability of metastasis. (Fig. 2.4H and I) The KRS expression of cancer cells and the infiltration pattern of macrophages around cancer cells were confirmed by IHC in the mouse lung tissues. The KRS expression was higher in the tumor-forming region than in the normal lung tissue region, and the infiltration of M2 macrophages, not M1 macrophages, was noticeable around cancer cells with high expression of KRS. (Fig. 2.4J) KRS expression of cancer cells was found to induce attraction and infiltration of the surrounding macrophages, especially, macrophages with the M2 phenotype were found around cancer cells with high expression of KRS. As the physical distance between cancer cells and macrophages approaches, suggesting that the interaction between cancer cells and macrophages is activated, thereby creating a tumor microenvironment that facilitates metastasis of colon cancer cells.

A positive relationship between KRS-positive colon cancer cells and M2 macrophages is important in favoring tumor microenvironment for KRS-positive metastatic phenotypes.

Interaction of cancer cells with high expression of KRS and surrounding macrophages may be expected to have an influence on the tumor microenvironment in which they are present. It is well known that various cells are present in the tissue, and among them, fibroblasts that form ECM greatly contribute to the migration of cancer cells. Thus, normal fibroblasts present in the tumor microenvironment were expected to be activated by cancer-associated fibroblasts,

which are known to create a favorable environment for tumors through the positive loop interaction of cancer cells and macrophages. To confirm this hypothesis, CCD18CO, a normal colon cell line, was embedded in 3D collagen 1 gel and the prepared macrophage CM was treated for 4 days. THP1 were each differentiated into M1 and M2 macrophages, respectively, and then M1 macrophages were treated with CM of HCT116 stable cell lines (shCon, shKRS # 2, KRSWT). As a result, CM of M1 macrophages treated with CM of KRS positive cancer cells caused a morphological change with a broad fibroblast with a rough surface. And it increased LN expression of fibroblast. This result was as if the CM of M2 macrophages was treated. (Fig. 2.5A and B). Under these conditions, we examined the mRNA levels of laminin and fibronectin, known as ECM, which may affect cancer cell metastasis. The CM of M1 macrophages treated with KRS positive cancer CM increased the mRNA of ECM components of fibroblast as much as the CM of M2 macrophages. (Fig. 2.5C) It is well known that when CAF is activated, collagen contraction occurs. When the collagen contraction phenomenon of fibroblast was examined under the same conditions, the CM of M1 macrophages treated with KRS positive cancer CM showed similar results to the CM of M2 macrophages. In other words, CM of KRS positive cancer cells can be expected to transit M1 macrophages to M2 macrophages. (Fig. 2.5D) Co-culture in 3D collagen environment was performed by making HCT116 or CCD18CO and HCT116 as one spheroid. When incubated with HCT116 alone, or when HCT116 and CCD18CO were co-cultured together, the results of these 2 cases were not significantly different under normal media conditions. However, when M2 CM was treated, co-culture of CCD18CO was found to increase the dissemination of cancer cells more than HCT116 alone. (Fig. 2.5E) In colorectal cancer cell lines, the secretion of IL8 and ANG, which are cytokines related to angiogenesis, was found to be highly correlated with KRS. Thus, to investigate the effect of KRS positive cancer cells on angiogenesis in tumor microenvironment, HUVEC and colon cancer cells were co-cultured using a 3D microfluidic

device. When co-cultured with KRS positive cells than when co-cultured with KRS negative cancer cells, HUVEC were extended to the direction of cancer cells. Through this, it can be expected that, within the tumor environment, KRS positive cancer cells will further promote angiogenesis. (Fig. 2.5F)

Cancer cells undergoing epithelial-mesenchymal transition (EMT) and M2-polarized macrophage (tumor-associated macrophages (TAMs)) at the invasive front of tumors suggests that these two cell types may mutually communicate positively for enhanced metastatic activities. KRS-positive colon cancer cells activate macrophages to a TAM-like phenotype by Gas6 / IL8 / ANG. Reciprocally, FGF2 / GROα / M-CSF from TAMs induces cancer cell dissemination, forming a positive feedback loop, in co-culture systems. These findings suggest that a positive feedback loop between FGF2/ GROα/M-CSF and Gas6/IL8/ANG is importantly involved in the cross-talks between macrophages and KRS-positive cancer cells for an efficient colon cancer metastasis. (Fig. 2.5G)

SHN-Fig. 1

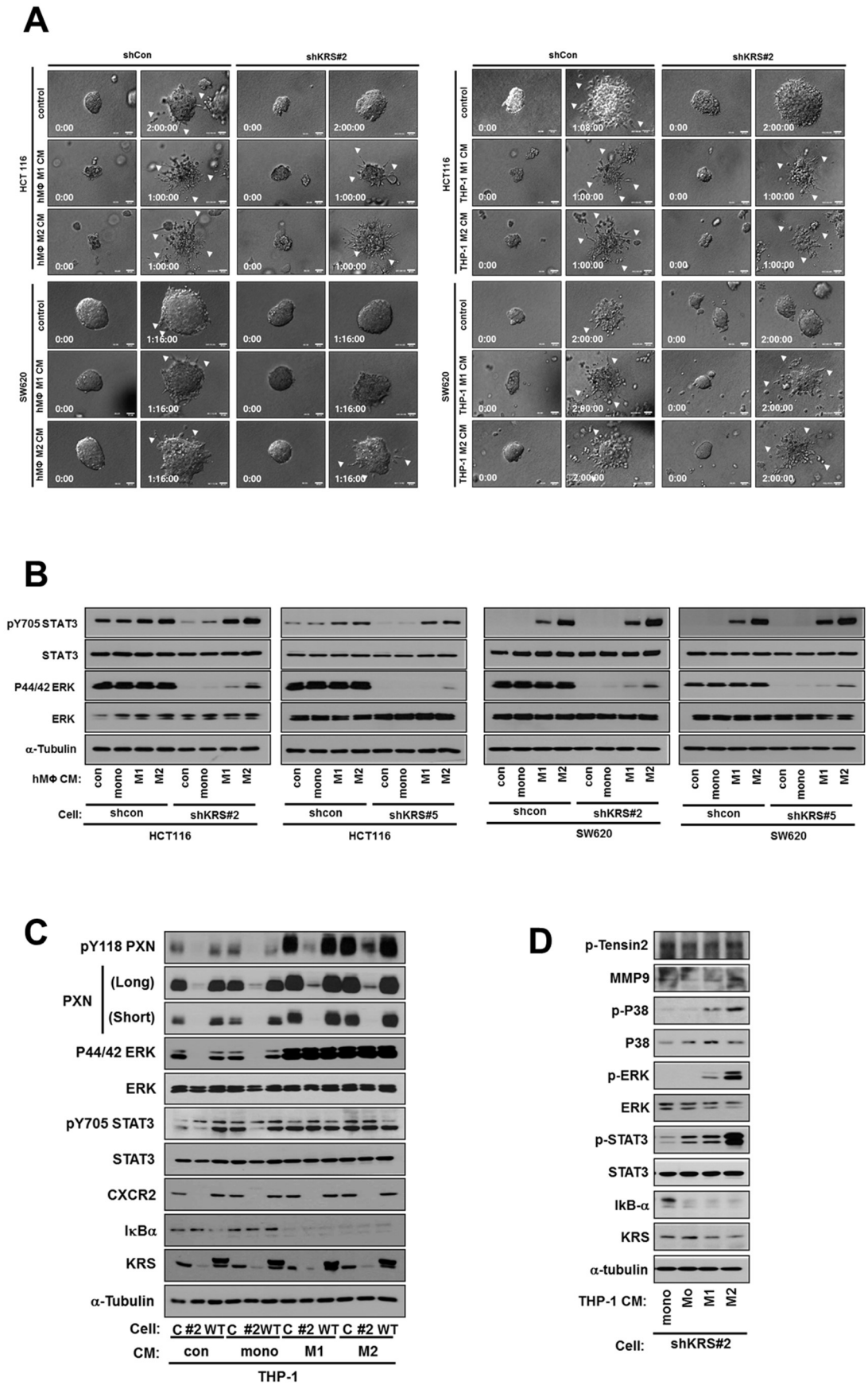
A
shCon
shKRS#2
HCT 116
SW620
control
hMΦ M1 CM
hMΦ M2 CM
HCT116
THP-1 M1 CM
THP-1 M2 CM
B
pY705 STAT3
STAT3
P44/42 ERK
ERK
α-Tubulin
hMΦ CM:
con
mono
M1
M2
Cell:
shcon
shKRS#2
shKRS#5
HCT116
SW620
C
pY118 PXN
PXN
(Long)
(Short)
P44/42 ERK
ERK
pY705 STAT3
STAT3
CXCR2
IκBα
KRS
α-Tubulin
Cell:
C #2 WT
CM:
con
mono
M1
M2
THP-1
D
p-Tensin2
MMP9
p-P38
P38
p-ERK
ERK
p-STAT3
STAT3
IkB-α
KRS
α-tubulin
THP-1 CM:
Mo
Cell:
shKRS#2

SHN-Fig. 1 continued

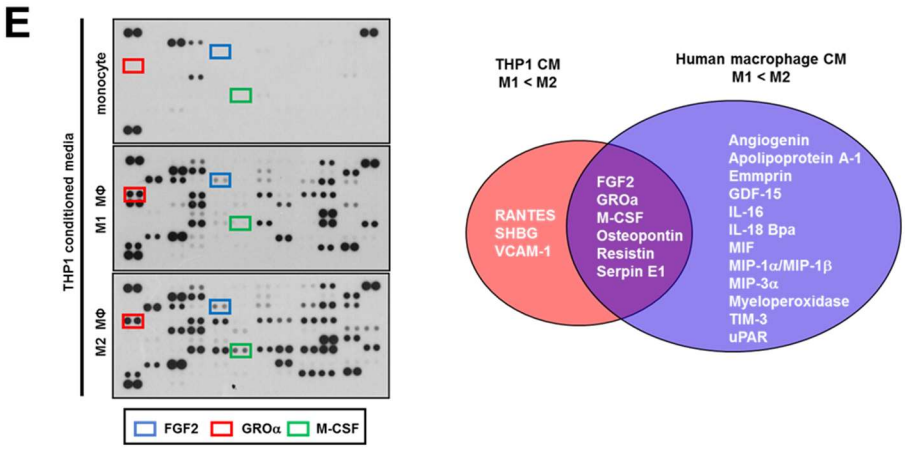

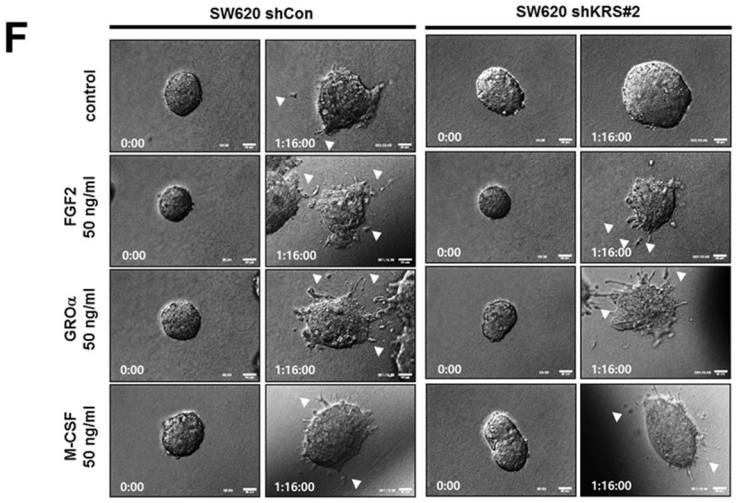

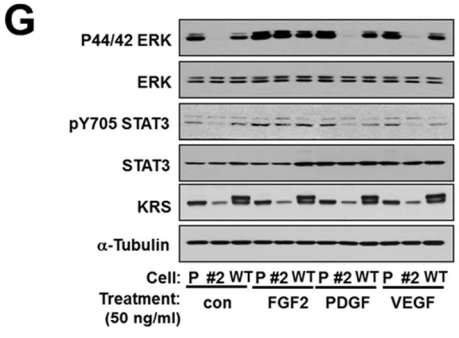

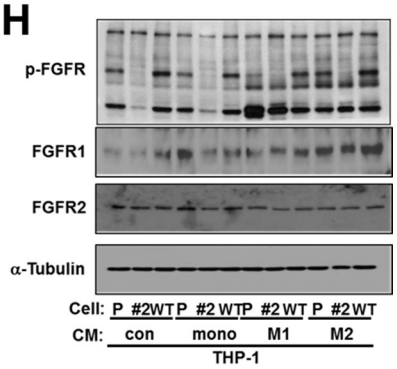

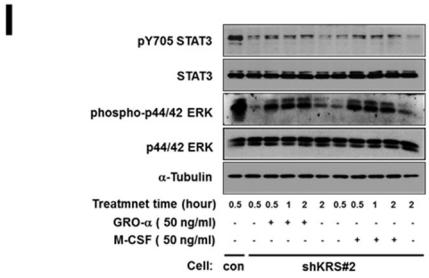

SHN-Fig. 1 continued

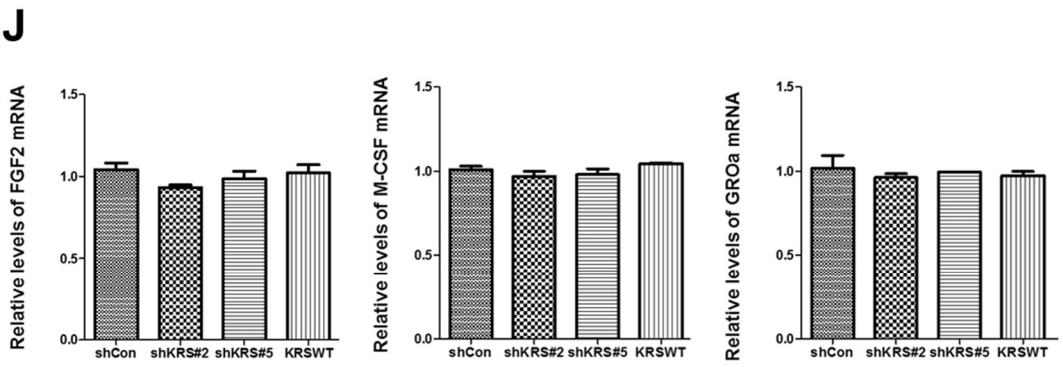

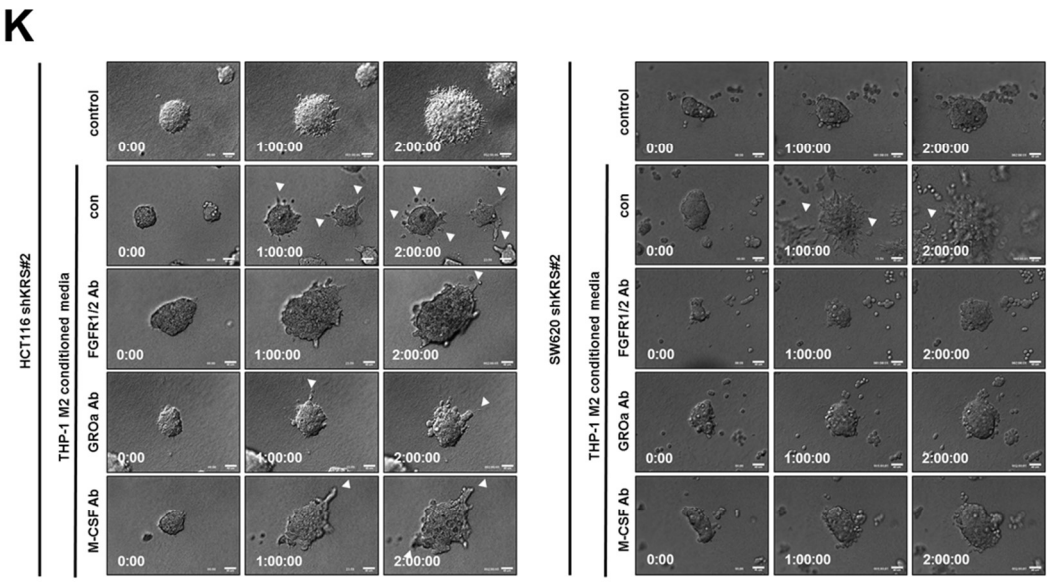

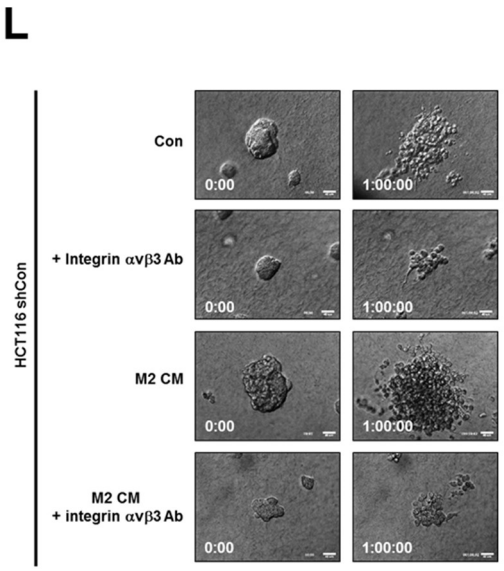

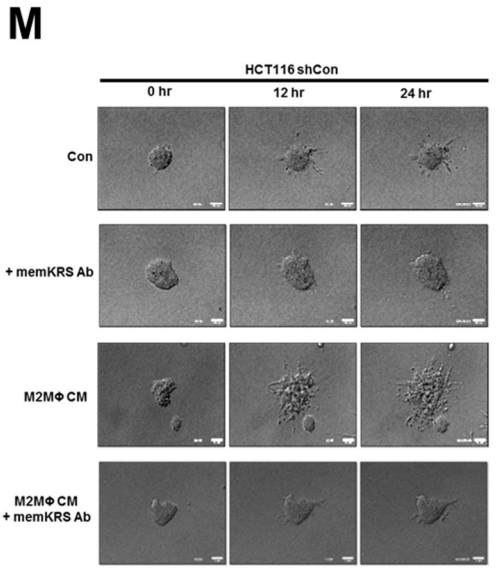

Fig. 2.1. FGF2/GROa/M-CSF cause the dissemination from colon cancer spheroids embedded in 3D collagen I gels.

(A) HCT116 and SW620 (shControl, KRS-suppressed stable cells) spheroids were embedded in 3D collagen I with concomitant treatment of conditioned media (CM, 30%) from monocytes or macrophages derived from human healthy donor blood (M1-, M2-polarized cells) or THP-1 (M1-, M2-polarized cells). Then, the spheroids were imaged by time-lapse microscopy for 48 h. **(B to D)** Spheroids of HCT116 cells (shControl, KRS-suppressed stable cells) embedded in 3D collagen I gels in the presence of the macrophages CM (derived human blood or THP-1 cells) were harvested for whole-cell extracts prior to performing standard western blots for the indicated molecules. **(E)** The Human Cytokine Array was used to simultaneously detect cytokine differences between supernatants of THP-1, human macrophage (monocyte, M1-, M2-polarized) cells. The relative expression levels of 102 human soluble proteins were determined. Blue, red and green rectangles depict for FGF2, GROα and M-CSF, respectively. **(F)** Spheroids of SW620 cells (shControl, KRS-suppressed stable cells) embedded in 3D collagen I gels in the presence of the FGF2 (50 ng/ml), GROα (50 ng/ml) and M-CSF (50 ng/ml) were imaged by time-lapse microscopy for 40 h. **(G to I)** Spheroids of HCT116 cells (shControl, KRS-suppressed stable cells) embedded in 3D collagen I gels in the presence of the FGF2 (50 ng/ml), GROα (50 ng/ml) and M-CSF (50 ng/ml) were harvested for whole-cell extracts prior to performing standard western blots for the indicated molecules. **(J)** mRNA expression of FGF basic(FGF2), GROα and M-CSF in HCT116 cells (shCon, KRS-suppressed stable cells, KRSWT) was measured by pRT-PCR. **(K)** Spheroids of HCT116, SW620 cells (shControl, KRS-suppressed stable cells) embedded in 3D collagen I gels in the presence of the M2 conditioned medium or M2 conditioned medium adding functional anti-human cytokine (FGFR1/2 or GROα, M-CSF) blocking antibody (10 μg/ml) were imaged by

time-lapse microscopy for 48 h. **(L)** Spheroids of HCT116 shControl stable cell lines embedded in 3D collagen I gels in the presence of the M2 CM and/or integrin αvβ3 antibody (10 μg/ml) were imaged by time-lapse microscopy for 24 h. **(M)** Treatment of anti-KRS antibody targeting KRS on membrane of HCT 116 colon cancer cells with wild type KRS expression or KRS suppression, mutant KRS expression embedded on 3D collagen 1 gel.

SHN-Fig. 2

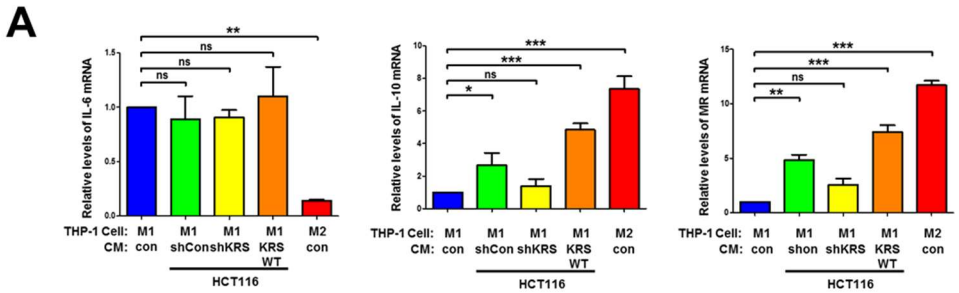

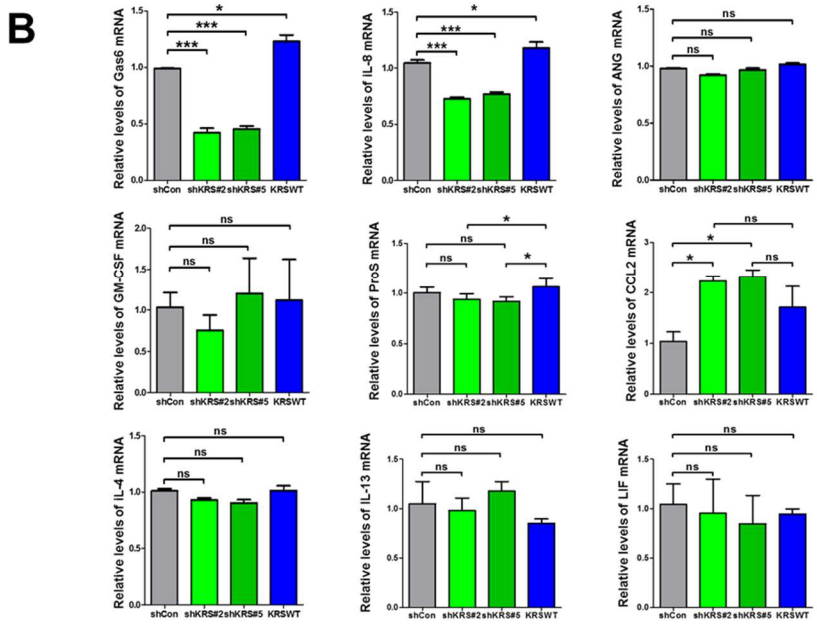

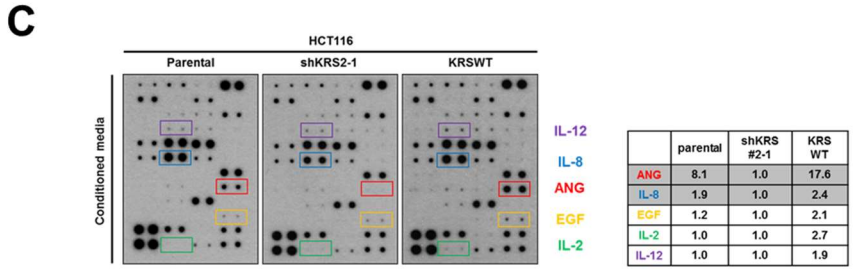

	parental	shKRS #2-1	KRS WT
ANG	8.1	1.0	17.6
IL-8	1.9	1.0	2.4
EGF	1.2	1.0	2.1
IL-2	1.0	1.0	2.7
IL-12	1.0	1.0	1.9

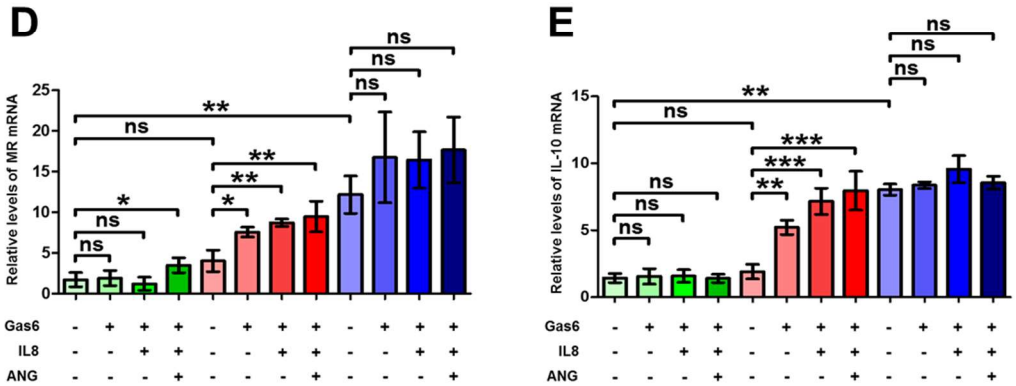

SHN-Fig. 2 continued

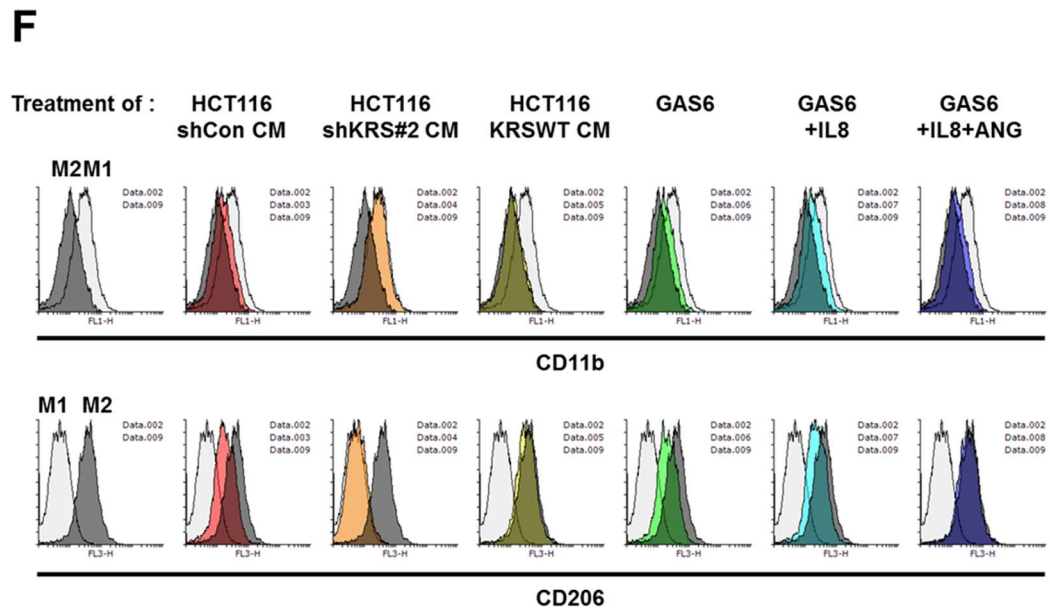

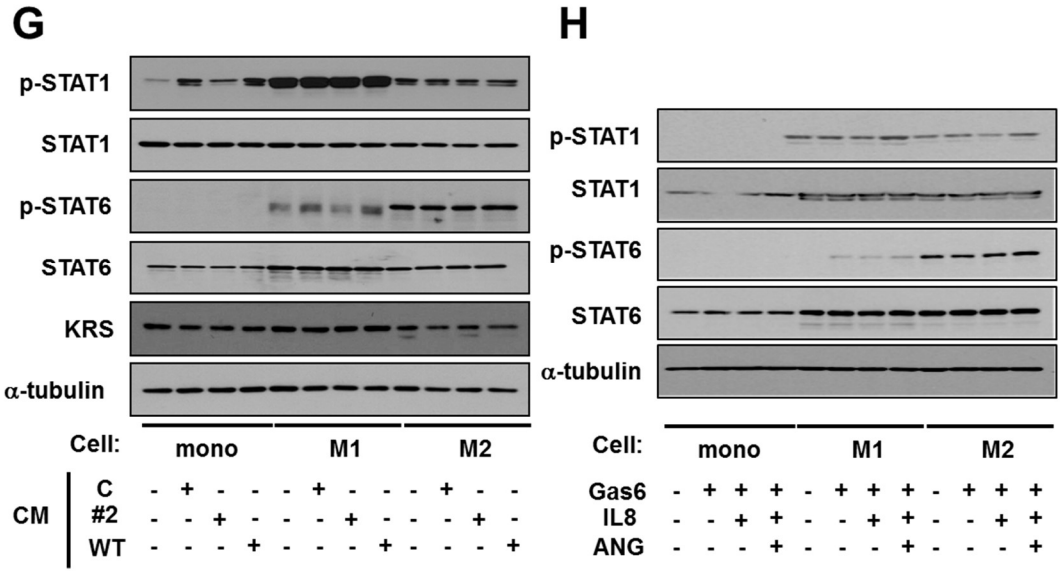

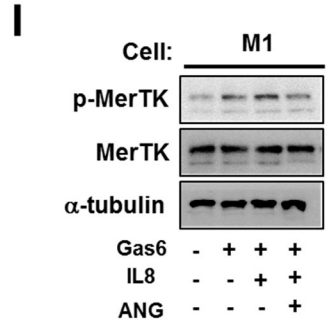

Fig. 2.2. GAS6 from KRS-positive tumor cells causes the polarization of macrophages from M1 to M2 populations.

(A) Cytokine mRNA levels of macrophages (M1 or M2) treated with the CM (30%) prepared from indicated-tumor HCT116 spheroids, by qRT-PCR. **(B)** mRNA levels of several genes related to M1-M2 macrophages transitions were measured in HCT116 cells by pRT-PCR. **(C)** Human cytokine antibody array was used to measure the synthesis or secretion levels of 42 cytokines by HCT116 spheroids (of parental, KRS-suppressed cells, or KRS-overexpression cells) embedded in 3D collagen I gels. Shown in rectangle enclosed boxes are the factors that were highly down-regulated upon KRS suppression in the conditioned media of the HCT116 spheroids. **(D)** mRNA levels of cytokines related macrophage polarization in spheroids of HCT116 (stable shControl, KRS-suppressed stable cells, and stably myc-KRS WT overexpressing cells) colon cancer cells embedded in 3D collagen I gels were analyzed by qRT-PCR. **(E)** Cytokine mRNA levels of monocytes or macrophages (M1 or M2) treated with GAS6 (10 ng/ml), IL8 (50 ng/ml), and/or angiogenin (50 ng/ml) into their culture media for 4 days. **(F)** When M1 macrophages were treated with HCT116 cancer cells (shCon, shKRS # 2, KRSWT) CM or Gas6 and / or IL8 and / or ANG, markers of macrophages were identified by FACS. **(G to I)** Monocytes or macrophages (M1 or M2) treated with HCT116 (stable shControl, KRS-suppressed stable cells, and stably myc-KRS WT overexpressing cells) conditioned media or GAS6 (10 ng/ml), IL8 (50 ng/ml), angiogenin (50 ng/ml) into their culture media for 4 days were were harvested for whole-cell extracts prior to performing standard western blots for the indicated molecules.

SHN-Fig. 3

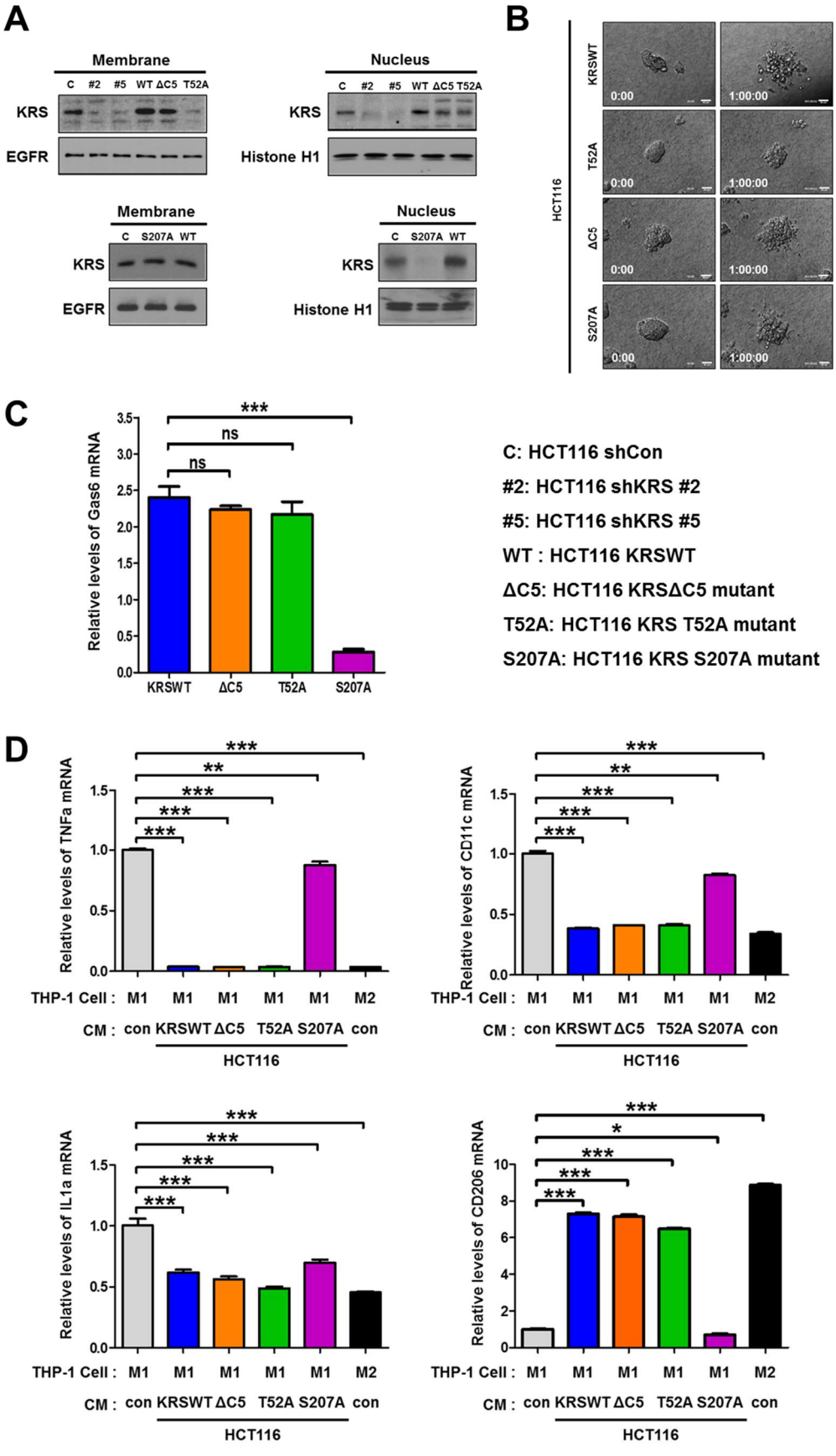
A
Membrane
C #2 #5 WT ΔC5 T52A
KRS
EGFR
Nucleus
C #2 #5 WT ΔC5 T52A
KRS
Histone H1
Membrane
C S207A WT
KRS
EGFR
Nucleus
C S207A WT
KRS
Histone H1
B
HCT116
KRSWT
T52A
ΔC5
S207A
0:00
1:00:00
C
Relative levels of Gas6 mRNA
***
ns
ns
KRSWT
ΔC5
T52A
S207A
C: HCT116 shCon
#2: HCT116 shKRS #2
#5: HCT116 shKRS #5
WT : HCT116 KRSWT
ΔC5: HCT116 KRSΔC5 mutant
T52A: HCT116 KRS T52A mutant
S207A: HCT116 KRS S207A mutant
D
Relative levels of TNFa mRNA
Relative levels of CD11c mRNA
Relative levels of IL1a mRNA
Relative levels of CD206 mRNA
THP-1 Cell : M1 M1 M1 M1 M1 M2
CM : con KRSWT ΔC5 T52A S207A con
HCT116

SHN-Fig. 3 continued

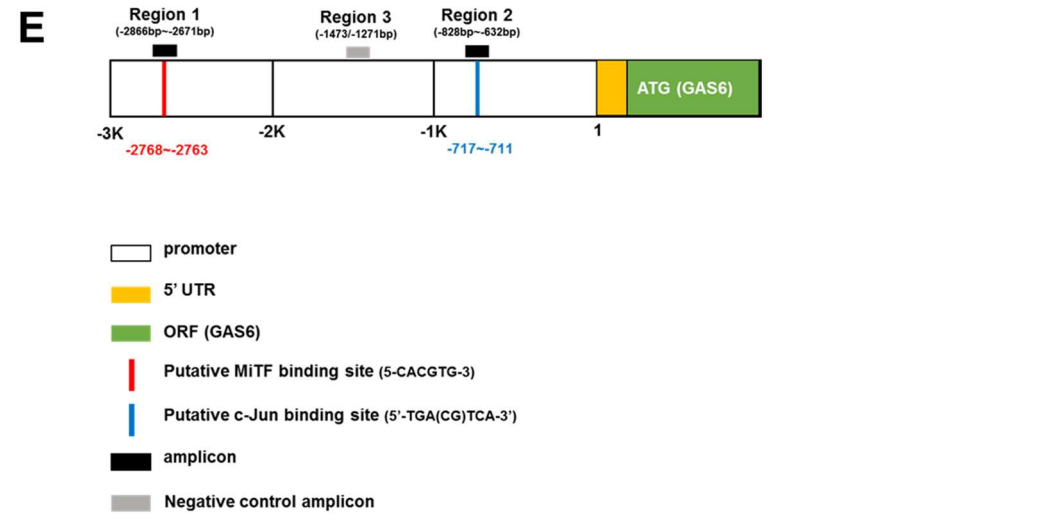

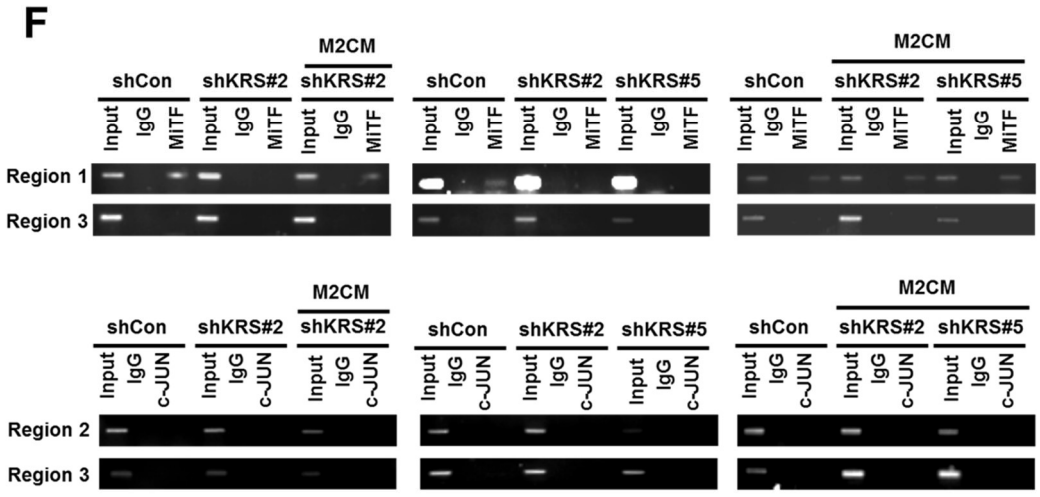

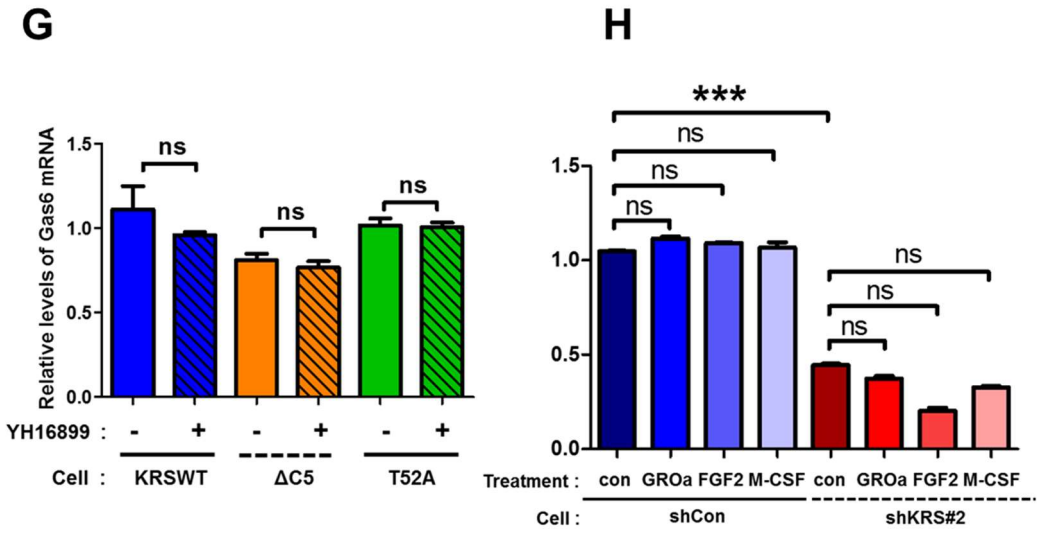

Fig. 2.3. KRS translocated into nucleus promotes GAS6 mRNA level through transcription factor MiTF.

(A) The localization of KRS in HCT 116 colon cancer cells with wild type KRS expression or KRS suppression, mutant KRS expression was confirmed by proteome extraction kit. **(B)** Spheroid of HCT 116 colon cancer cells with wild type KRS expression and mutant KRS expression embedded on 3D collagen 1 gel. Then, the spheroids were imaged by time-lapse microscopy. **(C)** The transcription level of GAS6 in HCT 116 colon cancer cells with wild type KRS expression or KRS suppression, mutant KRS expression was measured by qRT-PCR. **(D)** When M1 macrophages were treated with HCT116 cancer cells (wild type KRS expression and mutant KRS expression), markers of macrophages were measured by qRT-PCR. **(E)** Schematic representation of the promoter regions of the human *GAS6* gene with putative MiTF or c-JUN binding sites and the PCR amplification region of the chromatin immunoprecipitates. **(F)** Chromatin immunoprecipitated from cells using normal IgG or anti-MiTF (Region 1) or anti-c-JUN (Region 2) antibodies without or with M2 CM treatment were processed for PCR using primers for the *GAS6* promoter regions or control regions without binding sites. **(G)** When treated with YH 16899 on HCT116 KRS mutant cell lines, GAS6 mRNA levels were confirmed by qRT-PCR. **(H)** The transcription level of GAS6 was examined when FGF2, GROα, and M-CSF were treated with HCT116 cells (shCon, shKRS#2).

SHN-Fig. 4

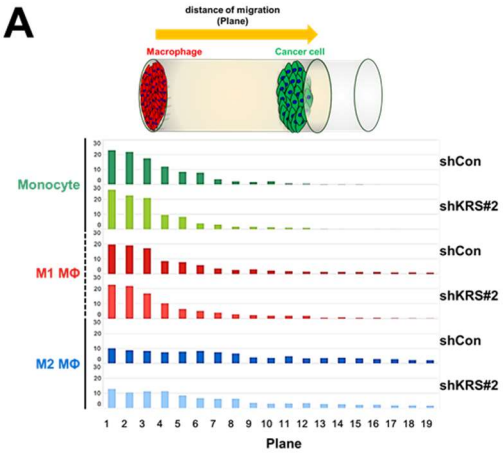
A
distance of migration
(Plane)
Macrophage
Cancer cell
Monocyte
M1 MΦ
M2 MΦ
shCon
shKRS#2
shCon
shKRS#2
shCon
shKRS#2
1 2 3 4 5 6 7 8 9 10 11 12 13 14 15 16 17 18 19
Plane

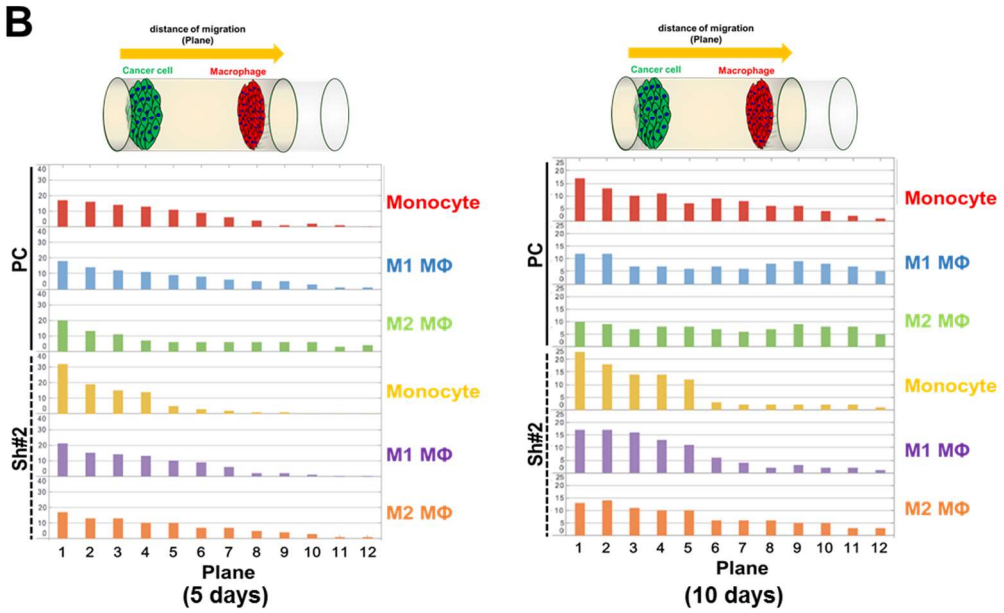
B
distance of migration
(Plane)
Cancer cell
Macrophage
PC
Sh#2
Monocyte
M1 MΦ
M2 MΦ
Monocyte
M1 MΦ
M2 MΦ
1 2 3 4 5 6 7 8 9 10 11 12
Plane
(5 days)
distance of migration
(Plane)
Cancer cell
Macrophage
PC
Sh#2
Monocyte
M1 MΦ
M2 MΦ
Monocyte
M1 MΦ
M2 MΦ
1 2 3 4 5 6 7 8 9 10 11 12
Plane
(10 days)

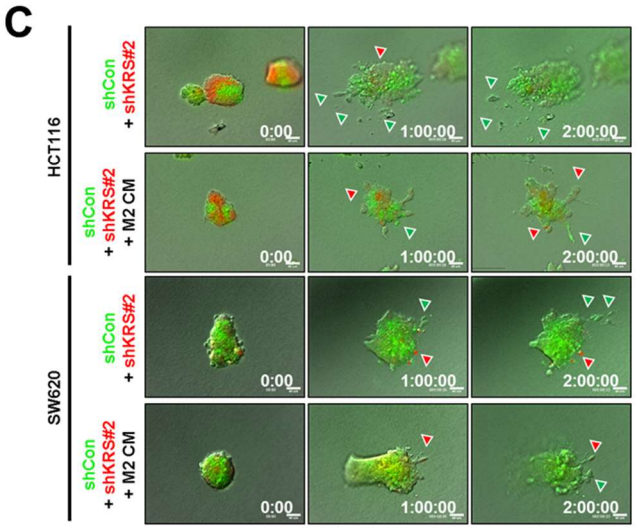
C
HCT116
SW620
shCon
+ shKRS#2
shCon
+ shKRS#2
+ M2 CM
shCon
+ shKRS#2
shCon
+ shKRS#2
+ M2 CM
0:00
1:00:00
2:00:00

SHN-Fig. 4 continued

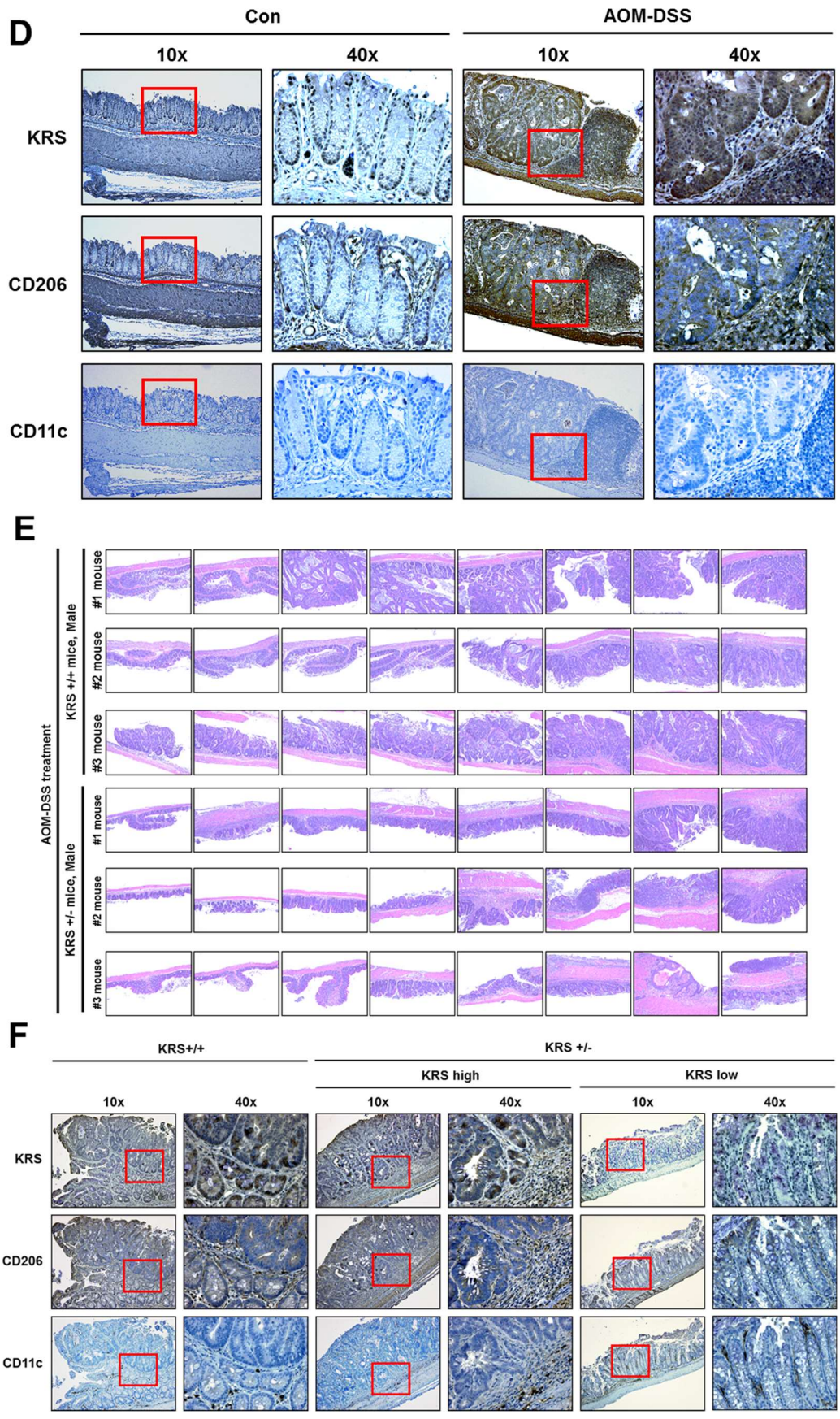

SHN-Fig. 4 continued

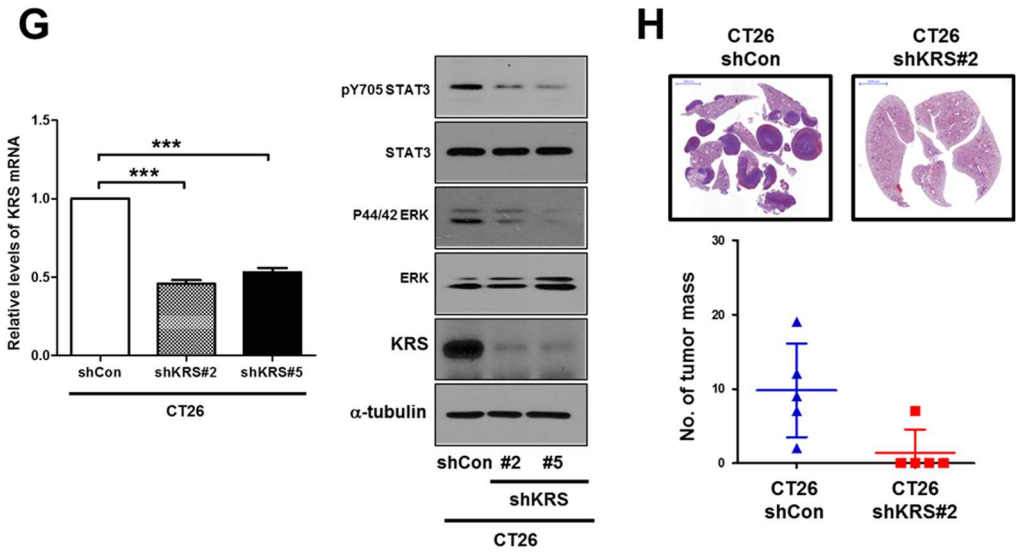

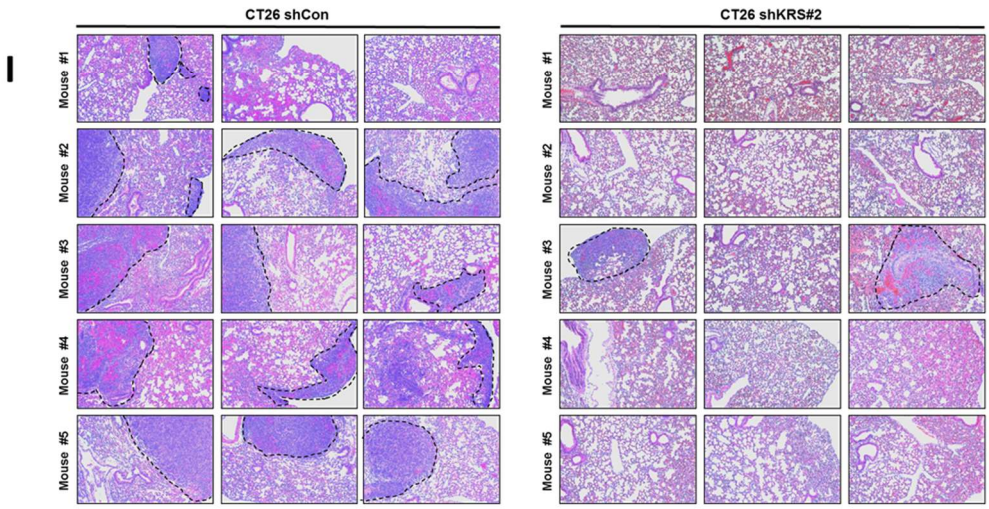

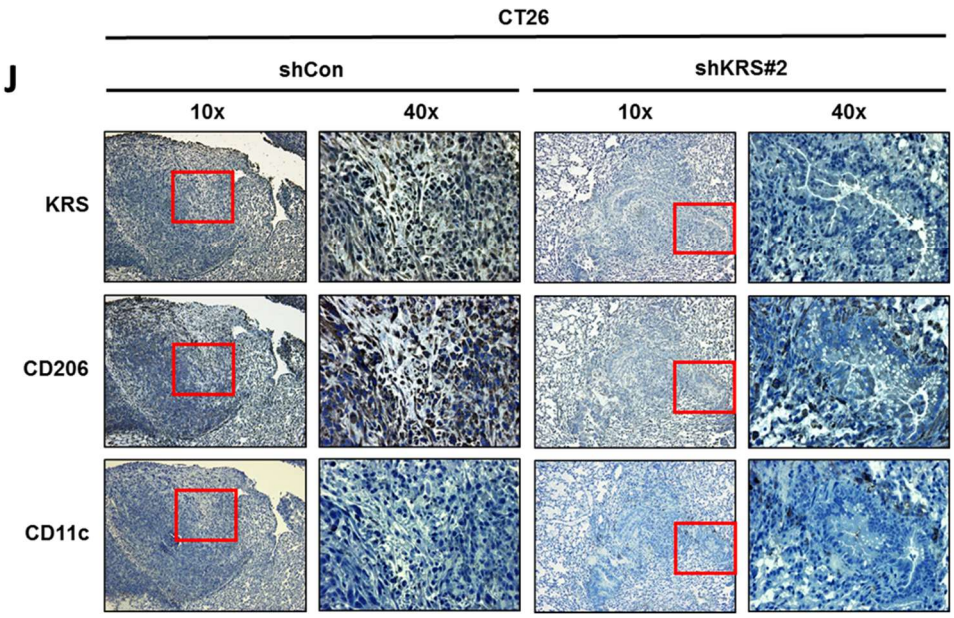

Fig. 2.4. KRS-positive HCT116 tumor cells prefer to communicate with M2 macrophages rather than with M1 macrophages.

(A) Monocytes or macrophages were embedded at the bottom of the gels, and KRS level-modulated HCT116 cancer cells were embedded at the upper side of the gels. Migration of cells analysed using Operetta ®/ Harmony® High Content Screening (HCS) Platform. **(B)** KRS level-modulated HCT116 cancer cells were embedded at the bottom of the gels, and monocytes or macrophages were embedded at the upper side of the gels. HCT116 cancer cells were stained with Cell Tracker Green (CMFDA), and macrophages were stained with Cell Tracker Red (CMTPX). The location of cells in the gels were taken at Day 5 and Day 10 after embedding. **(C)** HCT116 shControl stable cells were stained with CMFDA, and shKRS#2 stable cell lines were stained with CMTPX. These two cell lines were performed co-culture in 3D collagen environment. **(D to F)** Expression pattern of macrophages and M1/M2 macrophage subpopulations in colonic tissue during ulcerative colitis-colorectal carcinoma (UC-CRC) carcinogenesis. The expression pattern of macrophages was assessed by immunohistochemistry using an anti-CD11c antibody, anti-CD206 antibody and anti-KRS antibody. Hematoxylin was used to stain the nuclei. **(G)** KRS suppressed stable cell line was constructed in CT26 colon cancer cells and confirmed by qRT-PCR and immunoblotting. **(H to J)** The tumor formed by CT26 stable cell lines (shCon, shKRS#2) through tail vein injection in Balb/c mice was confirmed by H & E and immunohistochemistry.

SHN-Fig. 5

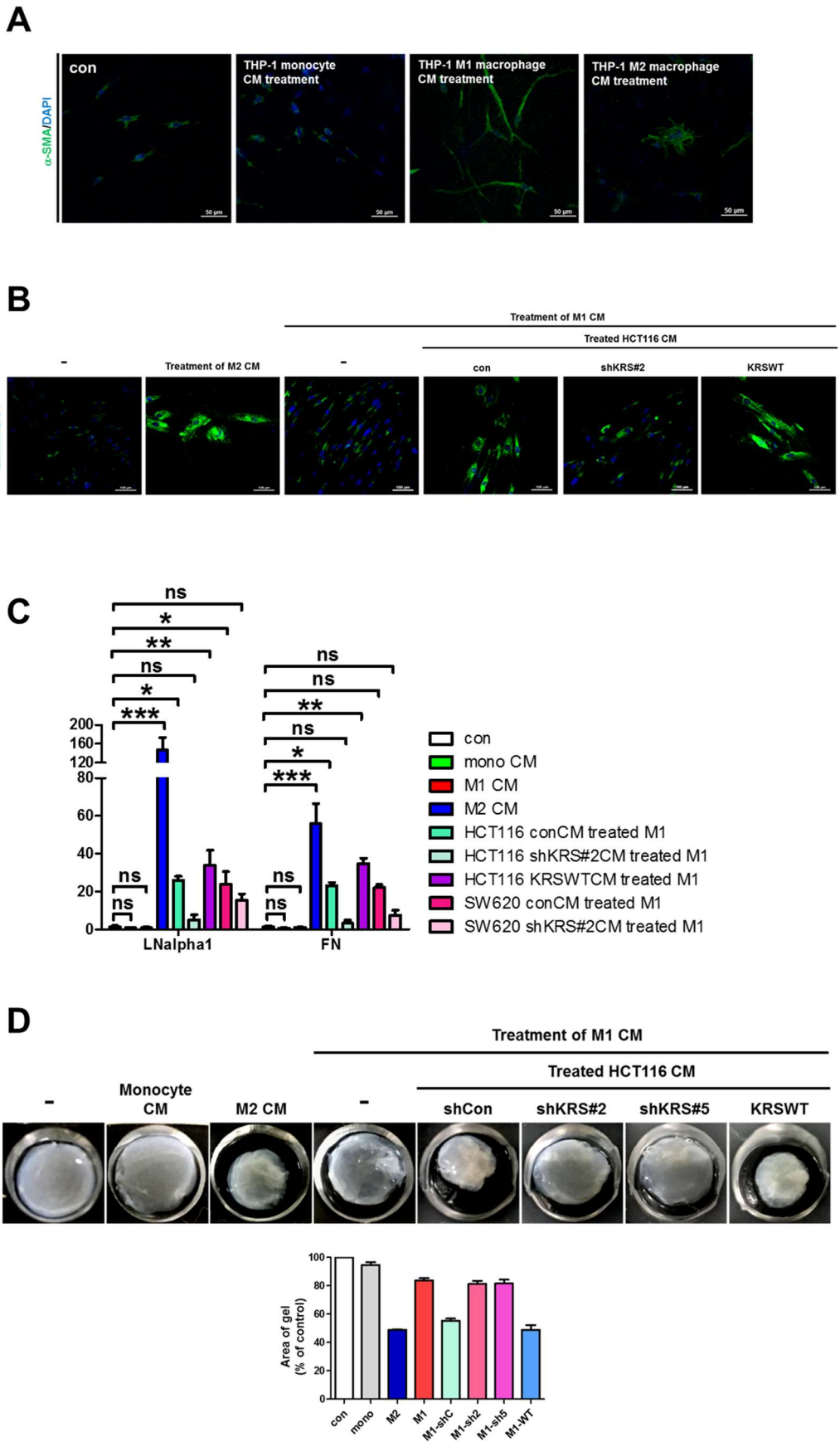
A
con
THP-1 monocyte CM treatment
THP-1 M1 macrophage CM treatment
THP-1 M2 macrophage CM treatment
α-SMA/DAPI
B
Treatment of M1 CM
Treated HCT116 CM
-
Treatment of M2 CM
-
con
shKRS#2
KRSWT
Laminin/DAPI
C
ns
*
**
***
LNalpha1
FN
con
mono CM
M1 CM
M2 CM
HCT116 conCM treated M1
HCT116 shKRS#2CM treated M1
HCT116 KRSWTCM treated M1
SW620 conCM treated M1
SW620 shKRS#2CM treated M1
D
Treatment of M1 CM
Treated HCT116 CM
-
Monocyte CM
M2 CM
-
shCon
shKRS#2
shKRS#5
KRSWT
Area of gel (% of control)
con
mono
M2
M1
M1-shC
M1-sh2
M1-sh5
M1-WT

SHN-Fig. 5 continued

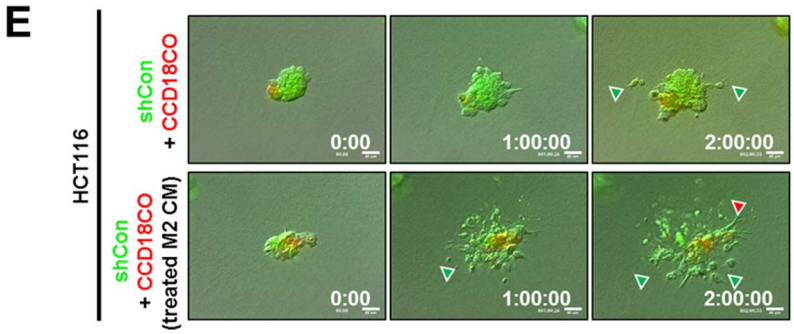

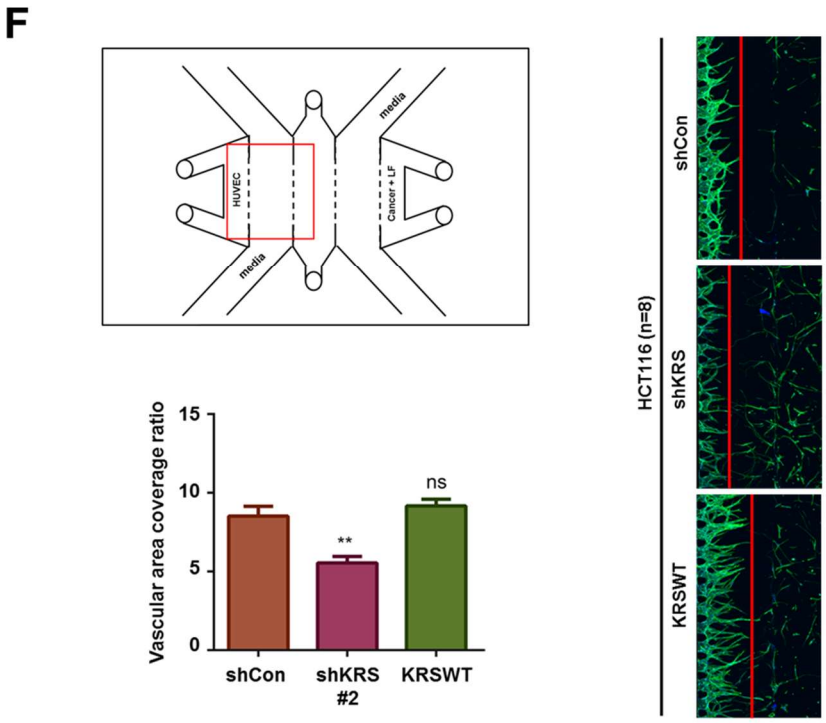

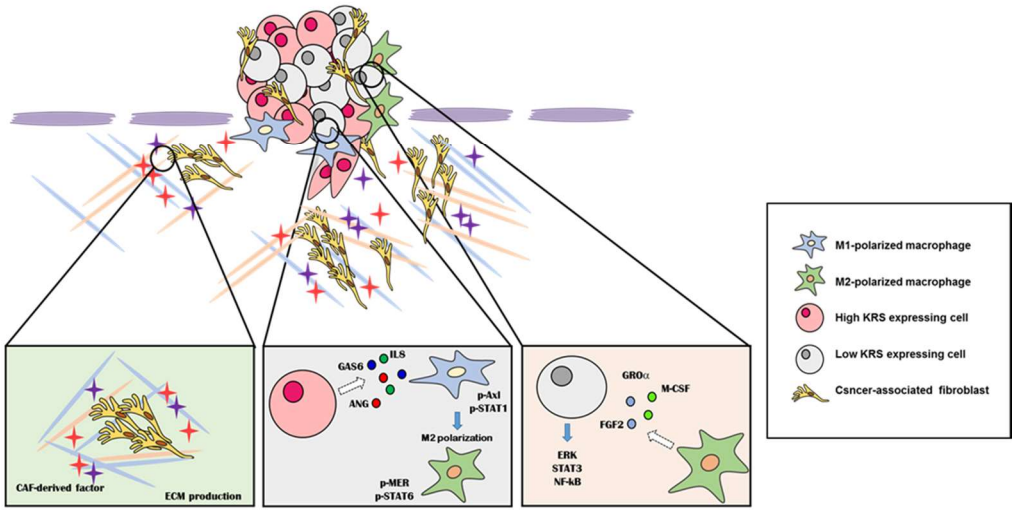

Fig. 2.5. A positive relationship between KRS-positive colon cancer cells and M2 macrophages is important in favoring tumor microenvironment for KRS-positive metastatic phenotypes.

(A) Human colon normal fibroblast CCD18CO in 3D collagen environment were treated with CM of THP1 monocytes or macrophages (M1 or M2) into their culture media. After 4 days, CCD18CO cells were immune-stained with α-sma. **(B to D)** After differentiation of THP-1 into M1 and M2, M1 macrophages were treated with HCT116 cancer cells CM. The CM of macrophages was treated with CCD18CO. Extracellular matrix (laminin alpha1, fibronectin) mRNA levels of human colon fibroblast CCD18CO treated with THP1 monocytes or macrophages (M1 or M2) into their culture media for 4 days measured by qRT-PCR. Representative images of fluorescent Laminin/DAPI staining in fibroblasts. And collagen contraction by fibroblasts was measured. **(E)** CM of M2 macrophages was treated with CCD18CO for 2 days. 3D co-culture of HCT116 cells stained with CMFDA (green) and CCD18CO stained with CMTPX (red) was performed. **(F)** HCT116 cells (shCon, shKRS#2, KRSWT) and HUVEC were co-cultured in a 3D microfluidic system. **(G)** A scheme that models the phenomenon that affects tumor microenvironment through positive-loop interaction between cancer cells with high expression of KRS and macrophages in 3D collagen environment.

Discussion

The most important cause of cancer mortality is metastasis. Metastasis is the growth of cancer cells through the interaction of cancer cells in new places, starting with the delivery of cancer cells to specific organs by blood flow and other factors [30]. Cancer epithelial cells are regulated in the activity and expression of proteins FAK, Src, paxillin, and ERK, which are involved in adhesion, invasion and migration of cells, and cell-cell adhesion, extracellular matrix (ECM) attachment. Recently, it has been confirmed that metastatic heterogeneity in circulating tumor cells (CTC), incomplete EMT phenotype cells, which maintain some epithelial type tendency may have the advantage of colonization again at the distal metastatic site.in order to transfer [42].

The various functions of metastatic cancer cells, including cell migration and invasion, are greatly influenced by the microenvironment around the cells during cell metastasis [32]. Various cells and factors present in the microenvironment of the tumor promote tumor angiogenesis and assist in the invasion and metastasis of tumor cells [33]. Tumor Inflammatory cytokines expressed in cancer cells as well as various immune cells in the microenvironment provide a good environment for tumor cells to grow and migrate and infiltrate while forming an inflammatory network [43]. IL-1β, IL-6, IL-8 and TNF-α, which are the most frequently expressed cytokines in many cancers, are regulated by NF-κB and STAT3 and induce cancer promotion. These cytokines are produced in the tumor microenvironment and induce the expression of MMP-like metastatic and angiogenic genes and growth factors such as VEGF, IL-8, IL-6, TNF-α and TGF-β [44-46]. Cytokines secreted from immune cells and tumor cells affect the signaling pathway through autocrine/paracrine method, allowing various physiological functions in the cell [47]. Thus, the immune cells and tumor cells have an organic

relationship with each other and carry out studies to identify and analyze the organic networking of the cancer cells and the surrounding cell environment, and to identify the functions of the cell [32, 48]. In order to mimic the in vivo environment, a 3D cell culture study supplemented with the disadvantages of 2D with an artificial cell form was developed [49]. Therefore, in vitro 3D cell culture can be a good alternative to actual cell morphology and function studies, and furthermore, interactions with microenvironment [50]. By understanding the mechanisms by which the cell-mediated cell functions of the cancer cells, such as migration / invasion, are regulated through interaction between the cells and the microenvironment around the three-dimensional cell [51, 52].

This study was carried out to investigate the expression of KRS in the colon cancer cell line. KRS plays an important role in linking lysine to the corresponding tRNA using ATP [53]. Recently, it has been reported that KRS also plays an important role in various cellular physiological phenomena such as inflammation, virus assembly, autoimmune disease, and promotes cancer cell migration, in addition to protein synthesis [6, 7, 54]. Especially, in the 3D culture system, the KRS / LR / integrin interaction is important for dissemination in the tumor spheroid. ERK and PXN phosphorylation is important as a downstream signal, and they affect the focal adhesions, leading to a crawling force for dissemination [40]. The aim of this study is to analyze the interaction of KRS with cellular microenvironmental factors in the cellular environment composed of 3D collagen gel. To co-cultivate colon cancer cells, tumor-associated macrophages, and HUVECs (Human Umbilical Vein Endothelial Cells) to consider various cells and factors present in the microenvironment of the tumor. To confirm the role of these cell interactions in terms of metastasis of colon cancer cells, neovascularization of tumor vessels, and function of immune cells.

In this study, we found that cancer cells with high expression of KRS secrete GAS6

and activate macrophages into TAM-like phenotypes. It is well known that M2 macrophages play a major role in the tumor microenvironment [38]. Cancer cells are attracted to surrounding monocytes and differentiate into M1 or M2 macrophages [34]. Usually, M1 macrophages secretes cytokines such as TNFα, IL6, IL1α, and has anti-tumoric functions. The other hand, M2 macrophages are known to have protumoric function by secreting cytokines such as IL10 and TGFβ [55]. Thus, it is important to note that macrophages recruited by several cytokines secreted by colon cancer cells undergo transition from M1 to M2 by KRS-positive cancer cells. KRS-mediated GAS6 affects these M1-M2 transitions, indicating that KRS has a great ability to create a prometastatic environment.

Activated macrophages then produce FGF2, GROα, and M-CSF to induce dissemination of cancer cells to form a positive feedback loop. The dissemination ability of cancer cells is very important as a stepping stone to metastasis [56]. It is well known that several cancer cells having a heterogeniety property, which affects cancer cells [1]. KRS- high expressed cancer cells with high disseminating ability induce the surrounding macrophages to have a TAM-like phenotype, and activated macrophages eventually give dissemination ability to KRS-negative cancer cells. When FGF2, GROα, and M-CSF were treated, the activation rates of the molecules related to dissemination were different. This phenomenon suggests that GROα and M-CSF, which induce activation in a short time, are involved in the initial dissemination of cancer cells, and FGF2, which can maintain its activation for a long time, gives power to become the driving force even at the end of dissemination. These positive loops are essential for promoting the metastasis of colorectal cancer cells and the prognosis of patients with colorectal cancer is poor. Our results indicate that KRS-positive cancer cells located in the stromal region of the tumor have excellent ability to activate macrophages to form a tumor microenvironment for tumor formation and metastasis.

We report that changes in secreted cytokine profiles are important for cancer cell dissemination and macrophage activation. FGF2 / M-CSF / GROα secreted M2 macrophages induced dissemination of colon cancer cells through activation of STAT3, ERK. Among the cytokines induced during dissemination, GAS6 is also responsible for the transition from the M1 macrophage to the M2 macrophage [57]. Other increased cytokines have also been found to be important in other aspects of the tumor microenvironment, such as IL-8 and angiogenin in angiogenesis [58-62]. In vivo, it has been reported that colon cancer cells and macrophages move with each other and interact with each other to induce invasion of one another. It is shown that GAS6 of colon cancer cells with high expression of KRS and FGF2 / GROα / M-CSF of TAM form a positive feedback loop to maintain or promote the dissemination and metastasis of cancer cells. These results provide an explanation for the colocalization of TAM and cancer cells in the invasive front of the tumor with clinical sample analysis. As a results, these interaction affected fibroblast nearby cancer cell and macrophages and gained phenotype of cancer-associated fibroblasts. And these CAFs induced dissemination of colon cancer cells by producing extracellular matrix, such as laminin and fibronectin.

We have found that KRS is significantly induced in cancer cells with excellent dissemination ability, and that these cancer cells are involved in macrophage activation by increasing secretion of GAS6, further promoting dissemination of cancer cells to form a self-reinforcing loop. We also found that GAS6 acts much more on M2 macrophage polarization than IL8 or angiogenin. In addition, when KRS is blocked from transferring to the nucleus, there is no significant effect on macrophage activation by conditioned medium of KRS S207A mutant cancer cells. KRS suggests that it may be possible to play an essential role in initiating a positive feedback loop. In summary, positive loop interaction between cancer cells and macrophages through KRS promotes dissemination of cancer cells and has a significant effect on tumor-microenvironment formation. This study suggests a new approach to anti-cancer

research that considers the microenvironment of the tumor. Especially in inflammatory cytokines that affect the metastasis and neovascularization of colon cancer among cytokines that are abundant in the tumor microenvironment. In addition, this study can be used as a useful data for future cancer diagnosis markers for early diagnosis and prognosis of colon cancer using cytokine.

REFERENCES

1. Thiery, J.P. and C.T. Lim, *Tumor Dissemination: An EMT Affair.* Cancer Cell, 2013. **23**(3): p. 272-3.
2. Meng, F. and G. Wu, *The rejuvenated scenario of epithelial-mesenchymal transition (EMT) and cancer metastasis.* Cancer Metastasis Rev, 2012. **31**(3-4): p. 455-67.
3. Kim, S., S. You, and D. Hwang, *Aminoacyl-tRNA synthetases and tumorigenesis: more than housekeeping.* Nat Rev Cancer, 2011. **11**(10): p. 708-18.
4. Park, S.G., et al., *Human lysyl-tRNA synthetase is secreted to trigger proinflammatory response.* Proc Natl Acad Sci U S A, 2005. **102**(18): p. 6356-61.
5. Yannay-Cohen, N., et al., *LysRS serves as a key signaling molecule in the immune response by regulating gene expression.* Mol Cell, 2009. **34**(5): p. 603-11.
6. Kim, D.G., et al., *Interaction of two translational components, lysyl-tRNA synthetase and p40/37LRP, in plasma membrane promotes laminin-dependent cell migration.* FASEB J, 2012. **26**(10): p. 4142-59.
7. Kim, D.G., et al., *Chemical inhibition of prometastatic lysyl-tRNA synthetase-laminin receptor interaction.* Nat Chem Biol, 2013.
8. Canfield, S.M. and A.Y. Khakoo, *The nonintegrin laminin binding protein (p67 LBP) is expressed on a subset of activated human T lymphocytes and, together with the integrin very late activation antigen-6, mediates avid cellular adherence to laminin.* J Immunol, 1999. **163**(6): p. 3430-40.
9. Ardini, E., et al., *Co-regulation and physical association of the 67-kDa monomeric laminin receptor and the alpha6beta4 integrin.* J Biol Chem, 1997. **272**(4): p. 2342-5.
10. Berno, V., et al., *The 67 kDa laminin receptor increases tumor aggressiveness by remodeling laminin-1.* Endocr Relat Cancer, 2005. **12**(2): p. 393-406.
11. Artym, V.V. and K. Matsumoto, *Imaging cells in three-dimensional collagen matrix.* Curr Protoc Cell Biol, 2010. **Chapter 10**: p. Unit 10 18 1-20.
12. Lee, S.A., et al., *The extracellular loop 2 of TM4SF5 inhibits integrin {alpha}2 on hepatocytes under collagen type I environment.* Carcinogenesis, 2009. **30**(11): p. 1872-1879.
13. Harvey, C.D., et al., *A genetically encoded fluorescent sensor of ERK activity.* Proceedings of the National Academy of Sciences, 2008. **105**(49): p. 19264-19269.
14. Lee, J.W. and R. Juliano, *Mitogenic signal transduction by integrin- and growth factor receptor-mediated pathways.* Mol Cells, 2004. **17**(2): p. 188-202.
15. Jung, O., et al., *Tetraspan TM4SF5-dependent direct activation of FAK and metastatic potential of hepatocarcinoma cells.* J Cell Sci, 2012. **125**(Pt 24): p. 5960-73.
16. Schlaepfer, D.D., et al., *Integrin-mediated signal transduction linked to Ras pathway by GRB2 binding to focal adhesion kinase.* Nature, 1994. **372**(6508): p. 786-91.
17. Yu, M., et al., *Circulating breast tumor cells exhibit dynamic changes in epithelial and*

mesenchymal composition. Science, 2013. **339**(6119): p. 580-4.

18. Aktas, B., et al., *Stem cell and epithelial-mesenchymal transition markers are frequently overexpressed in circulating tumor cells of metastatic breast cancer patients.* Breast Cancer Res, 2009. **11**(4): p. R46.
19. Koyanagi, K., et al., *Prognostic relevance of occult nodal micrometastases and circulating tumor cells in colorectal cancer in a prospective multicenter trial.* Clin Cancer Res, 2008. **14**(22): p. 7391-6.
20. Uen, Y.H., et al., *Persistent presence of postoperative circulating tumor cells is a poor prognostic factor for patients with stage I-III colorectal cancer after curative resection.* Ann Surg Oncol, 2008. **15**(8): p. 2120-8.
21. Panetti, T.S., *Tyrosine phosphorylation of paxillin, FAK, and p130CAS: effects on cell spreading and migration.* Front Biosci, 2002. **7**: p. d143-50.
22. Webb, D.J., et al., *FAK-Src signalling through paxillin, ERK and MLCK regulates adhesion disassembly.* Nat Cell Biol, 2004. **6**(2): p. 154-61.
23. Lin, T.H., et al., *Integrin-mediated activation of MAP kinase is independent of FAK: evidence for dual integrin signaling pathways in fibroblasts.* J Cell Biol, 1997. **136**(6): p. 1385-95.
24. Wary, K.K., et al., *The adaptor protein Shc couples a class of integrins to the control of cell cycle progression.* Cell, 1996. **87**(4): p. 733-43.
25. Wary, K.K., et al., *A requirement for caveolin-1 and associated kinase Fyn in integrin signaling and anchorage-dependent cell growth.* Cell, 1998. **94**(5): p. 625-34.
26. Lu, K.K., et al., *Adhesion-dependent activation of CaMKII and regulation of ERK activation in vascular smooth muscle.* Am J Physiol Cell Physiol, 2005. **289**(5): p. C1343-50.
27. Bellis, S.L., J.T. Miller, and C.E. Turner, *Characterization of tyrosine phosphorylation of paxillin in vitro by focal adhesion kinase.* Journal of Biological Chemistry, 1995. **270**(29): p. 17437-41.
28. Guller, M.C., et al., *c-Fos accelerates hepatocyte conversion to a fibroblastoid phenotype through ERK-mediated upregulation of paxillin-Serine178 phosphorylation.* Mol Carcinog, 2009. **48**(6): p. 532-44.
29. Katoh, K., et al., *Focal adhesion proteins associated with apical stress fibers of human fibroblasts.* Cell Motility & the Cytoskeleton, 1995. **31**(3): p. 177-95.
30. Condeelis, J. and J.W. Pollard, *Macrophages: obligate partners for tumor cell migration, invasion, and metastasis.* Cell, 2006. **124**(2): p. 263-6.
31. Robinson, B.D., et al., *Tumor microenvironment of metastasis in human breast carcinoma: a potential prognostic marker linked to hematogenous dissemination.* Clin Cancer Res, 2009. **15**(7): p. 2433-41.
32. Allavena, P., et al., *The inflammatory micro-environment in tumor progression: the role of tumor-associated macrophages.* Crit Rev Oncol Hematol, 2008. **66**(1): p. 1-9.
33. Dirkx, A.E., et al., *Monocyte/macrophage infiltration in tumors: modulators of angiogenesis.* J Leukoc Biol, 2006. **80**(6): p. 1183-96.

34. Bronte, V. and P.J. Murray, *Understanding local macrophage phenotypes in disease: modulating macrophage function to treat cancer.* Nat Med, 2015. **21**(2): p. 117-9.
35. Liddiard, K. and P.R. Taylor, *Understanding local macrophage phenotypes in disease: shape-shifting macrophages.* Nat Med, 2015. **21**(2): p. 119-20.
36. Marech, I., et al., *Tumour-associated macrophages correlate with microvascular bed extension in colorectal cancer patients.* J Cell Mol Med, 2016. **20**(7): p. 1373-80.
37. Chen, J., et al., *CCL18 from tumor-associated macrophages promotes breast cancer metastasis via PITPNM3.* Cancer Cell, 2011. **19**(4): p. 541-55.
38. Su, S., et al., *A positive feedback loop between mesenchymal-like cancer cells and macrophages is essential to breast cancer metastasis.* Cancer Cell, 2014. **25**(5): p. 605-20.
39. Huang, H., et al., *M2-polarized tumour-associated macrophages in stroma correlate with poor prognosis and Epstein-Barr viral infection in nasopharyngeal carcinoma.* Acta Otolaryngol, 2017: p. 1-7.
40. Nam, S.H., et al., *Noncanonical roles of membranous lysyl-tRNA synthetase in transducing cell-substrate signaling for invasive dissemination of colon cancer spheroids in 3D collagen I gels.* Oncotarget, 2015. **6**(25): p. 21655-74.
41. Neufert, C., C. Becker, and M.F. Neurath, *An inducible mouse model of colon carcinogenesis for the analysis of sporadic and inflammation-driven tumor progression.* Nat Protoc, 2007. **2**(8): p. 1998-2004.
42. Chua, K.N., et al., *Target cell movement in tumor and cardiovascular diseases based on the epithelial-mesenchymal transition concept.* Adv Drug Deliv Rev, 2011. **63**(8): p. 558-67.
43. Yeung, O.W., et al., *Alternatively activated (M2) macrophages promote tumour growth and invasiveness in hepatocellular carcinoma.* J Hepatol, 2015. **62**(3): p. 607-16.
44. Duluc, D., et al., *Interferon-gamma reverses the immunosuppressive and protumoral properties and prevents the generation of human tumor-associated macrophages.* Int J Cancer, 2009. **125**(2): p. 367-73.
45. Gocheva, V., et al., *IL-4 induces cathepsin protease activity in tumor-associated macrophages to promote cancer growth and invasion.* Genes Dev, 2010. **24**(3): p. 241-55.
46. Mancino, A. and T. Lawrence, *Nuclear factor-kappaB and tumor-associated macrophages.* Clin Cancer Res, 2010. **16**(3): p. 784-9.
47. Lazennec, G. and A. Richmond, *Chemokines and chemokine receptors: new insights into cancer-related inflammation.* Trends Mol Med, 2010. **16**(3): p. 133-44.
48. Mantovani, A. and A. Sica, *Macrophages, innate immunity and cancer: balance, tolerance, and diversity.* Curr Opin Immunol, 2010. **22**(2): p. 231-7.
49. Chu, J.H., et al., *Development of a three-dimensional culture model of prostatic epithelial cells and its use for the study of epithelial-mesenchymal transition and inhibition of PI3K pathway in prostate cancer.* Prostate, 2009. **69**(4): p. 428-42.
50. Bai, J., et al., *Identification of drugs as single agents or in combination to prevent carcinoma dissemination in a microfluidic 3D environment.* Oncotarget, 2015. **6**(34): p. 36603-14.

51. Aref, A.R., et al., *Screening therapeutic EMT blocking agents in a three-dimensional microenvironment.* Integr Biol (Camb), 2013. **5**(2): p. 381-9.
52. Foroni, L., et al., *The role of 3D microenvironmental organization in MCF-7 epithelial-mesenchymal transition after 7 culture days.* Exp Cell Res, 2013. **319**(10): p. 1515-22.
53. Freist, W. and D.H. Gauss, *Lysyl-tRNA synthetase.* Biol Chem Hoppe Seyler, 1995. **376**(8): p. 451-72.
54. Kim, B.H., et al., *Lysyl-tRNA synthetase (KRS) expression in gastric carcinoma and tumor-associated inflammation.* Ann Surg Oncol, 2014. **21**(6): p. 2020-7.
55. Pollard, J.W., *Tumour-educated macrophages promote tumour progression and metastasis.* Nat Rev Cancer, 2004. **4**(1): p. 71-8.
56. Zhang, L., et al., *Overexpression of fibroblast growth factor 1 in MCF-7 breast cancer cells facilitates tumor cell dissemination but does not support the development of macrometastases in the lungs or lymph nodes.* Cancer Res, 1999. **59**(19): p. 5023-9.
57. Graham, D.K., et al., *The TAM family: phosphatidylserine sensing receptor tyrosine kinases gone awry in cancer.* Nat Rev Cancer, 2014. **14**(12): p. 769-85.
58. Rozman, A., M. Silar, and M. Kosnik, *Angiogenin and vascular endothelial growth factor expression in lungs of lung cancer patients.* Radiol Oncol, 2012. **46**(4): p. 354-9.
59. Seyfarth, H.J., et al., *[Angiogenin, bFGF and VEGF: angiogenic markers in breath condensate of patients with pulmonary hypertension].* Pneumologie, 2015. **69**(4): p. 207-11.
60. Miyake, M., et al., *Angiogenin promotes tumoral growth and angiogenesis by regulating matrix metallopeptidase-2 expression via the ERK1/2 pathway.* Oncogene, 2015. **34**(7): p. 890-901.
61. Rogala, E., et al., *Assessment of the VEGF, bFGF, aFGF and IL8 angiogenic activity in urinary bladder carcinoma, using the mice cutaneous angiogenesis test.* Anticancer Res, 2001. **21**(6B): p. 4259-63.
62. Huang, S., et al., *Fully humanized neutralizing antibodies to interleukin-8 (ABX-IL8) inhibit angiogenesis, tumor growth, and metastasis of human melanoma.* Am J Pathol, 2002. **161**(1): p. 125-34.

ABSTRACT IN KOREAN

3차원적 콜라젠 환경에서 대장암세포의 침윤적 이탈을 위한 Lysyl-tRNA 합성효소의 기능

남 서 희

종양의 미세 환경은 암의 발생과 전이에 중요한 역할을 한다는 것이 잘 알려져 있다. 암세포의 세포-세포 및 세포-기질 부착 특성은 암 전이를 차단하기 위해 표적화 될 수 있다. 세포질의 lysyl-tRNA 합성 효소 (KRS 또는 KARS)는 본래 단백질 합성 과정에서 기능을 하지만, 세포막에 존재할 수 있는 KRS는 암전이에 관여한다고 확인한 바 있다.

본 연구는 3D 콜라겐 I 겔에서 KRS 양성 세포가 세포 이탈성 표현형을 명확하게 보인 반면, KRS 억제 세포는 이탈성 표현형이 차단된다는 것을 발견했다. 또한, KRS-의존적 침윤성 이탈 활성은 ERK/paxillin 활성을 유도하는 세포막 상의 인테그린 $\alpha 6$ 및 p67 라미닌 수용체와의 연관성 있음을 확인하였다. 그리고 KRS 억제에 의한 세포 이탈성 표현형의 감소는 ERK/또는 paxillin의 transfection에 의해 회복하였다. 따라서, 3차원 세포배양 환경에서 대장암세포 내의 KRS는 p67 라미닌 수용체 (p67LR)/인테그린α6β1/ERKs/Paxillin 신호 연결을 통해 암세포의 이탈 및 이동을 촉진시켰으며, 이는 세포가 이탈하는 동안

견인력이 생성됨을 추정할 수 있다.

침윤성 종양의 암세포 및 종양 관련 대식세포 (TAM; Tumor-associated macrophage)의 근접 가능성은 이 두 세포 유형이 상호 작용할 수 있음을 시사한다. 따라서 KRS-의존적 암덩어리에서 암세포의 이탈에 대식세포가 미치는 영향을 분석하였다. KRS 발현이 높은 대장암 세포에서 사이토카인을 분석한 결과, KRS 발현이 낮은 세포보다 KRS 발현이 높은 세포가 GAS6, IL8, angiogenin을 더 많이 발현하였다. 그 중에서 GAS6는 M1에서 M2 집단으로의 대식세포의 polarization 야기하는데 주로 역할을 하였다. 핵으로 이동한 KRS는 GAS6의 promoter에 결합이 가능한 MiTF를 통해 GAS6 mRNA의 발현을 증가시켰다.

이러한 KRS 매개 암세포의 이탈은 크게 2가지의 KRS 역할에 의해 의존적임을 밝혔다. 첫째, 핵으로 이동한 KRS는 GAS6의 전사를 조절하여 주변의 대식세포들을 M2 집단으로 분극화시킨다. M2 대식세포에서 분비되는 FGF2/GRO α/M-CSF는 암세포에서 ERKs/paxillin 및 STAT3와 NFκB를 포함하는 세포 내 신호 전달 경로를 활성화시켜 KRS 발현이 높은 세포뿐만 아니라 발현이 낮은 세포에서도 암세포 이탈 표현형을 유발한다. 둘째, 세포막으로 이동한 KRS는 라미닌 수용체와 함께 세포-ECM 상호작용에 매개하여, 세포 이동에 필요한 견인력 생성을 위한 세포 내 신호 전달 연계를 일으키는 역할한다.

정상 섬유아세포는 M2 대식세포 CM의 처리에 의해 암 관련 섬유 모세포 (CAF; Cancer-associated fibroblast)로 분화되는 것으로 나타났고, CAF의 라미닌 발현을 유도하여 KRS 양성 암세포의 이탈 및 이동을 유도할 수 있는 미세

환경을 구성한다. 결론적으로 대장암 세포 내에서의 높은 KRS 발현은 전이성 세포가 주변 조직으로의 침투 혹은 이탈을 용이하게 한다는 것을 알 수 있었기에, 이는 KRS가 대장암 전이를 막는 유망한 표적이 될 수 있음을 제시한다.

주요어 : lysyl-tRNA 합성효소; 암 전이; 3차원 세포배양; 항암전이제, 라미닌 수용체; 종양관련 대식세포, 암 미세환경, 사이토카인

학번 : 2012-30864